MODEL-BASED STATE ESTIMATION FOR FAULT DETECTION UNDER DISTURBANCE

A Dissertation

by

XINGHUA PAN

Submitted to the Office of Graduate and Professional Studies of
Texas A&M University
in partial fulfillment of the requirements for the degree of

DOCTOR OF PHILOSOPHY

Chair of Committee,	M. Nazmul Karim
Committee Members,	M. Sam Mannan
	Costas Kravaris
	A. Rashid Hasan
Head of Department,	M. Nazmul Karim

December 2016

Major Subject: Chemical Engineering

ABSTRACT

The measurement of process states is critical for process monitoring, advanced process control, and process optimization. For chemical processes where state information cannot be measured directly, techniques such as state estimation need to be developed. Model-based state estimation is one of the most widely applied methods for estimation of unmeasured states basing on a high-fidelity process model. However, certain disturbances or unknown inputs not considered by process models will generate model-plant mismatch. In this dissertation, different model-based process monitoring techniques are developed and applied for state estimation under uncertainty and disturbance.

Case studies are performed to demonstrate the proposed methods. The first case study estimates leak location from a natural gas pipeline. Non-isothermal state equations are derived for natural gas pipeline flow processes. A dual unscented Kalman filter is used for parameter estimation and flow rate estimation. To deal with sudden process disturbance in the natural gas pipeline, an unknown input observer is designed. The proposed design implements a linear unknown input observer with time-delays that considers changes of temperature and pressure as unknown inputs and includes measurement noise in the process. Simulation of a natural gas pipeline with time-variant consumer usage is performed. New optimization method for detection of simultaneous multiple leaks from a natural gas pipeline is demonstrated. Leak locations are estimated by solving a global optimization problem. The global optimization problem contains

constraints of linear and partial differential equations, integer variable, and continuous variable. An adaptive discretization approach is designed to search for the leak locations.

In a following case study, a new design of a nonlinear unknown input observer is proposed and applied to estimate states in a bioreactor. The design of such an observer is provided, and sufficient and necessary conditions of the observer are discussed. Experimental studies of batch and fed-batch operation of a bioreactor are performed using *Saccharomyces cerevisiae* strain mutant SM14 to produce β-carotene. The state estimation of the process from the designed observer is demonstrated to alleviate the model-plant mismatch and is compared to the experimental measurements.

DEDICATION

To my parents, family, and friends

ACKNOWLEDGEMENTS

I would like to deeply thank my advisor Dr. M. Nazmul Karim for all his guidance and advice through my study. His support and encouragement about my research give me opportunities to learn many different aspects of chemical engineering including experimental bioengineering projects and process engineering technology. His constructive criticism keeps me learning consistently and improving myself.

I would like to greatly thank my committee members, Dr. Mannan, Dr. Kravaris, and Dr. Hasan for their guidance and help throughout this research. I also want to thank Dr. Pistikopoulos, Dr. Jayaraman, and Dr. Balbuena for their support as my teaching assistant advisor.

I deeply appreciate and thank all my colleagues in Dr.Karim's group: Weiting, Alim, Chao Liang, Jon, Tejasvi, Melanie, Alex, Chiru, Carl, Zheng, and Yuxin. I can't finish this dissertation without the help and support from the group. I also want to thank Toni, Louis, Ashley, and Towanna for their help which makes my life much easier.

Thanks also go to many friends and colleagues in the chemical engineering department. Also I want to thank all my friends that I met in College Station, who make my life colorful.

Finally, thank my parents and all my family members for their love and support.

CONTRIBUTORS AND FUNDING SOURCES

Contributors

This work was supervised by a dissertation committee consisting of Professor M. Nazmul Karim, Professor M. Sam Mannan and Costas Kravaris of the Department of Chemical Engineering, and Professor A.Rashid Hasan of the Department of Petroleum Engineering.

The experimental data for Chapter V was conducted in part by Tejasvi Jaladi and Melanie R. DeSessa of the Department of Chemical Engineering.

All other work conducted for dissertation was completed by the student independently.

Funding Sources

Graduate study was supported by ‘Michael O’Connor Chair II’ from Texas A&M University.

TABLE OF CONTENTS

Page

LIST OF FIGURES

Page

LIST OF TABLES

Page

CHAPTER I

INTRODUCTION AND LITERATURE REVIEW

Introduction

This chapter briefly summarizes the research background and outlines the contribution and scope of the dissertation.

Process monitoring is an important practice for all engineering systems.[1] It is greatly associated with product quality and process safety. Production and transportation of petrochemical industries pay great attention to the process monitoring because the damage in these systems can be catastrophic.[2] Early detection of abnormal behavior of the process can help engineer identify the root cause and prevent further damage.

One of the key purposes of process monitoring is fault detection and diagnosis. [3–5] Fault in an engineering process is defined as abnormal deviations from normal behaviors, gradually or abruptly.[3,6] There are different types of faults in the system including additive process faults and multiplicative process faults.

For process fault detection and diagnosis, three tasks are required which are fault detection, fault isolation, and fault identification.[7] Fault detection is to identify abnormal behavior of the system. Fault isolation is to find the exact location and cause of the fault. Fault identification is to measure/estimate the size/magnitude of the fault. For some systems, fault identification and detection can be performed together. For a complex system, identification and isolation of multiple faults from a limited number of sensor

readings can be a challenge. Traditionally, process monitoring is performed by checking some key variables against their limit through the physical sensor.

The alarming limits of the process variables are set according to operator's previous experience or the machine configuration. Data-based process monitoring has been widely used in industry as statistical process control.[8–10] Data-based process monitoring is based on extensive previous operation data. Comparison between previous operation data and current monitored data is performed to monitor the current process. Several data analysis technique has been applied such as Principle Component Analysis and Partial Least Square.[11–13] Other advanced data analysis methods have been developed for different systems such as kernel Principle Component Analysis, time-series analysis, and multi-way and multi scale Principle Component Analysis.[11,14–18] Another method is model-based process monitoring which is based on the development of a mathematical process model. Comparisons between measured process variables and model predictions are studied to evaluate the process performance. Model-based process prediction techniques have been developed such as Kalman filter, observer, and optimization-based state estimation method.[19–25] Both data-based and model-based process monitoring methods have its advantage and disadvantage. The details about these two methods will be given at the next session. More attention will be given to the model-based process monitoring methods.

Literature review

Data-based process monitoring will be briefly introduced. Model-based process monitoring will be explained with more details.

Data-based process monitoring

Data-based statistical process control has been successfully implemented in various industries for process monitoring and improvement of product quality. The word 'control' in statistical process control aims to reduce process variation and to increase product quality.[26] The development of statistical process control as a system monitoring tool starts from Dr.Walter Shewhart at 1920s.[27] Namely, statistical process control uses statistical analysis method to understand and monitor a process. Commonly measured and calculated values of process variables include: mean, variance, probability density function, and cumulative distribution function.[26] For some processes with many process variables, process data needs to be analyzed and its dimension needs to be reduced. Data analysis and dimension reduction methods have been developed including single-block techniques including Principal Component Analysis, linear or Fisher's discriminant analysis, and independent component analysis, and dual-block techniques including canonical correlation analysis, reduced rank regression, Partial Least Squares, and maximum redundancy.[26,28–31]

Among the above-mentioned methods, Principle Component Analysis and Partial Least Square are variance/covariance-based techniques, which have been studied extensively. Principle Component Analysis is used to reduce the number of process variables to be monitored, which is a dimension reduction technique. It defines a reduced set of latent variables. The model construction is shown below:

$$X=TP'+E \quad (1.1)$$

$$y=Tc+f \quad (1.2)$$

$t_{pre}=x_{new}W(P'W)^{-1}$ (1.3)

where *T* is score of *X*. *P* and *c* are loadings corresponding to *X* and *y*, respectively. *E* and *f* are residuals. *W* is weight matrix from score calculation. t_{pre} is the estimated score corresponding to batch x_{new} and t_{pre} which is used to evaluate the batch-to-batch variation.

In contrast to Principle Component Analysis, Partial Least Square analyzes process input and process output. Partial Least Square calculates linear combinations of process variables to determine latent variables. The latent variables have similar effect in Principle Component Analysis, which is to capture process variations.[32]

In contrast to Principle Component Analysis, Partial Least Square analyzes process input and process output. Partial least square calculate linear combinations of the variables to determine latent variables.[32] The latent variables have similar effect in principle component analysis, which is to capture process variations. Partial Least Square is developed into the two-way data matrix *X* and vector of maturity variable y as followed.

$X=TP'+E$ (1.4)

$y=UQ'+f$ (1.5)

where *T* is scores of *X*. *P* and *Q* are loadings corresponding to *X* and *y*, respectively. *E* and *f* are the residuals.

Process monitoring charts have been developed to evaluate the performance of the process.[9] Basing on Principle Component Analysis and Partial Least Square models, the T-score variables describe variation that is introduced by the source vector. The T-

score variables are dimension reduced variables which can be plotted in scatter diagrams. Nonnegative quadratics statistical analysis including Hotelling's T^2 statistics and residual-based squared prediction error statistics, referred as Q statistics, can be performed on the plotted T-score variables. Hotelling's T^2 chart measures variation in the principal component subspace:

$$T_A^2 = \sum_1^A \frac{t_i^2}{s_{t_i}^2} \tag{1.6}$$

The Hotelling's T^2 chart calculates distance between new measurements and modeling dataset. With the assumptions of normal distribution and a known data mean value, the Hotelling's T^2 follows F-distribution. The limit for Hotelling's T^2 for a given significant level α is calculated as below.

$$T_\alpha^2 = \frac{l(N-1)}{N-l} F_{l,N-l,\alpha} \tag{1.7}$$

where $F_{l,N-1,\alpha}$ is the critical point for F distribution with (l, N-l) degrees of freedom with a significant level α.

Data analysis methods have been developed to analyze the plotted date including contribution charts, residual-based test, and variable reconstruction. Contribution charts reveal significance of the recorded variables. Variable reconstruction studies the correlation among the recorded process variables. Data-based process modeling relays on large-volume recorded process data. The data-based model can be used to monitor an existing process with significant amount of previous operation data. For a new process or operation under a new condition, data-based model is not able to estimate the process

variables. In these scenarios, model-based process monitoring and fault detection can be applied.

Model-based process monitoring

First principle models can be developed for a well-understood process. The models can be used to predict the process behavior under different operating conditions and inputs. The prediction of the model output is certain analytical forms of the measurement, which can be compared to the process measurement. A residual is defined as a comparison between model prediction and measurement. When a fault occurs in the process, an increased residual will be observed. As illustrate in Figure I.1, an alarm will be triggered if the residual exceed a pre-set threshold.

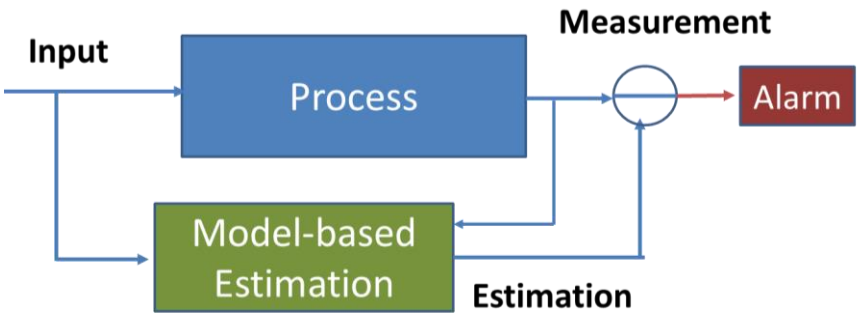

Figure I.1. Process configuration for model-based fault detection

The applied process model can be categorized as continuous model and discrete-event model. The continuous models are generally ordinary differential equation or partial differential equation, which can be further characterized as linear, nonlinear, and

time-variant equations. Continuous model is the most common process models for fault detection.

Continuous models for a chemical process are developed from theoretical analysis of the process, which is also called first principle modeling. Nature laws including mass balance, momentum balance, and energy balance are applied. Besides theoretical modeling, experimental modeling is based on the assumption of certain model structure. Input and output variables are measured to fit into an existing model structure. For both theoretical model and experimental model, model parameters are estimated using experimental data. The most common parameter estimation technique for linear system is the least square method.

State is the key information which is used to characterize a process such as temperature, pressure, degree of polymerization, and reactant concentration. This key information is required for process monitoring, such as evaluating the reaction kinetic, analysis of process safety, and determination of process control strategy. Some of the state variables are directly measureable such as temperature and pressure. Some of the state information cannot be measured directly or it has significant time-delay in measuring. Some state information is corrupted with process noise and process fault. State estimation techniques were developed to estimate unmeasured states or corrupted states. Analytical state estimation technique includes observer/filter design and parameterized mapping technique such as neural network and evolutionary algorithms.

Neural network and evolutionary algorithms

Neural network is a nonlinear mapping technique. The goal of neural network is to map between input and output space. It has been actively developed and applied in many engineering problems. The feed-forward artificial neural network includes multi-layer perceptron and radial basis function network. Evolutionary algorithm was developed by the inspiration of biological systems which can be conceived as a class of stochastic optimization algorithm. Two kinds of evolutionary algorithm have been developed including Genetic Algorithm and Genetic Programming. The algorithm has the following steps: population initialization, reproduction, recombination, mutation, and succession processes.

Design of observer and filter

Various design and applications of state estimation technique including observer-based and filter-based (stochastic method) have been extensively studied and applied. Luenberger observer and Kalman filter are the two most widely used state estimation techniques. Various new observers have been developed basing on these two methods. Design of observer can be categorized into linear and nonlinear observers. A linear observer design is demonstrated below.

Consider a linear time invariant continuous system:

$$\dot{x}(t)=Ax(t)+Bu(t) \tag{1.8}$$

$$y(t)=Cx(t) \tag{1.9}$$

where x, u, and y are the state, input, and output of the system, with $x \in \Re^n, u \in \Re^r, y \in \Re^p$. A, B, and C are parametric matrix with appropriate dimension. A full order feed-back observer was designed with the following structure.

$$\dot{\hat{x}}(t)=(A-KC)\hat{x}+Bu(t)+Ky(t) \quad (1.10)$$

$$\hat{y}(t)=C\hat{x}(t) \quad (1.11)$$

where *K* is a design parameter which needs to be determined such that the feedback matrix (A-KC) is asymptotically stable. The asymptotical stability of the observer guarantees the estimation error decay to zero. The pair (A, C) is observable equals to the controllability of the pair (A^T, C^T).

Kalman filter

Kalman filter is an optimal linear filter for state estimation. It propagates the mean and covariance of the state through time. To demonstrate the Kalman filter, a linear discrete-time system is given as the following equations:

$$x_k=F_{k-1}x_{k-1}+G_{k-1}u_{k-1}+w_{k-1} \quad (1.12)$$

$$y_k=H_K x_k+v_k \quad (1.13)$$

$\{w_k\}$ and $\{v_k\}$ are assumed white noise with known covariance matrix Q_k and R_k. The Kalman filter is initialized as follows:

Initialization: $\hat{x}_0^+=E(x_0)$; $P_0^+=E[(x_0-\hat{x}_0^+)(x_0-\hat{x}_0^+)^T]$ (1.14)

Estimation: for each time step $k = 1,2, \ldots$:

$$P_k^-=F_{k-1}P_{k-1}^+F_{k-1}^T+Q_{k-1}$$

$$K_k=P_k^-H_k^T(H_kP_k^-H_k^T+R_k)^{-1} \quad (1.15)$$

A priori state estimation: $\hat{x}_k^- = F_{k-1}\hat{x}_{k-1}^+ + G_{k-1}u_{k-1}$ (1.16)

A posteriori state estimation: $\hat{x}_k^+ = \hat{x}_k^- + K_k(y_k - H_k\hat{x}_k^-)$

$$P_k^- = (I - K_k H_k)P_k^-(I - K_k H_k)^T + K_k R_k K_k^T \quad (1.17)$$

Both the initial Luenberger observer and Kalman filter are designed for linear system. Extension of both observers to nonlinear system were also developed, which are called extended Luenberger observer and extended Kalman filter. Other type of nonlinear Kalman filter includes unscented Kalman filter. Successful application of Kalman filter is based on the following conditions: knowledge of mean and correlation of the noise at each time instant, knowledge of noise covariance, and knowledge of system model matrices.

Design of other linear observers

Besides the basic Luenberger observer and Kalman filter, researchers have developed different observers for a variety of systems for process monitoring and fault detection. Especially for certain systems with process disturbance and model-plant mismatch, design of observers for state estimation remains a challenge. Some other observers include: modified disturbance observer, Bode-ideal-cut-off observer, and sliding mode observers.[33] Adaptive state observer and backstepping observers are also developed based on basic idea of the Luenberger observer.

Linear observers were developed basing on linear process models, which are usually first principle models. However, most of the chemical process is highly nonlinear. Nonlinear observers were later developed to deal with the process

nonlinearity. One important consideration for designing an observer is the observability condition. Observability means for a system that all the initial condition is observable and its states can be estimated by its outputs. The first step to design an observer is to check the observability. There are many discussions in the literature on the observability and detectability of a process.[34–36]

The estimated states from an observer are usually the ones that are difficult to measure in a real-time manner. These are important states that need to be obtained for process monitoring. Validation between the state estimation and measurement is compared to test the efficiency of the observer. A whole design process for model-based observer is demonstrated in Figure I.2. Hybrid observers combine the design concept of different observers, which can be applied for more complex systems.

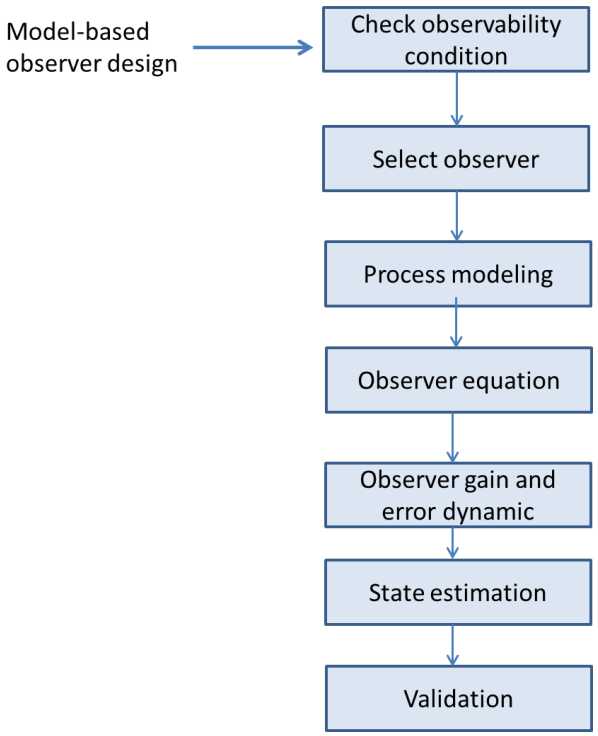

Figure I.2. Concept of design of model-based observer

Some reduced-order observer, low-order observer, high-gain observer, and asymptotic observer have been designed for chemical process systems with ordinary differential equation models. Certain observers are designed to estimate the state information in presence of faults and disturbance including disturbance observer, perturbation observer, equivalent input observer, uncertainty and disturbance estimator, generalized proportional integral observer, and unknown input observer. Unknown input observer and extended state observer are the two most extensively studied and applied observers.

Researchers have developed different disturbance and fault detection observers for estimation of disturbance and states. Wei et al. developed disturbance observer-based

disturbance attenuation control for a class of stochastic systems with multiple disturbances.[37] Chen et al. applied disturbance observer-based control system for a process with time-varying parameters and time delays.[38] Stobart et al. developed a robust uncertainty and disturbance estimator-based control strategy for uncertain linear time-invariant systems with state delays.[39] Zhong and Rees proposed an effective uncertainty and disturbance estimator for linear systems with uncertainties and disturbances.[40] Li et al. proposed an extended state observer-based control method for non-integral-chain systems with mismatched uncertainties. [41]

Generally, the observers for system with disturbance and uncertainties use a feedback design. A brief introduction of observer design for state estimation under disturbance is illustrated in the following section.

A concept of disturbance observer in frequency domain is illustrated in Figure I.3.[33,42] μ is the control input and $\bar{y}$ is the measured output, $G_n(s)$ is the nominal model used for control design, and $Q(s)$ is a stable filter. d_l is the lumped disturbance and $\hat{d}_l$ is the estimated lumped disturbance.

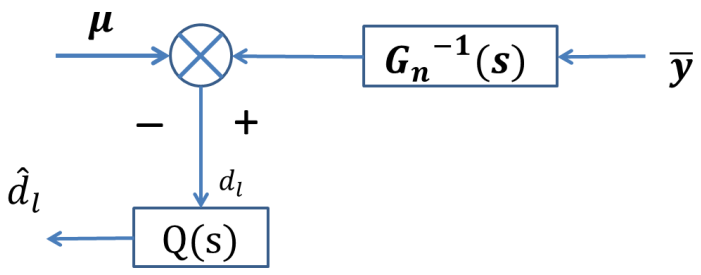

Figure I.3. Concept of disturbance observer in frequency domain

For a frequency domain disturbance observer design, the 'lumped disturbance' in the figure can be written as the following equation.

$$d_l(s)=\left[G(s)^{-1}-G_n(s)^{-1}\right]y(s)+d(s)-G_n(s)n(s) \quad (1.18)$$

where *G(s)* is the physical system and *d(s)* is the external disturbance. *n(s)* is the measurement noise. d_l captures all the system disturbance and uncertainty influence. The estimated lumped disturbance is obtained by passing a filter *Q(s)*, which is given in the following equation.[24,33]

$$\hat{d}_l(s)=G_{u\hat{d}}(s)u(s)+G_{y\hat{d}}(s)\bar{y}(s) \quad (1.19)$$

As one of the observes that can estimate both disturbance and states, extended state observer require less plant information than disturbance observer and unknown input observer.[41,43] As an example, extended state observer design for a single input single output system with disturbance is shown in the following equation.

$$y^{(n)}(t)=f\left(y(t),\dot{y}(t),\ldots,y^{(n-1)}(t),d(t),t\right)+bu(t) \quad (1.20)$$

where $y^{(l)}$ is the l^{th} derivative of the output *y*. *u* and *d* denote the input and disturbance. Let $x_1=y$, $x_2=\dot{y},\ldots,$ $x_n=y^{(n-1)}$, the following equation can be obtained.

$$\dot{x}_i=x_{i+1},\ i=1,\ldots,n-1 \quad (1.21)$$

$$\dot{x}_n=f\left(x_1,x_{2,\ldots}x_{n,},d,t\right)+bu \quad (1.22)$$

The state can be written as:

$$x_{n+1}=f(x_1,x_2,\ldots,x_n,d,t)$$

$$\dot{x}_{n+1}=h(t) \quad (1.23)$$

with $h(t)=\dot{f}(x_1,x_{2,\ldots}x_{n,},d,t)$

Extended state observer is designed to estimate all of the states and lumped disturbance term in the following equation.

$$\dot{\hat{x}}_i=\hat{x}_{i+1}+\beta_i\left(y-\hat{x}_i\right),\ i=1,\ldots,n \tag{1.24}$$

$$\dot{\hat{x}}_{i+1}=\beta_{n+1}(y-\hat{x}_1) \tag{1.25}$$

The extended state observer estimate unmolded dynamics and uncertainty as well as external disturbance. The extended state observer requires minimum information about a dynamic system. Different extensions of extended state observer have been developed. [44–46]

Unknown input observer is developed to deal with the system uncertainty and disturbance. There have been various developments of unknown input observer with different meanings.[47–50] For fault diagnosis and isolation, the unknown input observer is to estimate the fault which does not depends on unknown inputs. A typical unknown input observer is demonstrated in the following equations.

For a linear system:

$$\dot{x}=Ax+B_u u+B_d d \tag{1.26}$$

$$y=Cx \tag{1.27}$$

Unknown input observer estimate both state and disturbance. The observer can be designed to estimate both the state and disturbance simultaneously, as shown in the following equation:

$$\dot{\hat{x}}=A\hat{x}+B_u u+L_x\left(y-\hat{y}\right)+B_d\hat{d} \tag{1.28}$$

$$\hat{y}=C\hat{x} \tag{1.29}$$

where $\hat{x}$, L_x, and $\hat{d}$ are the estimates of the state, observer gain, and disturbance. In design of an observer, the observer gain is calculated so that the estimation error is stable.

Uncertainty and disturbance estimator is developed to estimate state in time delay system such as traffic network and chemical process.[51] It does not require assumptions about the uncertainty except its bandwidth. A basic design idea is illustrated in the following equation:

$$\dot{x}=Ax+B_u u+\Delta Ax+\Delta Bu+d \tag{1.30}$$

The lumped disturbance is described as the following:

$$d_l=\Delta Ax+\Delta Bu+d \tag{1.31}$$

It can be written as $d_l=\dot{x}- Ax-B_u u$.

Due to the absence of $\dot{x}$, d_l can be estimated by approximation through a filter by $\hat{d}_l=d_l \otimes q$, where $\otimes$ and q represent the convolution operator and impulse response of the filter.

Besides the above mentioned observers, generalized proportional integral observer is an enhanced version of disturbance estimator for time-varying disturbance. The generalized proportional integral observer is designed as the following.

$$\dot{\hat{x}}_i=\hat{x}_{i+1}+\beta_i\left(y-\hat{x}_1\right),\ i=1,\ldots,\ n-1$$

$$\dot{\hat{x}}_n=bu+\hat{\xi}_1+\beta_n(y-\hat{x}_1)$$

$$\dot{\hat{\xi}}_i=\hat{\xi}_{i+1}+\lambda_i\left(y-\hat{x}_1\right),\ i=1,\ldots,q-1$$

$$\dot{\hat{\xi}}_q=\lambda_q(y-\hat{x}_1) \tag{1.32}$$

where $\hat{x}_i$ is the estimate of the state x_i. $\hat{\xi}_i$ is the estimate of the lumped distribution term. The stability of estimation error is achieved by choosing observer gains β_i and λ_i.

Applications of disturbance and fault detection observer for bioreactor have been demonstrated using simulation or experimental validation. Rocha-Cózatl and Vouwer applied a linear quasi-unknown input observer to estimate concentrations, flow rates, and light intensity in phytoplanktonic cultures in the chemostat. The authors linearize the nonlinear process model at chemostat to apply the linear quasi-unknown input observer.[52] Lemesle and Gouzé developed bounded error observers for partially known bioreactor models. The hybrid bounded observers incorporate high gain observer and asymptotic observer to improve the error convergence rate depending on the knowledge of the model. Simulation study of a bioreactor model is provided.[53] Moisan et al. extended the bounded error observers to further improve the convergence properties. The extension use parallel internal observers to determine the inner envelop of the process.[54] Farze et al. propose an adaptive high gain observer for state and parameter estimation for a class of uniformly observable nonlinear systems with nonlinear parametrization and sampled outputs.[55] Ghanmi et al. extended Farze's work on an adaptive observer for state and parameter estimation of a nonlinear system basing on a high gain adaptive observer. Simulation study is applied to a bioreactor model.[56] Kravaris et al. proposed a systematic framework of nonlinear observer design to estimate process state variables and unknown process or sensor disturbances. Simulation study was performed using a bioreactor model.[22]

Design of nonlinear observers

Nonlinear observers have been studied for years due to the inherent nonlinearity of the chemical processes.[19,57,58] For the most common Kalman filter, nonlinear forms have been developed such as extended Kalman filter and unscented Kalman filter. There are several types of nonlinearity that have been well studied. A control-affine system is shown in the following equation:

$$f(x,u)=f_0(x)+g(x)u \tag{1.33}$$

Additive output nonlinearity is also well studied which is shown in the following equation:

$$\dot{x}=Ax+\varphi(Cx,u)$$

$$y=Cx \tag{1.34}$$

A nonlinear observer design for the system is proposed. If (A, C) is observable, an observer can be designed in the following format.

$$\dot{\hat{x}}=A\hat{x}+\varphi(y,u)-K(C\hat{x}-y) \tag{1.35}$$

K is calculated so that *(A-KC)* is stable.

For certain type of nonlinear systems, transformation-based design can be applied. Appropriate transformation can be done such as changes of states coordinates to estimate state information. A system described in the following equation:

$$\dot{x}=f(x,u)=f_u(x),\ x\in R^n,\ u\in R^m$$

$$y=h(x)\in R^p \tag{1.36}$$

is said to be equivalent to the system:

$$\dot{z}=F(z,u)=F_u(z)$$

$y=H(z)$ (1.37)

If there exists a diffeomorphism $z = \Phi(x)$ such that

$\forall u \in \mathbb{R}^m$, $\frac{\partial \Phi}{\partial x} f_u(x)_{|x=\Phi^{-1}(z)} = F_u(z)$ and $h \circ \Phi^{-1} = H$.

Another development for transformation-based observer design is immersion transformation. Immersion transformation for state estimation is to immerse the state space into a larger dimension space. The idea is demonstrated using a linear system.

$\dot{x}=-x+u$

$y=x+v$ (1.38)

where v is constant unknown measurement bias. Immersion of the system will include the bias term, which a second order system can be obtained.

$\dot{x}_1=-x_1+u$

$\dot{x}_2=0$

$y=x_1+x_2$ (1.39)

Definition of 'Immersion' is summarized in the reference and cited here[59]: '*an application $\tau: M \rightarrow M'$ is an immersion if its rank is $n=\dim M$ everywhere. If τ is an injective immersion, then it establishes a one-to-one correspondence of M and the subset $M''=\tau(M)$ of M'.*

Immersion of dynamical system: Consider two C^∞ system $S=(M, f_u, h)$ and $S'=(M', f_u', h')$ such that every input that is admissible for one of them is also admissible for the other. The system S is immersible into system S' if there exists a C^∞ map, $\tau: M \rightarrow M'$, such that:

1) for every pair $(x^{\circ}, x^{\bullet}) \in M \times M, h(x^{\circ}) \neq h(x^{\bullet}) implies\ h'(\tau(x^{\circ})) \neq h'(\tau(x^{\bullet}))$

2) for every pair (x,u)*, the domain of definition of* $y'_{\tau(x),u}$ *include the domain of definition of* $y_{x,u}$ *and on the intersection of their domains,* $y_{x,u}$ *and* $y'_{\tau(x),u}$ *coincide*.'

For observer design of other nonlinear systems, empirical observers are commonly used. The empirical observers approximate the nonlinear system for approximation of a theoretical best estimation such as extended Kalman filter. Although the extended Kalman filter losses global convergence while Kalman filer does. Other empirical observers include neural network, fuzzy logic, and genetic algorithm. Other studies have used Duncan-Mortensen-ZakaÏ equation to approximate the exact solution, which are used for stochastic problems. Such as a following stochastic system like the following:

$$dX(t)=f(X(t),u)dt+Q^{1/2}dW(t)$$

$$dY(t)=h(X(t),u)dt+R^{1/2}dV(t) \quad (1.40)$$

where $(t) \in \mathbb{R}^n, Y(t) \in \mathbb{R}^P$, nd $u \in \mathbb{R}^d$. W(t) and V(t) are two independent Wiener processes with

$$E\left[(Q^{1/2}W(t)(Q^{1/2}W(t)^{'}\right]=Q.t \quad (1.41)$$

where *Q* and *R* are the covariance matrix of the state noise and measurement noise. The explicit steps for applying Duncan-Mortensen-ZakaÏ equation are not demonstrated in this chapter. However, to briefly summarize the steps, two different methods are generally used. The first method is to simply the equations and linear and nonlinear

solutions can be applied. The second application is to use Monte-Carlo methods to solve the Duncan-Mortensen-ZakaÏ equation.

Optimization-based state estimation

Another type of nonlinear observer is nonlinear moving horizon observers.[20] Different from the analytic observers such as Kalman filter, optimization based observers apply the definition of observability to estimate the state. Optimization-based state observer searches for a minimal objective function $J(t,\zeta)$ which is the squared output prediction error over certain observation horizon to estimate state information. The advantages of optimization-based nonlinear observers include handling constraints and independence of the system model. Convergence is an important concern for optimization-based state estimation. There is no general algorithm to guarantee convergence for non-convex optimization problems. Real-time implement ability is another difficulty for optimization-based nonlinear observer. The time required for searching a minimal objective function may exceed the time available for control action.

For a system such as the following:

$$x(t)=F(t,t_0,x_0)$$

$$y(t)=h(t,x(t)) \qquad (1.42)$$

where $F: \mathbb{R}_+ \times \mathbb{R}_+ \times \mathbb{R}^n \to \mathbb{R}^n$ is a mapping function for state $x(t)$ based on the knowledge of the state $x(t_0)=x_0$. $y(t)$ is the output measurement at instant t.

An optimization-based observer with observation horizon $T = N\tau_s$ is shown as follows:

$$\hat{x}(t_k)=X(t_k,t_{k-N},\hat{\xi}(t_k))$$

$$\hat{\xi}(t_k) = \arg \min_{\xi \in X(t_{k-N})} [J(t_k,\xi)] := \sum_{i=k-N}^{k} \left\| y(t_i) - Y(t_i, t_{k-N}, \xi) \right\|^2_{Q_i(k)} \quad (1.43)$$

$Q_i(k) \in \mathbb{R}^{n_y \times n_y}$ is defined as a positive definite weighting matrix.

Differential form of moving horizon observers can be designed basing on a process model of ordinary differential equation.

$$\dot{x}(t) = f(t, x(t)) \quad (1.44)$$

$$y(t) = h(t, x(t)) \quad (1.45)$$

The cost function for differential form of receding-horizon estimation is given by the following:

$$J(t,\xi) = \int_{t-T}^{t} \left\| Y(\tau, t-T, \xi) - y(\tau) \right\|^2 d\tau \quad (1.46)$$

The differential form of the moving horizon estimation uses a gradient-based optimization method. However, existence of all the partial derivatives of the cost function needs to be guaranteed.

Optimization-based approaches have been developed to solve the nonlinear state estimation problem. Specially, the optimization can solve problem with state and parameter constraints.

Dual estimation of state and parameter

In some systems, the process model parameters are subject to certain uncertainty. These uncertainties either come from process disturbance or model uncertainty. With unknown process parameters, the observer is unable to give accurate state estimation. The concept of adaptive observer is developed to converge the observer estimation in the

presence of unknown parameters. In some cases, the process parameters and process state are estimated together, which is called joint parameter and state estimation.

Some research results show that adaptive state estimation is possible under 'passivity-like' condition. The unknown parameter is treated as inputs in the system. The definition of 'Passivity' is given in the reference and cited here:[59,60]

'*A system* $\dot{\xi}=f(\xi,u)$, $y=h(\xi,u)$ *is strictly state passive if there exists a storage function (positive semi-definite) V and a positive definite function* γ *such that*

$$u^T y \geq \frac{\partial V}{\partial x} f(x,u) + \gamma(x) \tag{1.47}$$

Adaptive state estimation with a linear unknown input parameter vector θ *can be written as the following.'*

$$\dot{x}(t)=f\big(y(t),z(t),v(t)\big)+g(y(t),z(t),v(t))\theta$$

$$y(t)=(I_p\ 0)x(t) \tag{1.48}$$

with $x(t)=\begin{pmatrix} y(t) \\ z(t) \end{pmatrix} \in \mathbb{R}^n, y(t) \in \mathbb{R}^n, v(t) \in \mathbb{R}^m, \theta \in \mathbb{R}^q$

Available theory about design of adaptive observers is given in the reference and summarized below.[59] *'For a system with a state estimation have a known parameter*(θ)*, a Lyapunov function V for* $\hat{x}_\theta$*-x: if* $\frac{\partial V}{\partial e} g(y,\sigma,v)=\varphi\big(\big[I_p\ 0\big]e,y,\sigma,v\big)$ *for function* φ *with g globally bounded, and f and g globally Lipschitz w.r.t. z, uniformly w.r.t.(u,y,t), then*

$$\lim_{t\to\infty}\big\|\hat{x}(t)-x(t)\big\|=0 \quad \text{when} \quad \dot{\hat{\theta}}=-\Lambda\varphi^T\big(\hat{y}-y,y,\hat{z},v\big),\ \Lambda>0 \tag{1.49}$$

if g is persistently exciting and $g^{\cdot}$ *is bounded then the following holds:* $\lim_{t\to\infty}\big\|\hat{\theta}(t)-\theta\big\|=0.$'

For joint parameter and state estimation, a method has been proposed and summarized below.[59,61]

'*If a system can be turned by a change of coordinates which may depends on time and parameters* $z=\Phi(x,\theta,t)$ *with* $x=\Psi(z,\theta,t)$ *bounded w.r.t. t*

$$\dot{z}=Z(z,y,u,t)$$

$$y=H(z,u,t)+D(z,u,t)\theta, \quad y \in \mathbb{R}^p, z \in \mathbb{R}^n, u \in \mathbb{R}^m, \theta \in \mathbb{R}^q \tag{1.50}$$

A decrescent positive definite C^1 *function V(t,e) exists, such that for any initial condition and any admissible input u, any* $z, e \in \mathbb{R}^n, y \in \mathbb{R}^p$, *and any* $t \geq 0$, *the following holds.*

$$\frac{\partial V}{\partial t}(t,e)+\frac{\partial V}{\partial e}\left[Z(e+z,y,u(t),t)-Z(z,y,u(t),t)\right] \leq -\gamma(e) \tag{1.51}$$

The following equation holds for any admissible input u and trajectories z(t). D is persistently exciting and uniformly bounded by some d, with

$$\left\|D(e+z,u(t),t)-D(z,u(t),t)\right\| \leq \gamma_D\sqrt{\gamma(e)}$$

$$\left\|H(e+z,u(t),t)-H(z,u(t),t)\right\| \leq \gamma_H\sqrt{r(e)} \tag{1.52}$$

for any e, z, and some $\gamma_D, \gamma_H > 0$, *then an adaptive observer for estimation of both state x and parameter* θ *simultaneously can be designed in the following format:'*

$$\dot{\hat{z}}=Z(\hat{z},y,u,t)$$

$$\dot{\hat{\theta}}=-\lambda D^T(\hat{z},u,t)\left(D(\hat{z},u,t)\hat{\theta}+H(\hat{z},u,t)-y\right), \lambda>0$$

$$\hat{x}=\Psi(\hat{z},\hat{\theta},t) \tag{1.53}$$

The proof is to build error equations and establish Lyapunov function, which is given in their original research paper.

Scope and objective of this dissertation

To estimate the state under process disturbance for fault detection or process control is a challenging task for some complicated process. Data-based process monitoring technique can effectively monitor the process basing on a large volume of previous operation data. Model-based process monitoring technique can be applied into different operating situations. Accurate process model of a nonlinear system is required for model-based process monitoring. However, certain unmodeled disturbance will cause the model-plant mismatch and drift the model prediction from experiment measurements. In this dissertation, model-based state estimation technique is studied. Two different case studies are performed. The first case studies the leak location estimation from a natural gas pipeline. State information which is flow rate in a natural gas flow case is estimated. This model-based state estimation is aimed to estimate leak location from a natural gas pipeline under different conditions. Different situations can make the state estimation difficult which are discussed in each chapter. These situations include the parameter mismatch in a model, disturbance from environment or operation, and multiple leaks case. For each situation, different state estimation methods need to be developed. Due to the complexity of the natural gas flow model, certain simplification methods need to be developed.

Besides the fault detection, advanced process control is another important application for state estimation. For certain biological systems, accurate process model is difficult to obtain due to the inherent uncertainty in the biology system. However, model-based advanced process control technique has great potential to increase the

productivity of the process. A methodology which can accurate estimate the state will be great beneficial for the advanced process control algorithm. An online state estimation technique is required to estimate the state in a bioreactor efficiently.

The specific objectives of the dissertation are:

1. To model the natural gas flow process in a straight pipeline, considering the effect of thermal properties such as natural gas inlet temperature, ground temperature, and heat transfer coefficient.

2. To study the effect of thermal properties using simulation.

3. To design an online state estimation technique for non-isothermal natural gas flow model in presence of parameter mismatch.

4. To estimate the state information of a natural gas pipeline under disturbance from temperature change and operation pressure change.

5. To develop leak detection and location estimation method for subsequent multiple leaks and simultaneous multiple leaks.

6. To design estimation method for state estimation for a bioreactor under unknown disturbance.

Contribution of this dissertation

In this dissertation, research results have the following contributions in the area of process modeling, optimization, and state estimation.

1. Developed a first principle non-isothermal natural gas process model considering leak event in a pipeline. Effect of leak on temperature profile and parameter change is studied using simulation.

2. Applied an efficient state and parameter dual estimation techniques to estimate the parameter and flow rate from a natural gas pipeline.

3. Modified a previous design of linear unknown input observer.

4. Developed a model reduction process to simplify the non-isothermal natural gas flow model for the unknown input observer.

5. Proposed a global optimization algorithm with partial differential equation and linear constraints and continuous and integer variables for location estimation of multiple leaks.

6. Designed a nonlinear unknown input observer to estimate the state in a bioreactor.

Organization of this dissertation

The thesis is organized as the following. Chapter II demonstrates non-isothermal natural gas flow models and studies the effect of leak and thermal properties. Dual state and parameter estimation for leak detection in a natural gas pipeline is proposed and compared with extended Kalman filter. Chapter III shows the model reduction of the non-isothermal flow model and modifies an existing unknown input observer for the natural gas pipeline. Effect of process disturbance such as temperature change and inlet pressure change is studied. The effect of process disturbance on state estimation from the unknown input observer is also studied. Chapter IV extends the linear unknown input observer design to detect and locate multiple subsequent leaks. An optimization-based state estimation for multiple simultaneous leaks identification is also proposed which contain partial differential equation constrains, linear constraints, integer variables, and

continuous variables. Chapter V develops a nonlinear unknown input observer and sufficient and necessary conditions are provided. Application of the nonlinear unknown input observer is provided using a bioreactor. Experimental validation using both batch and fed-batch experiments is performed.

CHAPTER II

DUAL UNSCENTED KALMANFILTER FOR NATURAL GAS PIPELINE LEAK DETECTION: NON-ISOTHERMAL MODELING AND EFFECT OF THERMAL PROPERTIES

Introduction

Pipelines are one of the most economical transportation solutions for natural gas and crude oil. However, leakage of the transported material from pipelines can harm the environment and can cause explosions. Over the last twenty years, there have been over two hundred million barrels of chemicals spilled from the pipelines, causing billions of dollars of property damage. Thus, a rapid and reliable leak detection method is urgently needed. Currently, the hardware leak detection method includes acoustic sensor, fiber optic sensor, soil monitoring, ultrasonic flow meter, and vapor monitoring instrumentations. Software methods include mass/volume balance, real time transient modeling, and statistical approaches such as Pressure Point Analysis (PPA).[62]

Different from the hardware methods, which are based on measuring the physical property change of the fluid and/or pipeline such as acoustic noise, electrical properties, and temperature change, the software methods are based on the conservation of mass, momentum, and energy with accurate flow rate and pressure measurements at the inlet/outlet of the pipeline. Some software methods have been commercialized for pipeline leak detection such as The Real-Time Transient method, mass balance-based method and Pressure Point Analysis.[63] However, the Real-Time Transient Method

requires extensive instrumentations for thermal measurements and Pressure Point Analysis can't estimate the leak location accurately.[62,64,65]

Model-based fault detection methods have been studied for decades.[6667] Unlike methods based on statistical analysis of measurements, model-based methods use dynamic models to estimate the key information of the process, which are the states of the process. To monitor the process, state estimations from the model-based estimation techniques are compared with measurements from the system. Process faults are identified if the difference between the estimated states and measurements exceeds a preset threshold. The state information of the pipeline system is defined as the flow rate of the pipeline. To estimate the flow rate in a pipeline, modeling and simulation of the natural gas flow in pipelines have been extensively studied.[68–73] A variety of simulation methods have been proposed considering the non-isothermal circumstance and pipeline networks.[74–76] However, the effect of leaks on the gas flow profile has not been studied yet. In this study, a leak term is incorporated into the non-isothermal modeling, and its effect on pressure, flow rate, and temperature is studied.

In order to apply the model-based fault detection method to detect leaks in a pipeline, the state information, which is the flow rate in the pipeline, is estimated at the nominal condition by simulation. To detect leak locations in a pipeline, a comparison between state (flow rate) measurement and estimation from the model-based estimation is performed. State estimation is based on the boundary pressure measurements. Due to the existence of the process noise, filtering techniques are required to obtain an accurate estimation of the state. Currently, there is a variety of options of filtering techniques for

state estimation at nominal conditions. Kalman filter is an optimal observer for the linear Gaussian case. For the non-linear process, filters such as extended Kalman filter, moving horizon estimator, unscented Kalman filter, and particle filter can be used.

The extended Kalman filter linearizes the non-linear model and applies the Kalman filter. For the nonlinear process and non-Gaussian disturbances, a moving horizon estimator solves an optimization problem over a moving horizon of the past measurements. H∞ filter provides a more rigorous method for model uncertainty and unmodeled noise and dynamics. An unscented Kalman filter is a nonlinear state estimator especially for a nonlinear system with high degree of nonlinearity and where the Jacobian matrix is not available.[77–79] A particle filter has more estimation accuracy for the nonlinear system than unscented Kalman filter, while requiring more computational effort.

Filter-based leak detection methods for natural gas pipelines using dynamic models were studied by Benkherouf and Allidina, who used extended Kalman filter for simultaneous state and parameter estimation.[80] Liu et al. improved the accuracy of the estimation using adaptive particle filter to estimate the leak location,[81] and Emara-Shabaik et al. applied a modified extended Kalman filter for leak estimation.[82] Hauge et al. designed an adaptive Luenberger observer for monitoring oil and gas pipelines for leak detection.[83] Model-based leak detection methods for water pipeline have also been developed.[84]

Model-based state estimation depends on a reliable model. All the models used in the above-mentioned research were under an isothermal assumption with fixed

parameters. However, these ideal and simplified models cannot study the effect of the thermal properties of the environment and the transported material through the pipeline. The ideal-gas assumption in the reported modeling efforts neglected the change of gas compressibility under different pressures and temperatures in the pipeline. Reddy et al. proposed a state estimator for leak detection based on the transfer function.[76] However, the effect of change of thermal properties on the flow was not studied. Of particular interests are the changes of the flow rate due to thermal properties, which are crucial for estimation of the location of the leak, as well as the temperature profile along the pipeline and its change when a leak occurs. In this paper, we developed non-isothermal equations of the gas flow in the pipeline with leak occurrence. Various thermal properties such as the ground temperature, heat transfer coefficient, gas compressibility, and inlet gas temperature were considered. According to the equations, the effect of thermal properties were simulated and studied with and without leak occurrence.

Besides measuring all the thermal-related parameters in the models, the parameters corresponding to thermal properties can also be estimated using parameter estimation techniques. To estimate the effect of thermal properties without measuring the thermal property for leak detection, a dual unscented Kalman filter (DUKF) was applied under process and measurement noise to estimate the state (flow rate). The dual unscented Kalman filter is a technique which combines parameter estimation and state estimation. The filter takes pressure measurements at the boundaries of the pipeline and estimates the flow rate. The estimation and measurement of flow rates are compared to determine a leak location. During the application of the dual unscented Kalman filter, the

parameter corresponding to the thermal properties in the isothermal model, which is subjected to change according to different thermal conditions was estimated and demonstrated in the results section. Estimation from a filter is compared with the measurements of the flow rate to detect a leak incident. Extended Kalman filter and unscented Kalman filter were applied and compared on isothermal model and non-isothermal model to estimate the flow rate.

Modeling of the non-isothermal natural gas flow

Natural gas pipeline modeling

A pipeline is the most widely applied mode of transportation for natural gas. Gas flow in the pipeline is driven by compression pumps. In this paper, we describe the one-dimensional gas flow dynamic through a gas duct, which was obtained by applying the conservation of mass, moment, and energy to derive the equations. The composition of natural gas is assumed as 95% methane, 2.5% ethane, 1.6% nitrogen, 0.7% carbon dioxide, and 0.2% propane. The pressure heat capacity (C_P) is assumed to be constant at 2170 (J/kg K). The pipeline is 100 km in length (L = 100 km), and 0.6 m in diameter (D = 0.6 m). Heat transfer coefficient along the pipeline is assumed to be uniform. The inlet pressure (P_{in}) is 50 bar, and the outlet pressure (P_{out}) is 40 bar. The flow rate, pressure, and temperature across the pipeline cross-section were assumed to be constant as the flow is highly turbulent.[85] The derivations of the natural gas flow model were based on the mass balance, momentum balance, and energy balance equations, which are shown in the Appendix. The following model equations were used, in which 'x' stands for the location in a pipeline and '*t*' refers to time. The modeling equations are:

The continuity balance equation: $\frac{\partial \rho v}{\partial x}+\frac{\partial \rho}{\partial t}+\frac{q_L}{A\Delta x}=0$ (2.1)

The momentum balance equation:

$$\frac{\partial(\rho v)}{\partial t}+\frac{\partial \rho v\cdot v}{\partial x}+\frac{\partial P}{\partial x}+\frac{q_L\cdot v}{A\Delta x}=-\rho g\sin\theta-\frac{fq^2}{2DA^2P}ZRT \quad (2.2)$$

The energy balance equation:

$$\rho\frac{\partial H}{\partial t}+\rho v\frac{\partial H}{\partial x}-v\frac{\partial P}{\partial x}-\frac{\partial P}{\partial t}=\frac{\rho f v^3}{2D}-\frac{4U(T-T_g)}{D} \quad (2.3)$$

Equation of state: $\frac{P}{\rho}=ZRT$ (2.4)

In the above equations, q_L is the leak mass flow rate in the pipeline, f is the friction factor, and θ is the inclined angle between the pipeline and the ground, which is set as zero here. A is the cross sectional area of the pipeline, and $q=\rho vA$ is the mass flow rate. Z is the compressibility factor which is a function of P and T. H is the enthalpy of natural gas and its derivate can be written as $dH=C_P dT+\left\{\frac{T}{\rho}\left(\frac{\partial \rho}{\partial T}\right)_P+1\right\}\frac{dP}{\rho}$. U is the overall heat transfer coefficient between the pipeline and environment and T_g is the ground temperature, which is assumed to be uniform along the pipeline.

The above equations were rearranged as follows:

$$\frac{\partial P}{\partial t}=\frac{-\frac{1}{A}\frac{\partial q}{\partial x}-\frac{1}{A\Delta x}q_L+\left(\frac{1}{ZC_P}\frac{\partial Z}{\partial T}+\frac{1}{TC_P}\right)\left(\frac{fq^3z^2R^2T^2}{2DA^3P^2}-\frac{4U(T-T_g)}{D}-\frac{q}{A}C_P\frac{dT}{dx}+\left(\frac{T}{Z}\frac{\partial Z}{\partial T}+1\right)\frac{q}{AP}ZRT\frac{dP}{dx}\right)}{\left(\frac{1}{ZRT}-\frac{P}{Z^2RT}\frac{\partial Z}{\partial P}\right)\left(\frac{\partial Z}{\partial T}\right)^2\frac{T}{Z^2C_P}-\frac{2}{ZC_P}\frac{\partial Z}{\partial T}-\frac{1}{TC_P}} \quad (2.5)$$

$$\frac{\partial q}{\partial t}=-A\frac{\partial P}{\partial x}-\frac{AP}{ZRT}g\sin\theta-\frac{fq^2}{2DAP}ZRT-\frac{1}{A}\frac{q_L}{\Delta x}\left(\frac{q}{P}\right)ZRT \quad (2.6)$$

$$\frac{\partial T}{\partial t}=\frac{\left(\frac{1}{ZRT}-\frac{P}{Z^2RT}\frac{\partial Z}{\partial P}\right)\frac{\partial P}{\partial t}}{\left(\frac{P}{Z^2RT}\frac{\partial Z}{\partial T}+\frac{P}{ZRT^2}\right)}+\frac{\frac{1}{A}\frac{\partial q}{\partial x}}{\left(\frac{P}{Z^2RT}\frac{\partial Z}{\partial T}+\frac{P}{ZRT^2}\right)}+\frac{q_L}{A\Delta x}\frac{1}{\left(\frac{P}{Z^2RT}\frac{\partial Z}{\partial T}+\frac{P}{ZRT^2}\right)} \quad (2.7)$$

In these equations, the compressibility of the natural gas (Z) and its derivatives $(\frac{\partial Z}{\partial P}, \frac{\partial Z}{\partial T})$ were calculated based on the equation proposed by Dranchuck and Abou-Kassem.[86]

For the purpose of comparison, the isothermal models use constant compressibility, in which $\frac{P}{\rho} = c^2$. (2.8)

$|q|$ is used to ensure the positive value of the flow rate in the model development. Equations for the isothermal models are:

$$\frac{\partial P}{\partial t} + \frac{c^2}{A}\frac{\partial q}{\partial x} + \frac{c^2}{A\Delta x} q_L = 0 \quad (2.9)$$

$$\frac{\partial q}{\partial t} + A\frac{\partial P}{\partial x} + \frac{fc^2 q|q|}{2DAP} + \frac{c^2}{A\Delta x}\left(\frac{q}{p}\right) q_L = 0 \quad (2.10)$$

$$\frac{\partial T}{\partial t} = 0 \quad (2.11)$$

In the results and discussion section, isothermal models will be used for parameter estimation.

Extended Kalman filter & unscented Kalman filter

A Kalman filter is an optimal state and parameter estimator for inaccurate and uncertain observations, such as the presence of process noise and measurement noise. It minimizes the mean square error of the estimated states (or parameters). For nonlinear system, an extended Kalman filter can be used by linearizing the nonlinear functions using Tylor series expansion. Unscented Kalman filter is another estimation method for nonlinear systems, which does not require linearization. The difference between extended Kalman filter and unscented Kalman filter was discussed in the reference.[77,78,87]

A continuous extended Kalman filter has the following mathematical description. Consider a nonlinear system:

$$x_{k+1}=f_k(x_k)+w$$

$$y_k=Cx+v \tag{2.12}$$

where w and v are Gaussian white noises with covariance matrices Q_k and R_k.

The extended Kalman filter design for the linearized system around the current estimate of the state is the following:

$$\hat{x}_{k+1|k+1}=f_k(x_{k|k})+K_{k+1}(y_{k+1}-C\hat{x}_{k+1|k}); \tag{2.13}$$

$$K_{k+1}=P_{k+1|k}C^T[CP_{k+1|k}C^T+R_{k+1}]^{-1};\quad P_{k+1|k}=F_kP_{k|k}F_k^T+Q_k$$

$$P_{k+1|k+1}=[I-K_{k+1}C]P_{k+1|k}$$

where F_k is the Jacobian matrices of $f(.)$ and K is the Kalman filter gain. $P_{k+1|k}$ is the a *priori* estimate of the error covariance matrix and $P_{k+1|k+1}$ is the a *posteriori* estimate of the error covariance matrix.

In an unscented Kalman filter, a set of sigma points is selected deterministically to represent the statistical properties of a random variable/function. Assuming that the mean and the covariance of the Gaussian random variable (GRV) are $\bar{x}$ and P_x, the sigma points, χ_i , are calculated as follows:

$$x_0=\bar{x} \tag{2.14}$$

$$\chi_i=\bar{x}+\sqrt{((L+\lambda))P_x}\ ,\ i=1,\ldots.L\ ;\ \chi_i=\bar{x}-\sqrt{((L+\lambda))P_x}\ ,\ i=L+1,\ldots.2L$$

$$W_0^m = \frac{\lambda}{L+\lambda} \tag{2.15}$$

$$W_0^c = \frac{\lambda}{L+\lambda} + 1 - \alpha^2 + \beta$$

$$W_i^c = W_i^m = \frac{1}{2(L+\lambda)}, \; i = 1, \ldots\ldots 2L \tag{2.16}$$

Here $\lambda = \alpha^2(L+K) - L$ is a scaling parameter. α determines the spread of the sigma points around $\bar{x}$, which is usually set as a small number (it is set as 10^{-3} in our case). α is applied to control the resulting covariance matrix from becoming non-positive semi-definite, which can be case-dependent. β is used to incorporate the prior knowledge of the distribution of X. $\beta = 2$ is optimal for Gaussian distribution, and K is a secondary scaling parameter, which is usually set to 0 or 3-L for Gaussian distribution .The choice of K determines the fourth and higher (even) moments of the sigma point distribution, which will affect the prediction accuracy of the mean and covariance. W_i^c and W_i^c are used in the time prediction equations and measurement update equations. (Equations (2.20) to (2.25)).

A dual unscented Kalman filter is a joint unscented Kalman filter estimation of both state and parameters, which applies for the state estimation in nonlinear systems with parameter uncertainty. DUKF uses two parallel estimators, which sequentially estimates states and parameters. In the state estimator, the parameters are treated as constants for estimating the states; while in the parameter estimator, the previous estimated states are fed to the algorithm as inputs to update the parameters. These two estimators update the states and parameters, recursively. The recursion of a dual unscented Kalman filter is described in the following steps:

Given $\hat{x}_0=E(x_0)$, $P_0=E[(x_0-\hat{x}_0)(x_0-\hat{x}_0)^T]$ (2.17)

Calculate the sigma points:

$$\chi_{k-1}=[\hat{x}_{k-1} \quad \hat{x}_{k-1}+\sqrt{((L+\lambda))P_{k-1}} \quad \hat{x}_{k-1}-\sqrt{((L+\lambda))P_{k-1}}\,] \tag{2.18}$$

The time prediction equations are: $\chi_{k|k-1}=f(\chi_{k-1})$ (2.19)

$$\hat{x}^-_{k|k-1}=\sum_{i=0}^{2L} W_i^m \chi_{i,k|k-1} \tag{2.20}$$

$$P^-_{k|k-1}=\sum_{i=0}^{2L} W_i^c(\chi_{i,k|k-1}-\hat{x}^-_{k|k-1})(\chi_{i,k|k-1}-\hat{x}^-_{k|k-1})^T+Q \tag{2.21}$$

$$Y_{k|k-1}=h(\chi_{k|k-1}) \tag{2.22}$$

$$\hat{y}^-_{k|k-1}=\sum_{i=0}^{2L} W_i^m Y_{i,k|k-1} \tag{2.23}$$

The measurement update equations are:

$$P_{yk}=\sum_{i=0}^{2L} W_i^c \left(Y_{i,k|k-1}-\hat{y}^-_{k|k-1}\right)\left(Y_{i,k|k-1}-\hat{y}^-_{k|k-1}\right)^T+R \tag{2.24}$$

$$P_{x_k y_k}=\sum_{i=0}^{2L} W_i^c(\chi_{k|k-1}-\hat{x}^-_{k|k-1})\left(Y_{i,k|k-1}-\hat{y}^-_{k|k-1}\right)^T \tag{2.25}$$

$$K_k=P_{x_k y_k}P_{yk}^{-1} \tag{2.26}$$

$$\hat{x}_{k|k-1}=\hat{x}^-_{k|k-1}+K_k(y_k-\hat{y}^-_{k|k-1}) \tag{2.27}$$

$$P_k=P^-_{k|k-1}-K_k P_{yk} K_k^T \tag{2.28}$$

where K_k is the Kalman filter gain. P_{yk} is the measurement noise covariance of y_k. $P_{x_k y_k}$ is the noise covariance of y_k and x_k. Q and R are defined in Equation (2.12). The measurement model is an identity mapping with the inlet and outlet pressure as measured variables. x_k represents state x at time k. y_k represents the measurement at time

k. The spatial distribution is represented as follows, e.g, for pressure P at time k and length '0' is P(k,0), pressure P at time 'k' and length 'Δx' is P(k, Δx). Similarly, P at other spatial intervals are: P(k, 2Δx), P(k, 3Δx) … P(k, L). Thus, flow rate and temperature are expressed as q(k,0), q(k, Δx), q(k, 2Δx), … q(k, L), T(k,0), T(k, Δx), T(k, 2Δx), … T(k, L). The states x_k at each node of the pipeline (P, q, and T) are calculated as a vector when applying both extended Kalman filter and an unscented Kalman filter. 'n' is the discretization number of the pipeline. x_k is a vector containing a total number of 3n states.

Both extended Kalman filter and unscented Kalman filter were applied on isothermal and non-isothermal models to compare their capability for accurate estimation of states. The two filters were given the same covariance of process and measurement noise.

Numerical solutions

Many numerical methods have been used to solve gas pipeline models. In our previous work, we have showed that the Method of Line is among the most efficient and accurate methods for solving the hyperbolic-type partial differential equations governing the gas pipeline model.[88] The fixed boundary conditions are set as follows:

$$\frac{\partial P}{\partial t}_{x=0} = 0, \quad \frac{\partial T}{\partial t}_{x=0} = 0, \quad \frac{\partial P}{\partial t}_{x=L} = 0$$

The leak was introduced at the location of 1/4, 1/2, and 3/4 of the pipeline length and with amplitudes of 2%, 5%, and 10% of the total flow rate in the pipeline. For the detection of leak location, both 2% and 5% leaks were used in our simulation results.

Results and discussion

Effect of thermal properties on pressure, flow rate, and temperature distribution of the natural gas in the pipeline

Although most of the previous studies with model-based natural gas pipeline leak detection utilized isothermal models, some research has been done to understand the non-isothermal pipeline flow phenomena, either for steady state or transient state.[89] Osiadacz and Chaczykowski compared the isothermal and non-isothermal pipeline gas flow models.[90] They studied both the steady state and transient state flow dynamics. Chaczykowski derived one-dimensional non-isothermal flow model to study transient behavior of the fluid flow phenomena.[91] Abbaspour and Chapman studied the non-isothermal transient flow in the natural gas pipeline considering the convective inertia term, friction factor changes with Reynolds number, and compressibility factor as a function of the temperature and pressure.[92] However, the non-isothermal modeling of gas flow with a leak in a pipeline and influence of this leak on flow rate and pressure under non-isothermal condition have not been studied yet. The non-isothermal model we derived in this paper was based on the following assumptions: the friction factor and the heat capacity of the natural gas were constant. The ground temperature was constant and not influenced by the leak of gas. Three different inlet temperatures (T_{in}) of 313 K, 343 K, and 373 K were simulated to investigate the effects of inlet temperature on the pipeline parameter variations. Three different ground temperatures (T_g) of 273 K, 289 K, and 303 K were applied. The equations were solved using the Method of Line. Three heat transfer coefficients (U, accounting for heat transfer between the pipeline and

environment), 1.84, 2.84, and 3.84 J/ (m^2 K s) were used representing for fully buried, partially buried, and bare pipeline.[92,93]

The effects of thermal properties such as ground temperature variation, inlet gas temperature change, and heat transfer coefficient variation were studied at steady state. The ground temperature contributes to the heat transfer between the environment and the pipeline. Three different ground temperatures were studied, which account for high, medium, and low environment temperature around the pipeline. Figure II.1 shows the effect of ground temperature on the pressure, flow rate, and temperature profile of natural gas along the pipeline. The inlet temperature was set at 313 K, and the heat transfer coefficient is set as 2.84 J/ (m^2 K s). Figure II.1a shows lower temperature generates a more uniform pressure drop. Figure II.1b shows variations of flow rate at different ground temperatures along the length of the pipeline. The flow rate decreased 3.31% from a total flow rate of 96.4 kg/s when ground temperature increases from 273 K to 303 K. A lower ground temperature increased the mass flow rate by increasing the gas density. Figure II.1b shows different flow rate at different ground temperature at steady state. Figure II.1c shows variations of the temperature along the length of the pipeline due to the different ground temperatures. A significant drop of temperature along the pipeline is observed at a lower ground temperature.

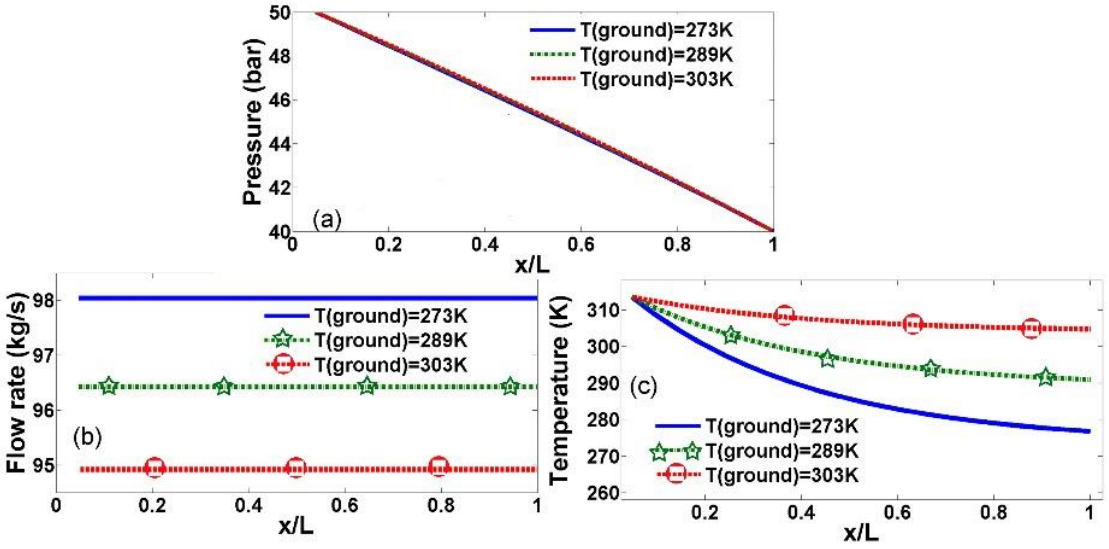

Figure II.1. Effect of ground temperature on pressure, flow rate, and temperature distribution of the pipeline at steady state

Figure II.2 shows the effects of the inlet temperature change on the pressure, flow rate, and temperature distribution. The ground temperature was set up as 289 K, and the heat transfer coefficient used is 2.84 J/ (m2 K s). Higher inlet temperature does not significantly affect the pressure drop profile as shown in Figure II.2a. From Figure II.2b, it can be seen lower inlet temperature increased the flow rate at steady state, generating a 3.44% difference with inlet temperature of 313 K and 375 K of inlet temperature. Inlet temperature fluctuation causes a temperature change over the entire pipeline and a higher inlet temperature increased the overall temperature in the pipeline.

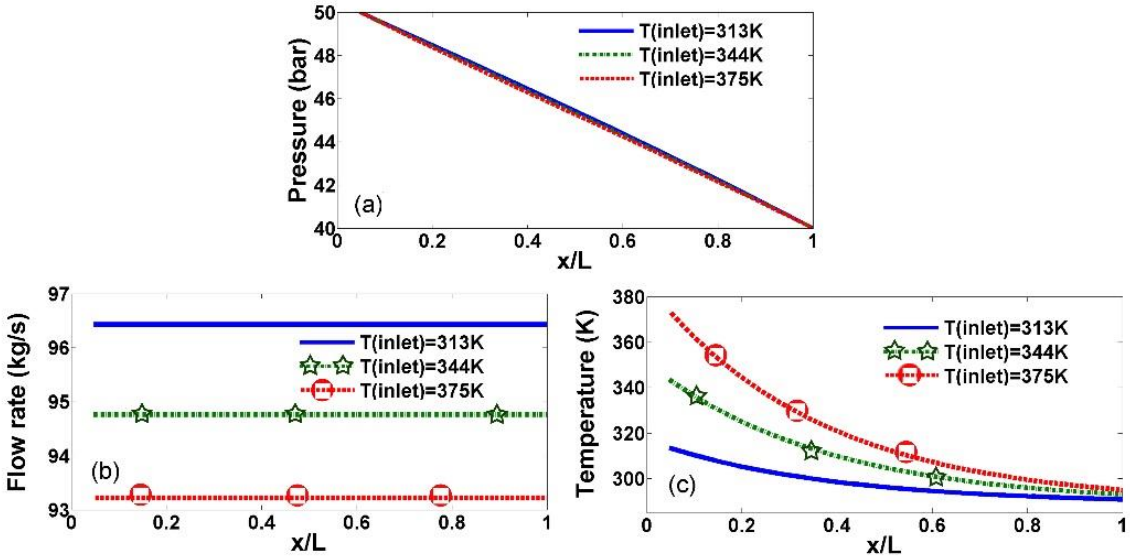

Figure II.2. Effect of inlet temperature on pressure, flow rate, and temperature distribution of the pipeline at steady state

Figure II.3 shows the effects of different heat transfer coefficients on the pressure, flow rate, and temperature profile. The ground temperature was set as 289 K, and the inlet temperature was set as 313 K. The effect of heat transfer coefficient on the pressure change across the pipeline is very small. The observed flow rate changes was 0.85% range when heat transfer coefficient was varied from 1.84 to 2.84 J/ (m^2 K s). Heat transfer coefficient affects the overall temperature profile as can be seen in the Figure II.3(c). Because the ground temperature was lower than the inlet gas temperature, higher heat transfer coefficient would decrease the pipeline temperature and subsequently increase the mass flow rate. If the ground temperature is higher than the inlet gas temperature, the effect of heat transfer coefficient will be the opposite.

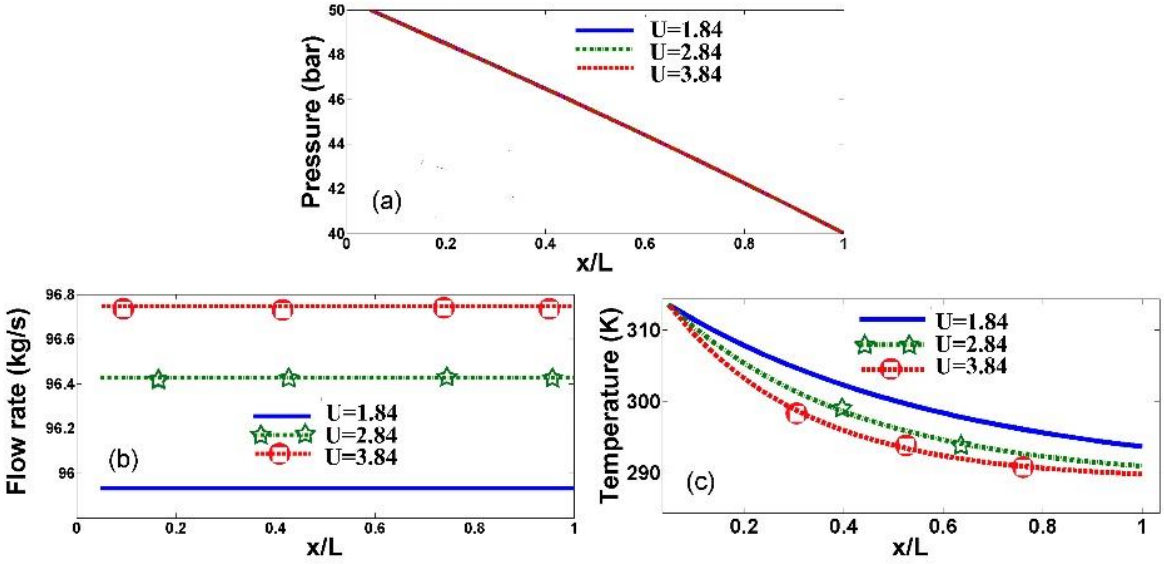

Figure II.3. Effect of heat transfer coefficient on pressure, flow rate, and temperature distribution of the pipeline at steady state; U represent heat transfer coefficient with unit of J/ (m^2 K s)

Figure II.3 Effect of heat transfer coefficient on pressure, flow rate, and temperature distribution of the pipeline at steady state; **U** represent heat transfer coefficient with unit of J/ (m^2 K s)

Many previous research efforts used non-isothermal model to study the transient and steady state behavior of the natural gas pipeline, but none of them considered leak occurrence. We incorporated a leak into the natural gas pipeline and studied the effect of leak on the pressure, flow rate, and temperature profile across the length of the pipeline. Different leak sizes (2%, 5%, and 10% of the total flow rate) and locations (L/4, L/2, and 3L/4) were tested. The effect of leak on the pressure and flow rate has been studied under an isothermal mode. In this paper, we are demonstrating the effect of a leak under a non-isothermal situation.

Figure II.4 shows the results of pressure change due to different amplitudes of the leak (Figure II.4a) and leaks with the same amplitude but at different locations (Figure II.4b) under non-isothermal condition. Due to the boundary conditions applied when solving the equations, the pressures at both ends do not change when responding to the leak. The effect of leak on pressure is to decrease the pressure at the leak sites. From Figure II.4b it can be seen that when a leak happens at L/4, L/2, and 3L/4, the pressure at the leak location decreases, and the decrease becomes larger with increased leak amplitudes, as shown in Figure II.4a.

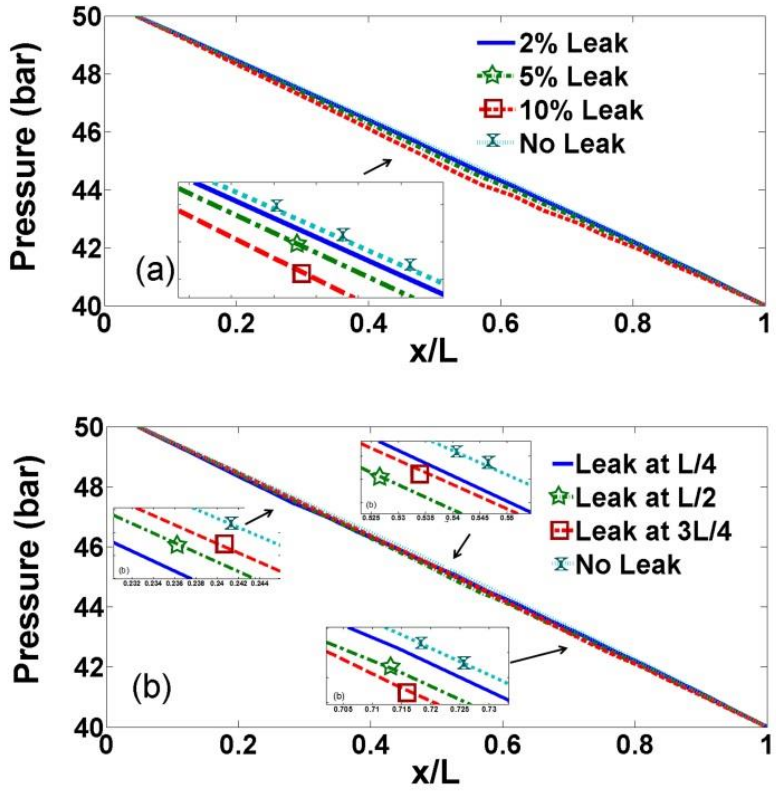

Figure II.4. Effect of leak on pressure distribution with (a) different leak sizes at L/2 location, and (b) 5% leak at different locations. L represents the total length of the pipeline

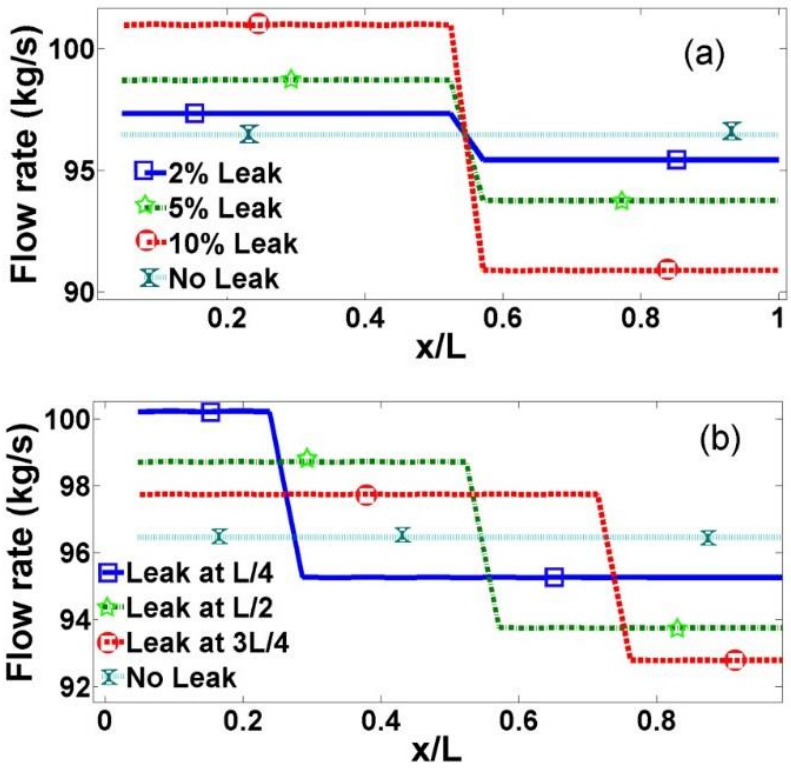

Figure II.5. Effect of leak on flow rate with (a) different leak magnitudes at L/2 and (b) 5% leak at different locations. L represents the total length of the pipeline

Figure II.5 illustrates the flow rate change due to a leak occurrence at the steady state. After the leak occurrence, the flow rate changes at both ends of the pipeline, i.e. upstream and downstream of the leak location. From Figure II.5a, it can be seen that the upstream flow rate increased while the downstream flow rate decreased. The difference between two ends is equal to the size of the leak. When the leak occurs, the pressure drop across of the pipeline will decrease due to the loss of flow rate and due to the operating condition of the pump station, the flow rate will increase to satisfy boundary condition which leads to increase in the inlet flow rate. In order to maintain the fixed

boundary pressure, more natural gas is pumped into the pipeline, which increases the upstream flow rate. The downstream flow rate decreases due to the presence of leak. Figure II.5b demonstrates the variation of flow rate profile due to leaks with the same amplitude occurring at different locations. The figure shows that the leak location will change the flow rate profile, which could be used for leak location identification. The difference between the flow rate with and without leak will change according to the leak location. The leak location identification equation is based on flow discrepancy, which is discussed by Wang et al. and showed as Equation (2.29).[89] E is the average of the discrepancies for ten previous measurements.

$$X_L = \frac{L}{1-\frac{E(q_{in}-q_s)}{E(q_{out}-q_s)}} \tag{2.29}$$

Here q_{in} and q_{out} represent the measured inlet, outlet flow rate after the leak and q_s is the flow rate at steady state without the leak. q_{in} and q_{out} are measured at both ends of the pipeline. q_s is estimated from the dual unscented Kalman filter using the measurement of boundary pressure at both ends of the pipeline. L is the total length of the pipeline. X_L is the estimated leak location. X_L is calculated when the difference between q_{out} and q_s exceeds a certain threshold.

The effects of a leak on the temperature profile across the length of the pipeline were studied by applying three different magnitudes of leaks in the middle of the pipeline. Figure II.6 shows the transient response of the temperature at different locations. From the figure it can be seen that when a leak occurs, the temperature at a location upstream of the leak point first decreases for a small amount, then increases,

and finally returns back to a steady state value. The decreasing temperature at the beginning of the leak is due to the pressure drop and Joule-Thomson effect. The subsequent temperature increase is due to the increased inlet flow rate at high temperature bringing in more energy, and the final steady state value is reached by the heat exchange with the environment. Figure II.7 demonstrates temperature change (at x=L/2) due to the leakage at different places. The leak with the same magnitude at different leak locations will affect the temperature change. The temperature change depends on the overall effect of inlet temperature, ground temperature, and pressure distribution.

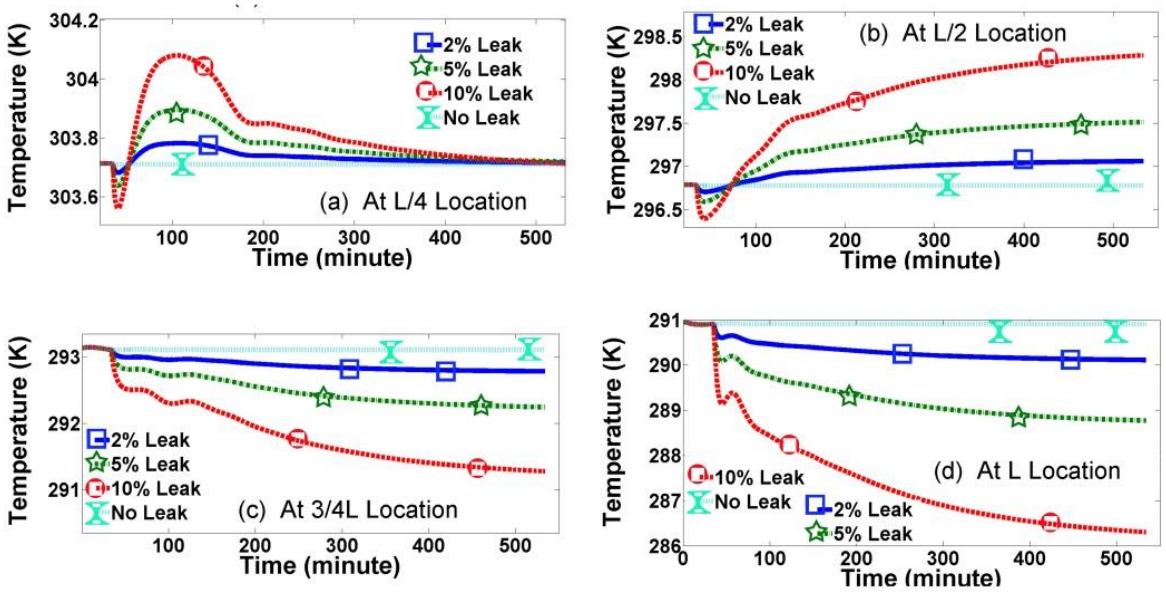

Figure II.6. Effect of leak (locating at L/2) on temperature change of the pipeline at different locations. L represents the total length of the pipeline

Leak detection using dual unscented Kalman filter

The unscented Kalman filter is a powerful state estimating technique for a nonlinear system. Compared to an extended Kalman filter, an unscented Kalman filter can be applied to a highly nonlinear system with higher accuracy. In our study, the flow rate is the process state of a gas flow process in a pipeline. In the application of the unscented Kalman filter, the generated sigma points will not violate the operational constraints because the process variance is small and the operation constraints in our study is the pressure at the pump station, which can tolerate significant variations. The number of sigma points is proportional to the discretization number of the pipeline, which is fixed in our study.

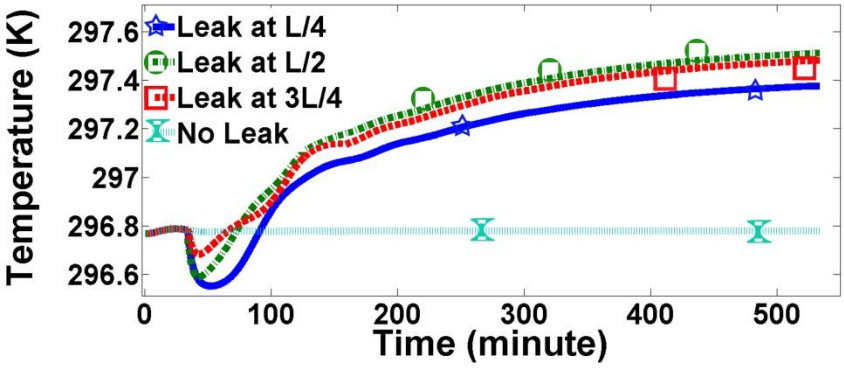

Figure II.7. Effect of leak on temperature change (at x=L/2 location) with leak occurring at different locations. L represents the total length of the pipeline

The non-isothermal model and the isothermal model were compared in the prediction of flow rate through the parameter estimation in the dual unscented Kalman filter. In the isothermal model, the parameter '*c*' is used to define the equation of state in

the isothermal model, which is closely related to the thermal properties such as temperature and compressibility factor, which is shown in Equations (2.4) and (2.8).

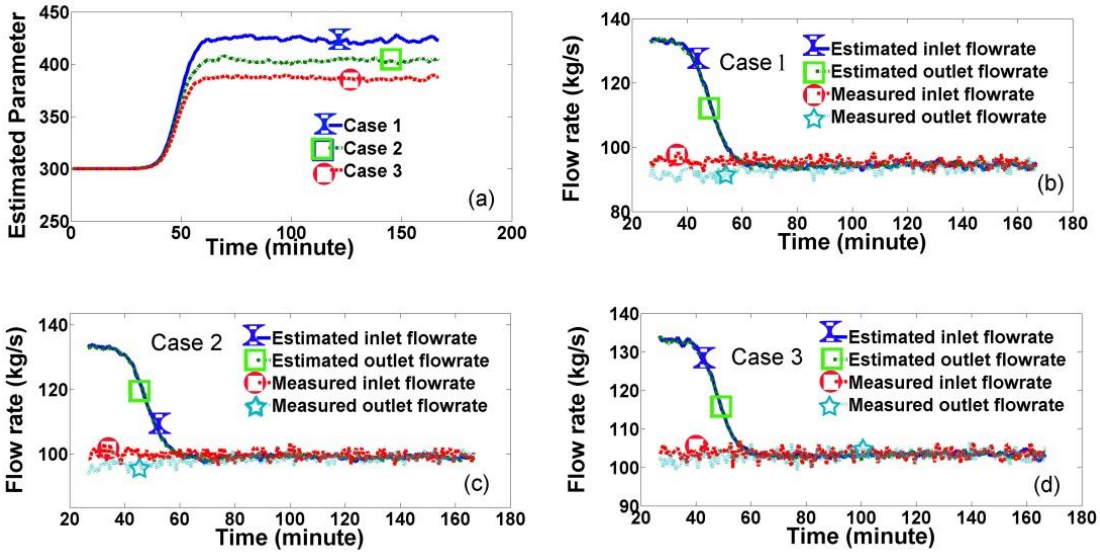

Figure II.8. Parameter estimation in three different cases and the match of flow rate with the simulated non-isothermal data. 'Estimated flow rates' are generated based on isothermal model and 'measured flow rates' are generated from non-isothermal model. Case 1, 2, and 3 respresent three different thermal conditions.

	Case 1	Case 2	Case 3
Ground temperature (K)	**303**	**273**	**289**
Inlet temperature (K)	**373**	**313**	**343**
Heat transfer coefficient (J/ (m^2 K s))	**1.84**	**3.84**	**2.84**

To demonstrate the effect of the estimated parameter, three different thermal situations were studied with randomly selected ground temperature, heat transfer coefficient, and inlet temperature. In Figure II.8 and the other figures, the 'measured' data was simulated through the non-isothermal model with process/measurement noise added (white noise, 1% of the flow rate at steady state), and the 'estimated' data was obtained by the dual unscented Kalman filter. Figure II.8a shows the estimated

parameter (‘*c*’ in Equation (2.4)) in three different thermal operating cases without leak occurrence. In each case, the parameter converges to a steady state value, and the fluctuation of the value was due to the noise of the measurements. From this figure it can be concluded that the parameter can be updated for different thermal operating conditions which matches the flow rate of non-isothermal model in Figures II.8b, II.8c, and II.8d. This parameter estimation technique can provide information about the thermal properties, such as ground temperature, gas heat capacity, material of a pipeline, and construction of a pipeline without having all these parameters measured.

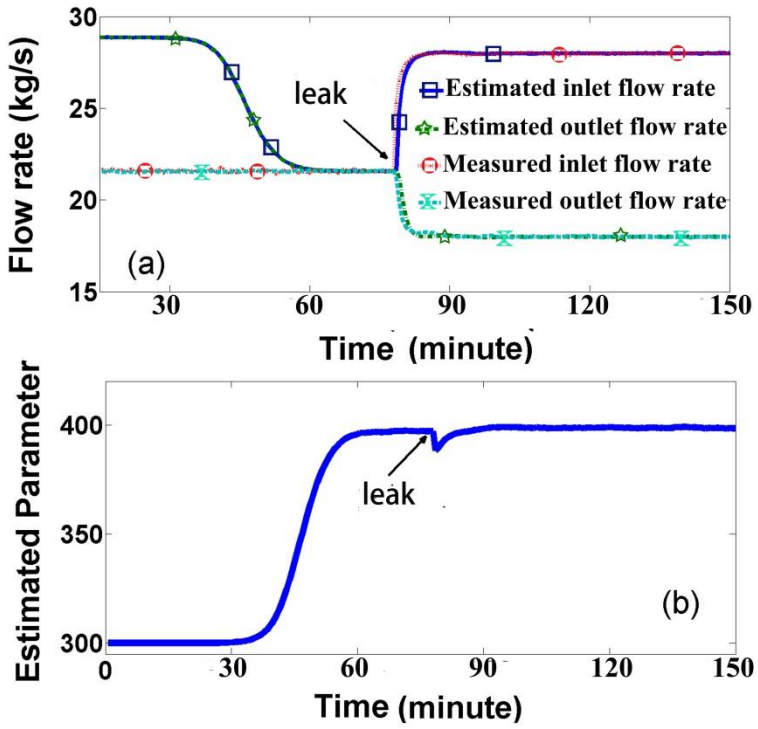

Figure II.9. Parameter estimation before and after leak occurrence: (a) match of flow rate due to parameter estimation, and (b) parameter estimation: parameter ‘*c*’ in isothermal model. ‘Estimated flow rates’ are generated based on isothermal model and ‘measured flow rates’ are generated from non-isothermal model.

Figure II.9 shows the estimation of the parameter in non-isothermal model with and without leak occurrence. As can be seen from Figure II.9a, the isothermal model can predict the flow rate of non-isothermal model before and after the leak happens through parameter estimation using dual unscented Kalman filter. The parameter estimation results in Figure II.9b indicate that the estimated parameter changes from 397.1 to 398.5 due to leak occurrence. The parameter '*c'* correlates with the thermal state of equation of the gas, and changes due to leak occurrence. The parameter changes accordingly when the leak changes the temperature profile of the gas in the pipeline.

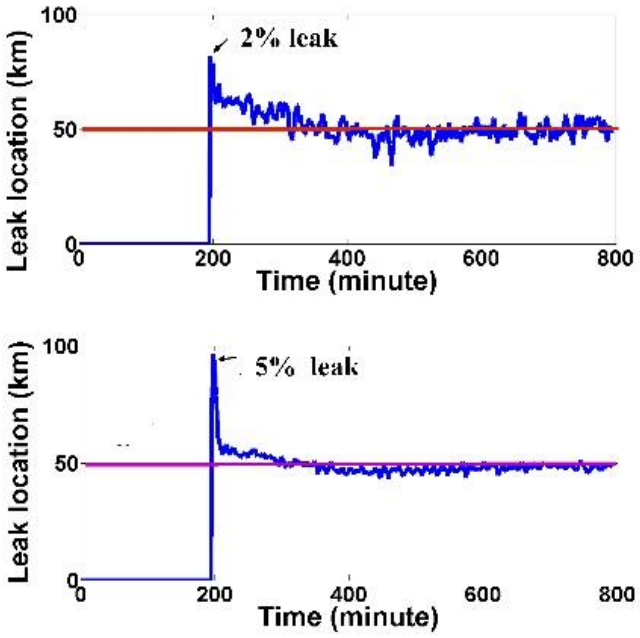

Figure II.10. Leak location identification using the dual unscented Kalman filter with 2% and 5% leakage

To detect a leak from the pipeline, an alarm will be triggered when the difference in flow rate between estimation from the filter and measurement exceeds a certain

threshold value according to the process noise level. Figure II.10 shows the leak location estimation using the DUKF algorithm. The leak location was calculated using Equation (2.29). The figure indicates that using a simplified model with parameter update, the DUKF can be applied for estimation of the leak location. As shown in Figure II.10, the estimation converges to a steady state value faster with larger leak magnitude. To eliminate the effect of noise, the moving window technique was applied, which averaged the data in a certain window time.

Comparisons between extended Kalman filter and unscented Kalman filter

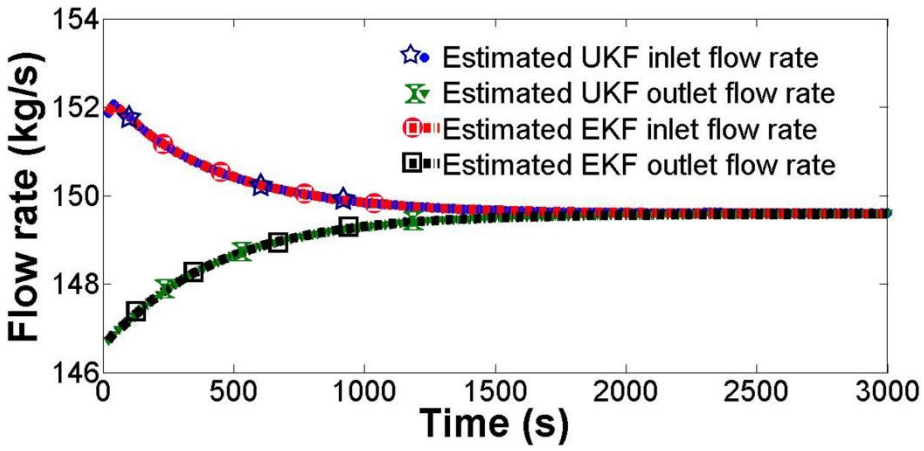

Figure II.11. Comparison between UKF and EKF for estimation of flow rate on isothermal model. 'Estimated flow rates' are generated based on isothermal model and 'measured flow rates' are generated from non-isothermal model.

To compare extended Kalman filter (EKF) and unscented Kalman filter (UKF), both isothermal and non-isothermal models were used. For the detection of a single leak in a pipeline, isothermal model with parameter estimation is sufficient. However, for detection of simultaneous multiple leaks, state and parameter estimations of non-

isothermal model are required. To compare unscented Kalman filter and extended Kalman filter fairly, the initial process covariance (P in Equation (2.13) for EKF and P_0 in Equation (2.17) for UKF) are set to the same value. The other covariance such as R_k and Q_k(in Equation (2.13) for EKF) are set equal to R and Q (in Equation (2.24) and (2.21) for UKF).

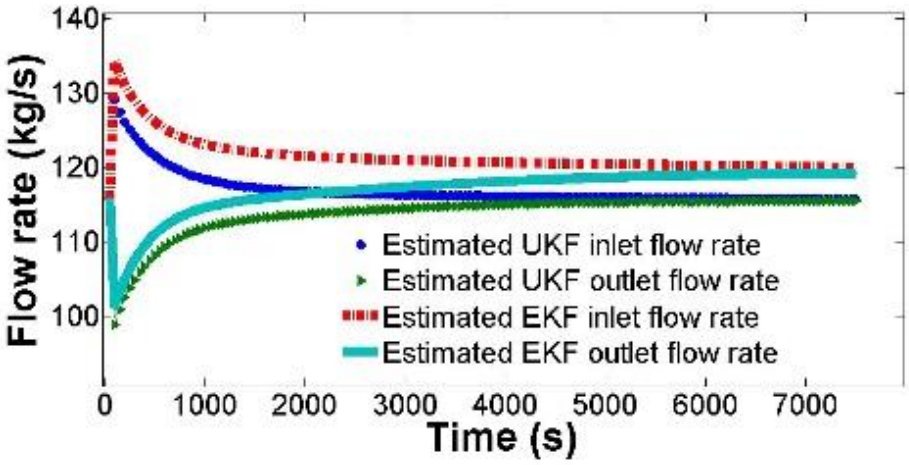

Figure II.12. Comparison between UKF and EKF for estimation of flow rate using non-isothermal model. Estimated flow rates are generated based on isothermal model and measured flow rates are generated from non-isothermal model.

Figure II.11 shows the comparison of extended Kalman filter and unscented Kalman filter on the isothermal model. The Jacobian matrix in the extended Kalman filter is calculated analytically. Both extended Kalman filter and unscented Kalman filter converge to the steady state value. 'Measurement' data applied in both Figure II.11 and Figure II.12 were generated by adding white noise term in the simulation. To compare both filters numerically, a simulation of 'measured' flow rate without process and measurement noise was provided, and the root mean square error (RMS error) from

the two filters was calculated. The estimation error is calculated using the following equation. Q_{in}^{filter} and Q_{out}^{filter} represent the inlet and outlet flow rate from filter estimation. Q_{in}^{state} and Q_{out}^{state} represent the inlet and outlet flow rate from simulation without any process noise.

$$\text{RMS } error = \sqrt{\sum((Q_{in}^{filter} - Q_{in}^{state})^2 + (Q_{out}^{filter} - Q_{out}^{state})^2)/2n}$$

The results showing estimation error for the isothermal and non-isothermal cases are provided in Table II.1.

Table II.1. RMS error from UKF and EKF estimation for isothermal and non-isothermal models

	UKF Error	EKF Error
Isothermal model	2.0×10^{-3}	6.0×10^{-5}
Non-isothermal model	0.265	2.68

The isothermal case study indicates that both unscented Kalman filter and extended Kalman filter has negligible estimation errors, and extended Kalman filter performs slightly better. It is because the isothermal model doesn't have high nonlinearity, and the slow dynamic of the system doesn't introduce significant linearization error. The errors in both cases are much smaller than the process noise.

The non-isothermal case study shows the superior of the unscented Kalman filter. In the application of extended Kalman filter on non-isothermal model, there are several physical parameters in the Jacobian matrix calculation that is not available. To calculate

the Jacobian matrix for non-isothermal model, the numerical values of high-order derivatives of the compressibility factor are needed, such as $\frac{\partial Z^2}{\partial P \partial T}$, $\frac{\partial Z^2}{\partial^2 P}$, and $\frac{\partial Z^2}{\partial^2 T}$. The relationships between gas compressibility and pressure/temperature are built on empirical models from experimental data, and these equations for the parameters are not continuous. So the Jacobian matrix for extended Kalman filter has to be calculated numerically. For the nonlinear system like the non-isothermal model when Jacobian matrix is hard to obtain, the unscented Kalman filter performs better than the extended Kalman filter. This case shows that the unscented Kalman filter has better performance when analytical Jacobian matrix of extended Kalman filter is not available. As can be seen in the Table II.1, extended Kalman filter provides large estimation error for the non-isothermal case. It is due to the error introduced in the first order linearization. The unscented Kalman filter provides better estimation of the process in the presence of process noise for the non-isothermal case.

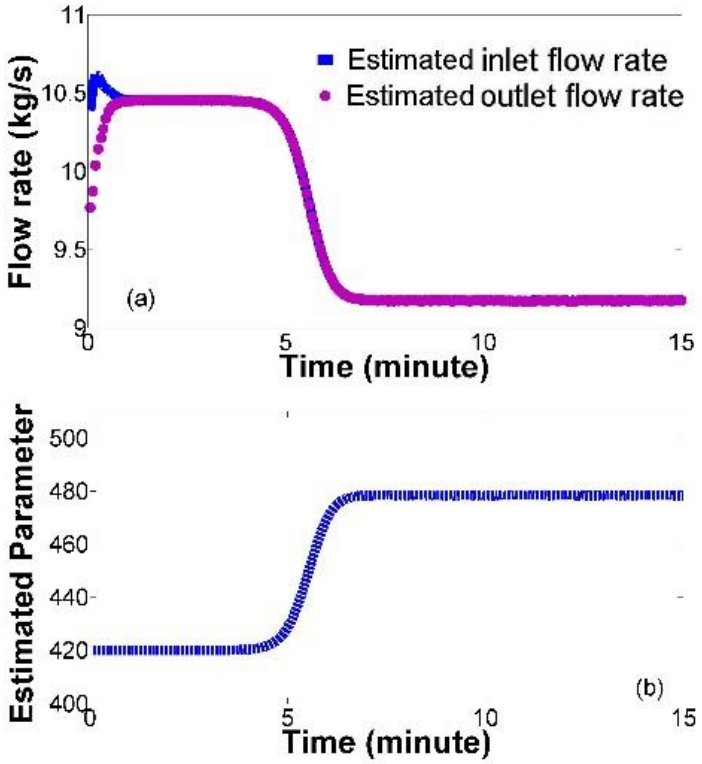

Figure II.13. An estimation of flow rate (a) and parameter: 'c' in isothermal model (b) using measurement data from PIPESIM

A case study using PIPESIM

To validate the dual unscented Kalman filter algorithm, a case study was performed using PIPESIM. PIPESIM is steady state simulation software used for the design and diagnostic analysis of oil and gas system including pipeline network developed by Schlumberger (PIPESIM software, 2015). A steady state natural gas pipeline flow simulation was performed with and without leak occurrence. The simulated straight pipeline has a length of 10 km, a pipe diameter of 0.3 m, and a heat transfer coefficient of 1.13 J/ (m^2 K s). The initial and ground temperature is set at 313 K

and 289 K, respectively. Inlet and outlet pressures (boundary conditions) are set at 10 bar and 8 bar. A comparison was performed between PIPESIM simulation and non-isothermal model developed in this paper using the same parameters. The PIPESIM calculated a flow rate of 9.2 kg/s at steady state while our non-isothermal models showed 10.6 kg/s. This difference may be due to the calculation of friction factor, which can be updated through the same parameter and state estimation technique. However, the non-isothermal model in our study is used to demonstrate the effect of thermal properties and generate 'measurement' data, which is used in the parameter and state estimation using the isothermal model. The parameter and state estimation can also be applied to non-isothermal model, which is not demonstrated here. In Figure II.13, the results shows that the flow rate estimation can be performed using the dual unscented Kalman filter. In PIPESIM, to simulate a pipeline with leak, a joint and an outlet 'sink' were added to the pipeline at a certain location with gas flowing out of the pipeline. We used our dual unscented Kalman filter algorithm on our isothermal model to estimate the parameter 'c' in Equations (2.9) and (2.10). Figure II.13 shows the updated flow rate and parameter 'c' using the simulation data obtained from PIPESIM. Leak location estimation was performed. The algorithm calculated the location of the leak to be at 6.09 km at 2% leak, whereas the actual location of the leak was at 6.00 km.

Summary of the chapter

Model-based fault detection method is one of the most widely used software solutions for leak identification in pipelines. In most previous natural gas pipeline leak detection studies, the gas flow models for natural gas pipelines were based on

assumptions that assume isothermal operation. In this paper, non-isothermal state equations were derived for natural gas pipeline flow processes considering the effect of gas compressibility, heat transfer coefficient, ground temperature, and leak occurrence in the pipeline. The effects of the above-mentioned thermal properties and the leak occurrence on the pressure, flow rate, and temperature profile along the pipelines were studied using MATLAB® simulations. The results showed that the ground temperature, heat transfer coefficient, and leak occurrence affected the flow rate values at steady state. Estimation of the leak location is extremely important from the point of view of safe operation of pipelines.

A dual unscented Kalman filter was used for parameter estimation and leak detection. To compare the isothermal and non-isothermal models, the parameter in the isothermal model was estimated for various thermal situations, including different inlet temperatures, ground temperatures, heat transfer coefficients, and leak occurrence. Together with the parameter update, the dual unscented Kalman filter was able to detect and identify the location of the leakage. A comparison study between unscented Kalman filter and extended Kalman filter is provided.

CHAPTER III

DESIGN OF AN UNKNOWN INPUT OBSERVER FOR LEAK DETECTION UNDER PROCESS DISTURBANCE

Introduction

Many chemicals in the petrochemical industry are transported through pipeline networks. However, leakage of chemicals from pipelines is always the main safety concern and may cause catastrophic failure. Hardware-based methods, such as fiber optic sensors, acoustic sensors, and vapor monitoring sensors, require extensive instrumentation for implementation.[62,94,95] Software-based methods are available for leak detection from a pipeline and generally only require measurements of flow rate and pressure at the boundary of the pipeline; the exception to this is Real-Time Transient Modeling, which needs temperature measurements.[96,97] However, for software-based methods, their high sensitivity to process noise and disturbances prevent them from detecting small leaks.[98]

A natural gas pipeline presents a complicated transportation problem, more so than a liquid phase pipeline, due to the possibility of phase change of the gas. Modeling and simulation of transient natural gas pipelines have been extensively studied considering non-isothermal conditions in single pipelines and networks.[71,74,75,99–103] For the purpose of leak detection in a natural gas pipeline, the effect of thermal properties cannot be ignored. The effects of changing thermal conditions on the natural gas flow in a pipeline through non-isothermal modeling has been demonstrated.[99]

Model-based methods for fault detection have been successfully demonstrated by many researchers. In these methods, key information regarding the state of the process is estimated. For transportation processes in pipelines, these estimated quantities include both flow rate and pressure. Many studies have proposed different methods for state estimation for leak detection in natural gas pipelines without considering the variation of thermal properties.[80,81,83,104,105] Methods such as optimization and neural networks have been developed for estimating the leak locations.[106,107] Most of the previous reports are based on ideal–gas assumptions for the natural gas. However, variations from the inlet gas temperature and ground temperature can be considered as disturbances in the process and can cause a change in thermal conditions of the gas, including phase changes. To deal with the effect of changing thermal conditions, one proposed method is to perform a real-time transient modeling with measurements of the thermal properties.[108]

Besides the variation of thermal properties, changes in boundary pressures at a pump station is also considered as a process disturbance. For a pipeline with a fixed delivering pressure at a pump station, consumer usage introduces time-variant oscillations in the pressure that further influence the leak detection. To compensate for the effect of these pressure oscillations, Reddy et al. applied a transfer function method on linearized partial differential equations of natural gas flow models to study the effect of the boundary pressure.[105] The Real-Time Transient Modeling method develops first-principle, non-isothermal models of the gas flow in pipelines and measures the corresponding parameters of the model, i.e. boundary pressure, inlet gas temperature, and ground temperature. Real-time transient modeling is performed using the measured

physical properties to monitor the pipeline operation.[96,97] However, this method not only introduces extra instrumentation but also exacerbates the effect of possible measurement (sensor) faults.

Observers for fault detection have been demonstrated by different researchers.[47,109–111] Observers and filters have also been applied for leak detection in water or natural gas pipelines, including extended Kalman filters, particle filters, high-gain observers, sliding mode observers, and Luenberger-type estimators.[81,83,112–116] Reducing the effect of process disturbances is a challenge for these observers unless real-time modeling and computation is performed. An unknown input observer is an observer designed to estimate the states when considering certain unknown inputs.[109,117–119] For a pipeline transportation process, disturbances such as unexpected changes in temperature and boundary pressure can be considered as unknown inputs and make the unknown input observer a better method than other filter and observers previously used.

In this paper, a linear unknown input observer is designed for a natural gas pipeline to estimate state (flow rate) information and reduce the effect of process disturbances. The pipeline is depicted with time-variant consumer usage at a certain known location. We provide a methodology to construct a linear unknown input observer to estimate the state for a natural gas flow process, which is modified from a previous research by Koenig et al.[47] The modified observer can be applied to the reduced pipeline model for leak detection under process disturbance. The modified observer also improved the performance of state estimation by considering the effect of process measurement noise. The robustness of the observer with respect to measurement

noise is analyzed. The corresponding sufficient and necessary condition for the modified observer is provided. With our new method, only two measurements (inlet and outlet flow rate) are needed to detect the leak location.

Modeling of non-isothermal natural gas flow

Non-isothermal modeling of natural gas flow in a pipeline

Non-isothermal modeling of natural gas flow is based on mass, momentum, and energy balances. Briefly, the composition of natural gas is assumed to be 95% methane, 2.5% ethane, 1.6% nitrogen, 0.7% carbon dioxide, and 0.2% propane. The length, diameter, inlet pressure, and outlet pressure are set as 10 km (L = 10 km), 0.3 m (D = 0.3 m), 10 bar (P_{in}), and 8 bar (P_{out}). A time-variant consumer usage is applied to the pipeline at a known location. The consumer usage is measured every 30 second, and is assumed constant in between measurements. The time-variant consumer usage is shown in Figure III.1, which is adapted from the work of Szoplik.[120] The compressibility factor was calculated based on the work of Dranchuk.[86]

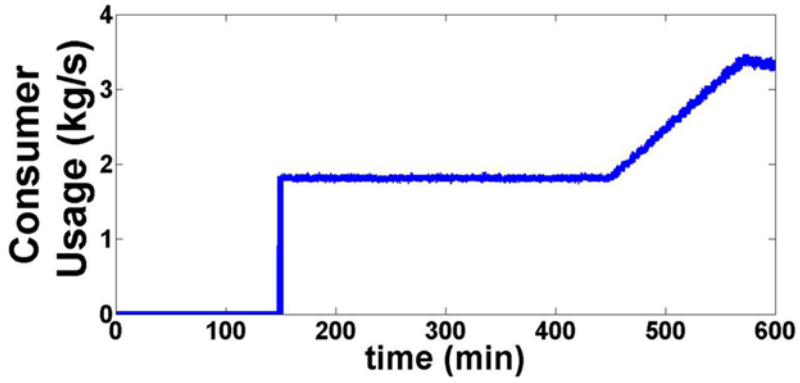

Figure III.1. Time-variant consumer gas usage

The development of the non-isothermal models is shown in Chapter II and as follows:

$$\frac{\partial P}{\partial t}=\frac{-\frac{1}{A}\frac{\partial q}{\partial x}-\frac{1}{A\Delta x}q_L+\left(\frac{1}{ZC_P}\frac{\partial Z}{\partial T}+\frac{1}{TC_P}\right)\left(\frac{fq^3z^2R^2T^2}{2DA^3P^2}-\frac{4U(T-T_g)}{D}-\frac{q}{A}C_P\frac{dT}{dx}+(\frac{T}{Z}\frac{\partial Z}{\partial T}+1)\frac{q}{AP}ZRT\frac{dP}{dx}\right)}{\left(\frac{1}{ZRT}-\frac{P}{Z^2RT}\frac{\partial Z}{\partial P}-\left(\frac{\partial Z}{\partial T}\right)^2\frac{T}{Z^2C_P}-\frac{2}{ZC_P}\frac{\partial Z}{\partial T}-\frac{1}{TC_P}\right)} \tag{3.1}$$

$$\frac{\partial q}{\partial t}=-A\frac{\partial P}{\partial x}-\frac{AP}{ZRT}g\sin\theta-\frac{fq^2}{2DAP}ZRT-\frac{1}{A}\frac{q_L}{\Delta x}\left(\frac{q}{P}\right)ZRT \tag{3.2}$$

$$\frac{\partial T}{\partial t}=\frac{\left(\frac{1}{ZRT}-\frac{P}{Z^2RT}\frac{\partial Z}{\partial P}\right)\frac{\partial P}{\partial t}}{\left(\frac{P}{Z^2RT}\frac{\partial Z}{\partial T}+\frac{P}{ZRT^2}\right)}+\frac{\frac{1}{A}\frac{\partial q}{\partial x}}{\left(\frac{P}{Z^2RT}\frac{\partial Z}{\partial T}+\frac{P}{ZRT^2}\right)}+\frac{q_L}{A\Delta x}\frac{1}{\left(\frac{P}{Z^2RT}\frac{\partial Z}{\partial T}+\frac{P}{ZRT^2}\right)} \tag{3.3}$$

In the above equations, P, q, and T are pressure, mass flow rate, and temperature in the pipe. A is the cross sectional area of the pipe. q_L is the mass flow rate of the leak and Δx is the corresponding discretization section of the pipe for the leak. The parameter Z is the compressibility factor of the gas, while U is the heat transfer coefficient of the pipe, T_g is the ground temperature, and f is the friction factor of the pipe. The non-isothermal model is used to generate measurement data in the following sections by using the Method of Line, which is shown in our previous work to be among the most efficient and accurate methods for solving the hyperbolic-type partial differential equations governing flow in natural gas pipelines. The fixed boundary conditions for solving the non-isothermal model are set as follows:

$$\left.\frac{\partial P}{\partial t}\right|_{x=0}=0,\quad \left.\frac{\partial T}{\partial t}\right|_{x=0}=0,\ \left.\frac{\partial P}{\partial t}\right|_{x=L}=0$$

The effect of temperature changes and pressure changes are also simulated using the non-isothermal model.

Model reduction

Both the oscillation of pressure and changes of temperature are nonlinear disturbances. To eliminate the effect of nonlinear disturbances in a nonlinear system, a nonlinear unknown input observer needs to be developed. However, to the best of our knowledge, there does not exist a general way to construct a nonlinear unknown input observer to compensate for nonlinear disturbances for nonlinear systems. Available methods for designing unknown input observers for nonlinear systems impose strict requirements on the system, such as satisfying local Lipchitz condition.[121] The linearization of nonlinear terms will introduce estimation errors, especially for nonlinear non-isothermal model, where an accurate Jacobian matrix is not available due to the calculation of numerical values of high-order derivative of compressibility factors, such as $\frac{\partial Z^2}{\partial P \partial T}$, $\frac{\partial Z^2}{\partial^2 P}$, and $\frac{\partial Z^2}{\partial^2 T}$, not available from experimental data.

To overcome this difficulty, a reduced linear process model is developed to construct a linear unknown input observer. Isothermal models are also derived using an ideal-gas assumption, which considers constant temperature along the pipeline and no change of gas phase. The isothermal model equations use constant compressibility $\frac{P}{\rho}=c^2$, as shown in the equations below:

$$\frac{\partial P}{\partial t}+\frac{c^2}{A}\frac{\partial q}{\partial x}+\frac{c^2}{A\Delta x}q_L=0 \tag{3.4}$$

$$\frac{\partial q}{\partial t}+A\frac{\partial P}{\partial x}+\frac{fc^2 q|q|}{2DAP}+\frac{c^2}{A\Delta x}\left(\frac{q}{p}\right)q_L=0 \tag{3.5}$$

For both the isothermal and non-isothermal models containing PDE equations, only boundary pressure and flow rate from the numerical solutions are used for leak

detection. The reduced linear model is designed to show the boundary flow rate of the pipeline under the influence of consumer usage. The disturbance from pressure and temperature changes can also be reduced to a linear disturbance.

The model reduction process begins with Equations (3.4a) and (3.5a), which can predict the behavior of the non-isothermal model by changing the corresponding parameters. The variable q_{usage} is used to represent the consumer usage at time *t*.

$$\frac{\partial P}{\partial t}+\frac{c^2}{A}\frac{\partial q}{\partial x}+\frac{c^2}{A\Delta x}q_{usage}=0 \tag{3.4a}$$

$$\frac{\partial q}{\partial t}+A\frac{\partial P}{\partial x}+\frac{fc^2q|q|}{2DAP}+\frac{c^2}{A\Delta x}\left(\frac{q}{p}\right)q_{usage}=0 \tag{3.5a}$$

The pipeline is divided into three sections depending on the location of the consumer usage, which have length of l_1, l_2, and l_3. The pressure drop in Equations (3.4a) and (3.5a) over each section is integrated with an assumption of a steady state flow rate. For a pipeline without usage, the pressure drop along the pipeline is shown in Equation (3.5b), which is the integral solution of Equation (3.5) over *x* at steady state where q_{usage} is set to 0.

$$P_1^2- P_0^2=l_1\frac{fc^2q_1^2}{DA^2}+l_2\frac{fc^2q_1^2}{DA^2}+l_3\frac{fc^2q_1^2}{DA^2} \tag{3.5b}$$

Here, the inlet and outlet pressure are represented by P_1 and P_0, and q_1 and q_0 are the flow rate before and after the leak location, respectively. For a pipeline without a leak or consumer usage the values of q_1 and q_0 are equal. For a pipeline with consumer usage, the flow rate at different sections will change correspondingly, and these changes are defined by Δq_1 before the section with consumer usage, Δq_0 inside the section with

consumer usage, and Δq_0 after the section with consumer usage. For the pipeline with consumer usage, the pressure drop along the pipeline becomes as follows:

$$P_1^2 - P_0^2 = l_1 \frac{f \times c^2 (q_1 + \Delta q_1)^2}{DA^2} + l_2 \frac{f \times c^2 (q_1 + \Delta q_0)^2}{DA^2} + \frac{c^2}{2A^2} q_{usage} (q_1 + \Delta q_0) + l_3 \frac{f \times c^2 (q_1 + \Delta q_0)^2}{DA^2} \quad (3.5c)$$

The consumer usage can be calculated from the change of the flow rate, for which $q_{usage} = \Delta q_1 - \Delta q_0$. The pressure drop in Equation (3.5b) and Equation (3.5c) will be equal since the pressure at the boundary of the pipeline is fixed, so the following equation can be derived:

$$l_1 \frac{f \times c^2 (2q_1 + \Delta q_1) \Delta q_1}{DA^2} + (l_2 + l_3) \frac{f \times c^2 (2q_1 + \Delta q_0) \Delta q_0}{DA^2} + \frac{c^2}{2A^2} (\Delta q_1 - \Delta q_0)(q_1 + \Delta q_0) = 0 \quad (3.5d)$$

If the consumer usage is relatively small compared to the nominal flow rate, we can assume $(2q_1 + \Delta q_1) \approx 2q_1$ and $(2q_1 + \Delta q_0) \approx 2q_1$, therefore $(q_1 + \Delta q_0) \approx q_1$. Using these approximations, Equation (3.5d) can be simplified to Equation (3.5e):

$$\frac{\Delta q_1}{\Delta q_0} = -\frac{(l_2 + l_3)}{l_1} = -\frac{\left(\frac{f \times (l_2 + l_3)}{D} \frac{1}{4}\right)}{\frac{f \times (l_1)}{D} + \frac{1}{4}} \quad (3.5e)$$

The overall boundary flow rates of a pipeline with stable consumer usage at steady state are given by the following equations:

$q_{in} = q_{st.} + q_{usage} \times a$; $q_{out} = q_{st.} + q_{usage} \times b$;

$a/b = \text{constant}$ (3.6)

In Equation (3.6), the variables q_{in} and q_{out} are the inlet and outlet flow rate and $q_{st.}$ is the flow rate at steady state without consumer usage. To evaluate the linear approximation, a simulation result is presented in Figure III.2, which shows the linear fit

between the consumer usage and boundary flow rate at steady state. The R^2 value for linear fit of inlet flow rate and outlet flow rate is 0.987 and 0.999, respectively.

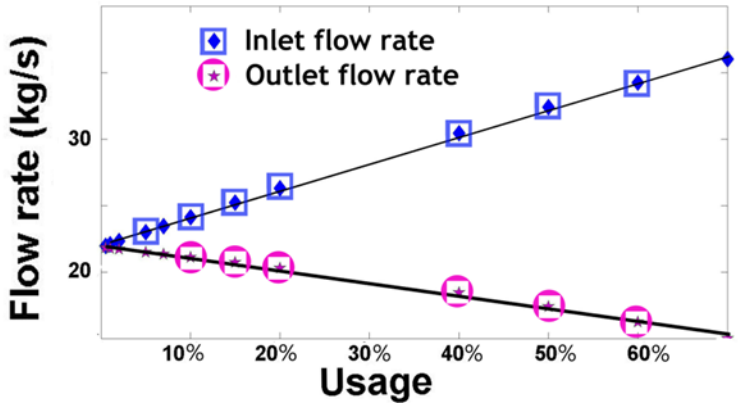

Figure III.2. Linear fit of boundary flow rate with consumer usage at steady state

For a pipeline with time-variant consumer usage, q_{in} and q_{out} will be subjected to the dynamic change of consumer usage. The response of the boundary flow rate corresponding to the consumer usage can be written as Equation (3.7) and Equation (3.8).

$$q_{in}(t)=q_{st.}+\sum_{i=0}^{n} a_i\, q_{usage}(t-i) \tag{3.7}$$

$$q_{out}(t)=q_{st.}+\sum_{i=0}^{n} b_i q_{usage}(t-i) \tag{3.8}$$

The parameters a_i and b_i model the effect of consumer usage on the flow rate, and are obtained by performing a simulation study. In the simulation study, artificial measured flow rate at the boundary of the pipe were generated using Equation (3.1), (3.2), and (3.3) with known q_{usage}, which is q_L in these equations. q_{in} and q_{out} from Equation (3.7) and (3.8) are calculated and compared to the simulation data from Equation (3.1-3.3). a_i and b_i are tuned so that $q_{in}(t)$ and $q_{out}(t)$ will fit the artificial measurement for each time step.

The comparison of the flow rates between the original model and the reduced model is shown in the results section. Different observers need to be designed for different process models for state estimation purpose. In the next session, design of observer for the process model in the format of Equation (3.7) and (3.8) is introduced.

Design of a linear unknown input observer

To apply the concept of model-based fault detection, a state estimation is obtained from filtering our observer and is then compared with the measurements. For a case study of a pipeline system, the state information is flow rate, pressure, and temperature. To detect leaks in the pipeline, a comparison between the estimated state and the measured state is performed to determine the leak occurrence and more importantly the leak location. There are several proposed state estimation methods for a pipeline system for leak detection, as introduced before, however these methods cannot efficiently estimate the state information in the presence of process disturbances. Thus, we propose using a new state estimation method to deal with the process disturbance. An unknown input observer is designed to estimate the state information as well as to eliminate the effect of unknown input, which is a perturbation with unknown size. The construction of a linear unknown input observer is demonstrated in the following steps.

Without loss of generality, a linear process model such as Equation (3.7) and Equation (3.8) can be written as follows:

$$x(t)=\sum_{i=0}^{n} A_i x\left(t-\tau_i\right)+\sum_{i=0}^{n} B_i u\left(t-\tau_i\right)+Ww(t) \tag{3.9}$$

$$y(t)=Cx(t)+Md(t)$$

where x(t) is the state, y(t) is the measurement, $u(t-\tau_i)$ is the input, d(t) is measurement noise, here assumed to be white noise, and w(t) is the unknown input. τ_i is the time delay constant. Equation (3.9) is a general format of Equation (3.7) and Equation (3.8). For the application of flow rate estimation, in Equation (3.9), x(t), y(t), and u are boundary flow rate, measured boundary flow rate, and consumer usage. Here, W is the parameter matrix for the unknown input, which was determined by the simulation results of the unknown input to the system. To obtain the W matrix in a simulation study, different values of w(t) are introduced into the system, and the changes of x(t) are calculated. The W matrix is calculated as $\Delta x_1(t)/\Delta x_2(t)$ in presence of w(t) at steady state . $\Delta x_1(t)$ and $\Delta x_2(t)$ represent the change of inlet and outlet flow rate. For the leak detection from a pipeline, w(t) is defined as pressure change at pump station and change of ground temperature. To perform the simulation study to obtain W matrix, drop of inlet pressure and change of ground temperature were introduced individually using Equation (3.1-3.3), the inlet and outlet flow rate which is x(t) in Equation (3.9) was recorded. W matrix is then calculated as $\Delta x_1(t)/\Delta x_2(t)$ at steady state.

A modified design of unknown input observer from Koenig et al.[24] is shown as follows:

$$z(t)= \sum_{i=0}^{n} F_i z(t-\tau_i)+ \sum_{i=0}^{n} TB_i u(t-\tau_i)+ \sum_{i=0}^{n} G_i y(t-\tau_i) \quad (3.10)$$

$$\hat{x}(t)=z(t)+Ny(t)$$

where F_i , T, N, B_i, and G_i are corresponding parameters for the observer and $\hat{x}(t)$ is an estimation of the state x(t).

Proving existence, stability and robustness of the unknown input observer

To utilize the unknown input observer described in Equation (3.10) for fault detection in pipelines, its existence, stability and robustness must be proven. The following lemma is applied for the existence of an observer for the system. The proof of Lemma 3.1 m is similar to Koenig et al., which is given in Appendix.[47]

Lemma 3.1: The necessary and sufficient condition for the existence of observer (Equation (3.10)) for a system (Equation (3.9)) is $rank\ CW = rank\ W$

Stability of an observer refers to the propagation of the estimation error over time, where a stable observer has an estimation error that decreases over time. The following theorem gives the stability criteria of an observer:

Theorem 3.1: The observer is asymptotically stable if and only if the following conditions hold:

1) $e(t)=\sum F_i\ e(t-\tau_i)+\sum G_i M\ d(t-\tau_i)+NM\ d(t)$ is asymptotically stable

2) $T+NC=I$

3) $TW=0$

4) $\bar{G}_i=G_i-F_iN,\ \ i=0,1,2,\ldots n$

5) $F_i=TA_i-\bar{G}_iC,\ i=0,1,2,\ldots n$

Theorem 3.1 has similar structure with Theorem 1 in the reference[47] except condition (1). Condition (4) and (5) introduce new variables for ease of solving the parameters. Condition (2) and (3) are used to derive the condition (1), which is shown as the following. The assumption for *W* is that it is not an identity matrix. From the design of the observer and Equations (3.9) and (3.10), the error of the observer is calculated as:

$$e(t)=\hat{x}(t)-x(t)=z(t)+(NC-I)x(t)+NMd(t)$$

$$=\sum F_i e(t-\tau_i)+\sum(T+NC-I)B_i u(t-\tau_i)+\sum(F_i-\overline{G_i}C-F_iCN+(NC-I)A_i)x(t-\tau_i)+$$

$$(NC-I)Ww(t)+\sum G_i Md(t-\tau_i)+NMd(t) \quad (3.11)$$

Asymptotic stability is defined as the speed of the decrease of the estimation error and condition (1) in **Theorem 3.1** guarantees this stability. Conditions (2), (3), (4), and (5) in **Theorem 3.1** can be used to simply Equation (3.11) to condition (1)**.** After the simplification of the estimation error of Equation (3.11) into condition (1) using conditions (2-5) in **Theorem 3.1**, **Theorem 3.2** is introduced to prove asymptotic stability criteria described by condition (1) and solve the parameter for the observer using a linear matrix inequality toolbox in MATLAB:

Theorem 3.2: The observer estimation error will be asymptotically stable if and only if the following conditions hold: there exist matrices $P=P^T>0$ and $Q_i>0$ satisfying the following linear matrix inequality:

$$\Xi=\begin{bmatrix} -P+\sum_{i=1}^{4}Q_i & 0 & 0 & 0 & 0 & F_0^tP \\ * & -Q_1 & 0 & 0 & 0 & F_1^tP \\ * & * & -Q_2 & 0 & 0 & F_2^tP \\ * & * & * & -Q_3 & 0 & F_3^tP \\ * & * & * & * & -Q_4 & F_4^tP \\ * & * & * & * & * & -P \end{bmatrix}<0 \quad (3.12)$$

The proof of **Theorem 3.2** is introduced in Appendix.

To solve for the parameters of the unknown input observer in Equation (3.10) which satisfy **Theorem 3.1**, the linear matrix inequality method is used and is

summarized in the following brief steps.[24] The unknown input parameter matrix W is set as $\begin{bmatrix} 1 & 1 \\ 1 & 1 \end{bmatrix}$, which corresponds to the pressure oscillation and temperature change at steady state. More discussion about the W matrix can be found in the following section. Conditions (2-5) in **Theorem 3.1** can be rewritten as the linear system shown in Equation (3.11b) based on the assumption of setting 'n' in Equations (3.9) and (3.10) equal to 4.

$$[T \quad N \quad F_0 \quad \bar{G}_0 \quad F_1 \quad \bar{G}_1 \quad F_2 \quad \bar{G}_2 \quad F_3 \quad \bar{G}_3 \quad F_4 \quad \bar{G}_4]\cdot\phi_1=\Psi_1 \tag{3.13a}$$

$$\phi_1=\begin{bmatrix} I_0 & W & A_0 & A_1 & A_2 & A_3 & A_4 \\ C & 0 & 0 & 0 & 0 & 0 & 0 \\ 0 & 0 & -I_n & 0 & 0 & 0 & 0 \\ 0 & 0 & -C & 0 & 0 & 0 & 0 \\ 0 & 0 & 0 & -I_n & 0 & 0 & 0 \\ 0 & 0 & 0 & C & 0 & 0 & 0 \\ 0 & 0 & 0 & 0 & -I_n & 0 & 0 \\ 0 & 0 & 0 & 0 & C & 0 & 0 \\ 0 & 0 & 0 & 0 & 0 & -I_n & 0 \\ 0 & 0 & 0 & 0 & 0 & C & 0 \\ 0 & 0 & 0 & 0 & 0 & 0 & -I_n \\ 0 & 0 & 0 & 0 & 0 & 0 & C \end{bmatrix} \qquad \Psi_1=[I_n \ 0 \ 0 \ 0 \ 0 \ 0 \ 0 \ 0] \tag{3.13b}$$

By rearranging Equations (3.13a) and (3.13b), the parameters F_i in Equation (3.11) can then be rewritten in as shown in Equation (3.13c). Here, ϕ_1^+ is a generalized inverse matrix of ϕ_1 and K is an appropriate matrix parameter to be determined.

$$F_i=\chi_i-K\beta_i, \ i=0,1,2,3,4 \tag{3.13c}$$

$$\chi_0= \Psi_1\Phi_1^+ \ [A_0^T \ 0 \ 0 \ -C^T \ 0 \ 0 \ 0 \ 0 \ 0 \ 0 \ 0 \ 0]^T$$

$$\chi_1 = \Psi_1\Phi_1^{+}\ [A_1^T\ 0\ 0\ \ 0\ \ 0\ -C^T 0\ 0\ 0\ 0\ 0\ 0]^T$$

$$\chi_2 = \Psi_1\Phi_1^{+}\ [A_2^T\ 0\ 0\ \ 0\ \ 0\ \ 0\ -C^T 0\ 0\ 0\ 0]^T$$

$$\chi_3 = \Psi_1\Phi_1^{+}\ [A_3^T\ 0\ 0\ \ 0\ \ 0\ \ 0\ \ 0\ 0\ -C^T 0\ 0]^T$$

$$\chi_4 = \Psi_1\Phi_1^{+}\ [A_4^T\ 0\ 0\ \ 0\ \ 0\ \ 0\ \ 0\ 0\ \ 0\ \ 0\ -C^T]^T$$

$$\beta_0 = \left(I-\Phi_1\Phi_1^{+}\right)\ [A_0^T\ 0\ 0\ -C^T\ \ 0\ 0\ 0\ 0\ 0\ 0\ 0\ 0]^T$$

$$\beta_1 = \left(I-\Phi_1\Phi_1^{+}\right)\ [A_1^T\ 0\ 0\ \ 0\ \ 0\ -C^T 0\ 0\ 0\ 0\ 0\ 0]^T$$

$$\beta_2 = \left(I-\Phi_1\Phi_1^{+}\right)\ [A_2^T\ 0\ 0\ \ 0\ \ 0\ \ 0\ \ 0\ -C^T 0\ 0\ 0\ 0]^T$$

$$\beta_3 = \left(I-\Phi_1\Phi_1^{+}\right)\ [A_3^T\ 0\ 0\ \ 0\ \ 0\ \ 0\ \ 0\ 0\ -C^T 0\ 0]^T$$

$$\beta_4 = \left(I-\Phi_1\Phi_1^{+}\right)\ [A_4^T\ 0\ 0\ \ 0\ \ 0\ \ 0\ \ 0\ 0\ \ 0\ \ 0\ -C^T]^T$$

After the rearrangement in Equation (3.13c), the parameter of F_i is introduced into Equation (3.12). Equation (3.12) is solved using the linear matrix inequality toolbox in MATLAB. The parameter F_i can be solved through the equation, and other parameters for the observer can be solved according to condition (4) and (5) in **Theorem 3.1**.

Another restriction for the parameters is that λ_1 and λ_2, the eigenvalues of the parameters F_i in Equation (3.12), need to be confined in a certain range.[47] The eigenvalues of the parameters F_i determine the speed of the convergence. It satisfies the following linear matrix inequality with $Q_1=Q_1^T$ and $U=Q_1K$:

$$Q_1 \sum \chi_i + \left(Q_1 \sum \chi_i\right)^T - U \sum \beta_i - \left(U \sum \beta_i\right)^T + 2\lambda_1 Q_1 < 0$$

$$Q_1 \sum \chi_i + (Q_1 \sum \chi_i)^T - U \sum \beta_i - (U \sum \beta_i)^T + 2\lambda_2 Q_1 > 0$$

To restrict the effect of measurement noise *d(t)* on the estimation error in condition (1) in **Theorem 3.1**, a robustness study is proposed using an H-infinity norm of the transfer function relating noise to estimation error. We introduce a combined noise term $n(t)$ to simplify the noise term in condition (1) in Theorem 1 to the following:

$$\sum G_i M d(t-\tau_i) + NMd(t) = (\sum G_i M + NM) \cdot n(t)$$

To ensure the effect of process noise on the estimation error is confined in a certain range, we define a H_∞ norm of the transfer function T_{en}, which is the transfer function of process noise to estimation error in condition (1) in **Theorem 3.1**. More applications of a transfer function for robust control can be found in Mahmoud's book.[122] This transfer function can be written as follows:

$$T_{en} = \frac{(NM + \sum G_i M)}{(I - \sum F_i e^{-\tau_i s})}$$

To solve the H_∞ robustness problem, which ensures $\|T_{en}\|_\infty \leq \gamma$ with $\gamma > 0$, **Theorem 3.3** is introduced. The proof of **Theorem 3.3** is introduced in Appendix B.

Theorem 3.3: The norm of transfer function of T_{en} will be smaller than γ if there exists matrices, and $P = P^T > 0$; $Q_i > 0$, which satisfy the following linear matrix inequality. *D* equals to$(NM + \sum G_i M)$.

$$\Omega=\begin{bmatrix} -P+\sum_{i=1}^{4} Q_i & 0 & 0 & 0 & 0 & 0 & F_0^tP & F_0^tP & 0 \\ * & -Q_1 & 0 & 0 & 0 & 0 & F_1^tP & F_1^tP & 0 \\ * & * & -Q_2 & 0 & 0 & 0 & F_2^tP & F_2^tP & 0 \\ * & * & * & -Q_3 & 0 & 0 & F_3^tP & F_3^tP & 0 \\ * & * & * & * & -Q_4 & 0 & F_4^tP & F_4^tP & 0 \\ * & * & * & * & * & -\gamma^2 & D^tP & D^tP & 0 \\ * & * & * & * & * & * & -P & 0 & 0 \\ * & * & * & * & * & * & * & 0 & P \\ * & * & * & * & * & * & * & * & -I \end{bmatrix} < 0 \qquad (3.14)$$

Theorem 3.3 is not used to solve the parameters for the observer, which is used to validate the effect of process noise on state estimation. In the application of **Theorem 3.3**, a given value of γ is provided, and parameters from **Theorem 3.2** such as F_i and D are introduced to validate the existence of the linear matrix inequality Equation (3.14) using the toolbox in MATLAB.

Application of an unknown input observer in pipeline monitoring

To apply the design of the unknown input observer in Equation (3.10) to a pipeline system, the parameters in Equations (3.9) and (3.10) are obtained from the reduced pipeline model, Equations (3.7) and (3.8), where the input term u(t) in Equation (3.9) is treated as the time variable consumer usage, q_{usage}. The flow rate and its estimated measurement value are given as x(t) and y(t) respectively in Equation (3.9). A real-time monitoring of the pipeline system is performed using the unknown input observer Equation (3.10). The estimation of the flow rate from the observer is compared with the simulated process flow rate generated from the non-isothermal model. Process disturbances such as pressure oscillation and change of ground temperature are added to

the non-isothermal modeling. The simulated process data, including the scenario with process disturbances, are fed into the unknown input observer for flow rate estimation.

Results and discussion

Effect of pressure change

Model-based fault detection methods involve solving dynamic models which are usually ordinary or partial differential equations. Boundary conditions for solving these equations relate to the control performance of actuators in applications. For a pipeline, boundary conditions such as fixed boundary pressure or flow rate relate to controlling the pump pressure at the pump station. However, these conditions are subject to disturbances such as leaks and consumer usage, which tend to reduce the boundary pressure. As indicated by Wang et al., both inlet and outlet pressure dropped due to a leak occurrence in an oil pipeline.[89] The unknown input observer method proposed in this paper is designed to handle the oscillation of the pressure and does not require an online model of the process. The effects of a pressure drop and pressure increase are simulated and its effect on boundary flow rate is demonstrated.

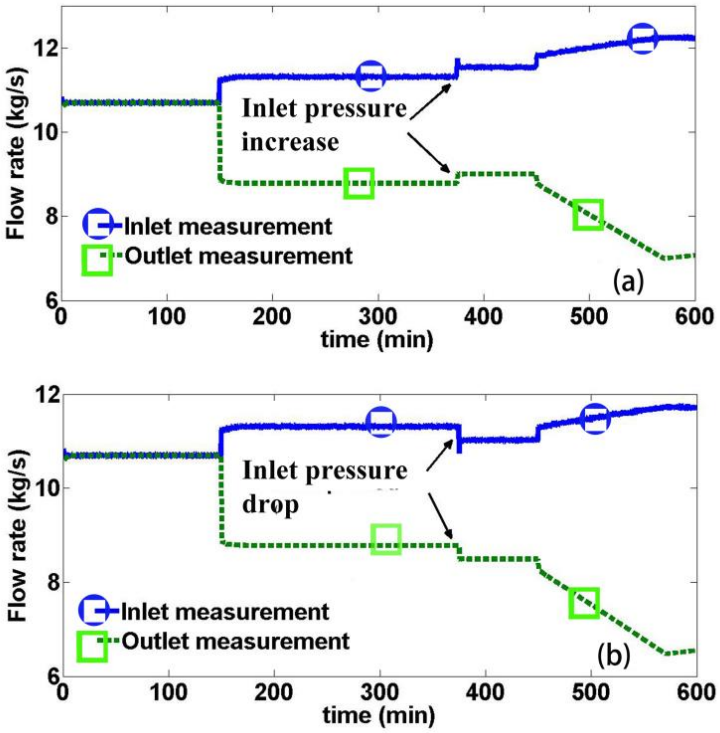

Figure III.3. The effect of inlet pressure drop/increase on boundary flow rate

Figure III.3 shows the effect of pressure drop or pressure increase on the flow rate at the boundary of the pipeline in a simulation study using the non-isothermal model. The pressure change is applied at the 375th minute when the consumer usage is stable so the change of flow rate will be solely the effect of pressure change rather than the variation of consumer usage. As indicated in the figure, both the inlet and outlet flow rate decrease correspondingly when an inlet pressure drop is applied. An increase in boundary pressure will result in an increase in both the inlet and outlet flow rate (not shown). Pressure drops are expected to be the more prevalent event affecting the pressure changes because leaks or consumer usage will tend to decrease the pressure.

As explained before, the unknown input matrix *W* in Equation (3.9) is calculated using a simulation study. Figure III.3 indicates the changes of inlet an outlet flow rate are equal at steady state when the inlet pressure change. So the W matrix is $\begin{bmatrix}1\\1\end{bmatrix}$ for the disturbance pressure change. W is set as $\begin{bmatrix}1 & 1\\1 & 1\end{bmatrix}$ for ease of solving the parameter in Equation (3.13a,b).

Effect of temperature change

The changing of thermal conditions can cause phase changes in natural gas. To analyze the role temperature plays on the pipeline process, the effects of changing ground temperature on boundary flow rate are simulated and the results are shown in Figure III.4. Conventional techniques use a commercial real-time modeling method to deal with the change of thermal properties by continuously measuring them along the length of the pipeline. In this paper, we develop a method to consider the effect of the change of thermal properties without acquiring the thermal measurement data. The effect of temperature change on the boundary flow rate was studied for the observer design.

Figure III.4 shows the effects of a 10 K increase or decrease in ground temperature in 30 seconds. For the case of a ground temperature drop (Figure III.4b), both the inlet and outlet flow rates increased at steady state. However, the boundary flow rates go through a small range of oscillation. A ground temperature increase (Figure III.4a) shows an opposite effect on the flow rate. The unknown input matrix for a temperature change can also be calculated as $\begin{bmatrix}1 & 1\\1 & 1\end{bmatrix}$, since the inlet and outlet flow rate change corresponding to a ground temperature change is also equal. For both inlet

pressure change and ground temperature change, the unknown input matrix W is the same. The same unknown input matrix can be used for both pressure change and temperature change scenarios.

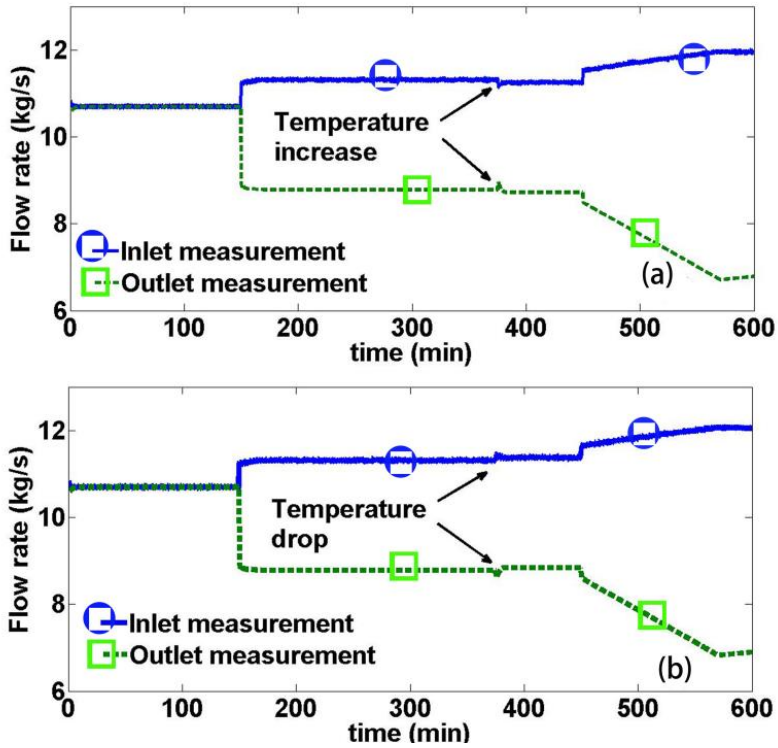

Figure III.4. Effect of ground temperature change on the boundary flow rate

Comparison between the reduced linear model and the non-isothermal model

The original nonlinear flow model was reduced to a linear model under certain assumptions as indicated before. The parameters for the dynamic linear model in Equation (3.7) and Equation (3.8) were obtained from non-isothermal simulation data and are shown in Table III.1.

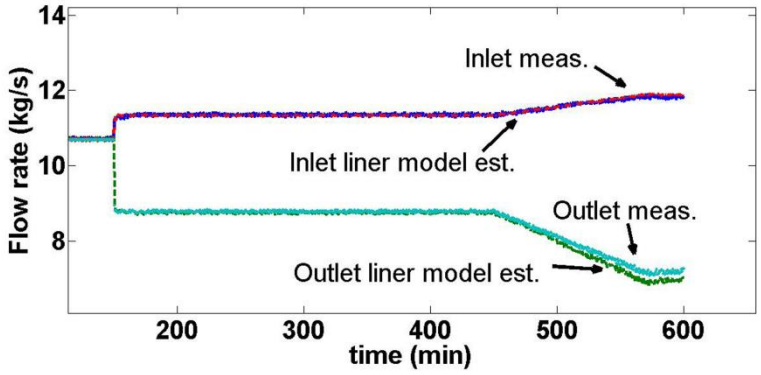

Figure III.5. Comparison of flow rate between the reduced linear model (inlet and outlet linear model estimation) and the non-isothermal model (inlet and outlet measurement)

Table III.1. Parameters for the linear model in Equation (3.7) and Equation (3.8)

a_0	a_1	a_2	a_3	a_4
0.227703	0.026773	0.000441	0.001321	0
b_0	b_1	b_2	b_3	b_4
-0.69458	-0.05688	0.01312	0.00766	0

Table III.2. Parameters for the unknown input observer in Equation (3.9)

F_0	F_1	F_2
$\begin{bmatrix} 3.012\times10^{-4} & 0 \\ 0 & 3.012\times10^{-4} \end{bmatrix}$	$\begin{bmatrix} 2.9218\times10^{-4} & 0 \\ 0 & 2.9218\times10^{-4} \end{bmatrix}$	$\begin{bmatrix} 2.9218\times10^{-4} & 0 \\ 0 & 2.9218\times10^{-4} \end{bmatrix}$
G_0	G_1	G_2
$\begin{bmatrix} -3.012\times10^{-4} & 3.012\times10^{-4} \\ 0 & 0 \end{bmatrix}$	$\begin{bmatrix} -2.9218\times10^{-4} & 2.9218\times10^{-4} \\ 0 & 0 \end{bmatrix}$	$\begin{bmatrix} -2.9218\times10^{-4} & 2.9218\times10^{-4} \\ 0 & 0 \end{bmatrix}$
F_3	G_3	F_4
$\begin{bmatrix} 2.9218\times10^{-4} & 0 \\ 0 & 2.9218\times10^{-4} \end{bmatrix}$	$\begin{bmatrix} -2.9218\times10^{-4} & 2.9218\times10^{-4} \\ 0 & 0 \end{bmatrix}$	$\begin{bmatrix} 5.3446\times10^{-4} & 0 \\ 0 & 5.3446\times10^{-4} \end{bmatrix}$
T	N	G_4
$\begin{bmatrix} 1 & -1 \\ 0 & 0 \end{bmatrix}$	$\begin{bmatrix} 0 & 1 \\ 0 & 1 \end{bmatrix}$	$\begin{bmatrix} -5.3446\times10^{-4} & 5.3446\times10^{-4} \\ 0 & 0 \end{bmatrix}$

Figure III.5 shows a comparison of the boundary flow rates between the reduced linear model and the non-isothermal nonlinear model. Boundary flow rates from both the

non-isothermal models and the reduced linear model are compared at steady state during the first 450^{th} minutes. As the figure shows, the steady state flow rate from the linear model is the same as the nonlinear model during this time. However, when the change of consumer usage is applied after 450^{th} minutes, the dynamic process introduces parameter uncertainty and causes a flow rate mismatch at high consumer usage between the linear reduced model and non-isothermal nonlinear model.

Figure III.6 shows the comparison of flow rates between estimation from the unknown input observer and the non-isothermal models without a leak. As the figure demonstrates, the observer can estimate the boundary flow rate due to its feed-back design. Table III.2 lists the parameters for the unknown input observer. The parameters obtained from **Theorem 3.2** were validated using **Theorem 3.3**. In Equation (3.14), γ is set as 1 and parameters in Table III.2 were introduced into the equation to validate the existence of the linear matrix inequality. Using MATLAB toolbox, the existence of Equation (3.14) is validated, which indicated the effect of process measurement noise on the estimation is smaller than 1 according to **Theorem 3**. This procedure is to validate a given γ value rather than to solve a minimal γ. If a given γ value cannot guarantee the existence of Equation (3.14), a higher value of γ need to be searched.

A residual signal is defined as the difference between the estimation and the measurement of a boundary flow rate. In our paper, the residual is calculated as the difference of flow rate from the observer estimation and the non-isothermal model. Only the residual signal from inlet flow rate is shown in our study as the outlet residual signal is always zero due to the calculated parameter of the observer listed in Table III.2.

Figure III.7 shows the simulation results of the residual signals from nominal operation (3.7a), a sudden pressure drop (3.7b), and a temperature increase or decrease (3.7c and 3.7d). The variation in the residual signal under the nominal operation is due to the addition of 0.5% measurement noise. As shown in Figure III.7b, a sudden change of operating condition can lead to a temporary drift of residual signal. The inlet pressure drops when a leak occurs or consumer usage increases. This pressure drop generates a negative residual value and the decrease of inlet pressure will decrease both the inlet and outlet flow rate.

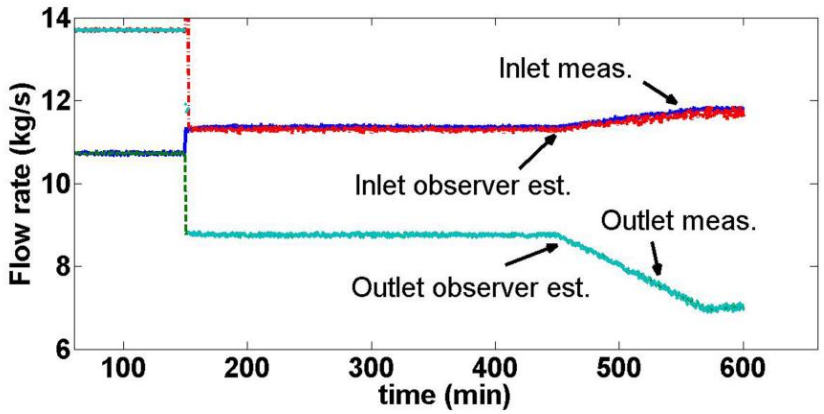

Figure III.6. Comparison between the unknown input observer (inlet and outlet observer estimation) and the non-isothermal model (inlet and outlet measurement)

In non-isothermal modeling, variations in ground temperature will cause a change in the boundary flow rate. Figure III.7c illustrates the effect of a sudden increase in ground temperature of 10 K over a 30 second time period, an extreme case meant to demonstrate the effect of temperature change. The figure shows that the increase of ground temperature will lead to a sharp negative residual signal, whereas a temperature

decrease will result in the opposite effect. The result of a case with a 2 K decrease in temperature in 30 second is shown in Figure III.7d, where the residual signal for this small temperature change cannot be distinguished from the background noise. The results indicate that a small change of temperature in short time will have negligible effect on the residual signal and leak detection in our simulation.

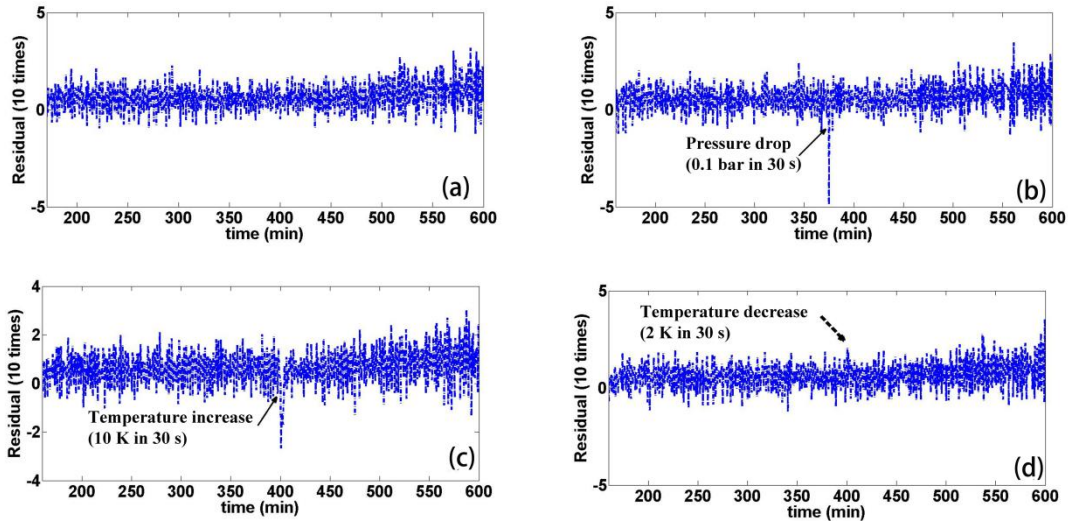

Figure III.7. Residual signals from the observer at different situations

Residual signals from a leak are demonstrated in Figure III.8. The residual signal from a leak occurrence leads to a consistent positive residual signal but the residual signal of pressure drop is a sharp decrease when assuming conventional control is applied to the pump to maintain constant pressure. Figure III.8a and III.8b show the simulation results of residual signals with leaks of varying sizes. In our simulation results, a 0.5% of measurement white noise is added to the process. The figure shows a 0.7% (of the original steady state flow rate) leak can be identified based on the residual

signal. The 1.5% leak result shows that a bigger leak will lead to higher residual signal. Figure III.8c shows the residual signal of a leak when the inlet pressure drops at the same time. As can be seen in the figure, the residual signal went through a sharp decrease due to a pressure drop then went back to a positive value because of the leak occurrence. Software-based leak detection methods sometimes fail due to process disturbances, but as Figure III.8 shows our work can detect leaks when it is slightly bigger than the noise level.

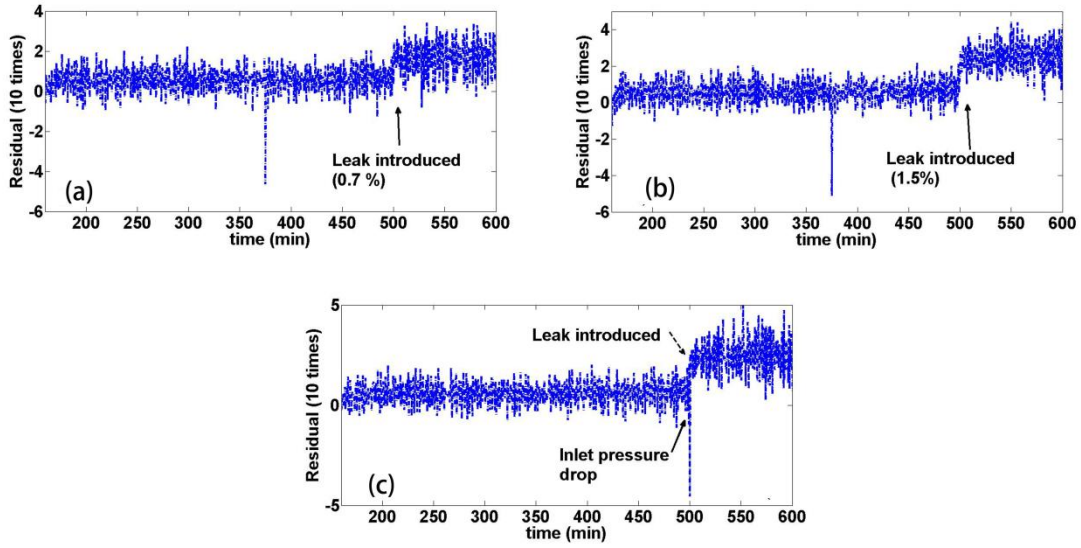

Figure III.8. Residual signals from observer with leaks of varying sizes: (a) 0.7% leak, (b) 1.5% leak and (c) 1.5% leak with an additional inlet pressure drop

Figure III.9 shows the boundary flow rates from the observer estimation and simulated measurement generated from the non-isothermal model. As demonstrated in our previous study, under the condition of fixed boundary pressure, the inlet flow rate will increase and the outlet flow rate will decrease due to the leak. Figure III.9a shows

an increase in the inlet flow rate measurement in the presence of a leak, but the flow rate estimate from the observer remains as if no leak had occurred. Since the inlet flow rate always increases when a leak occurs, the residual signal of a leak is always a positive constant. Figure III.9b demonstrates the comparison of boundary flow rates between the observer estimation and the measurement when a leak and pressure drop happen at the same time. As shown in the figure, the observer can estimate the flow rate in presence of a sudden pressure drop.

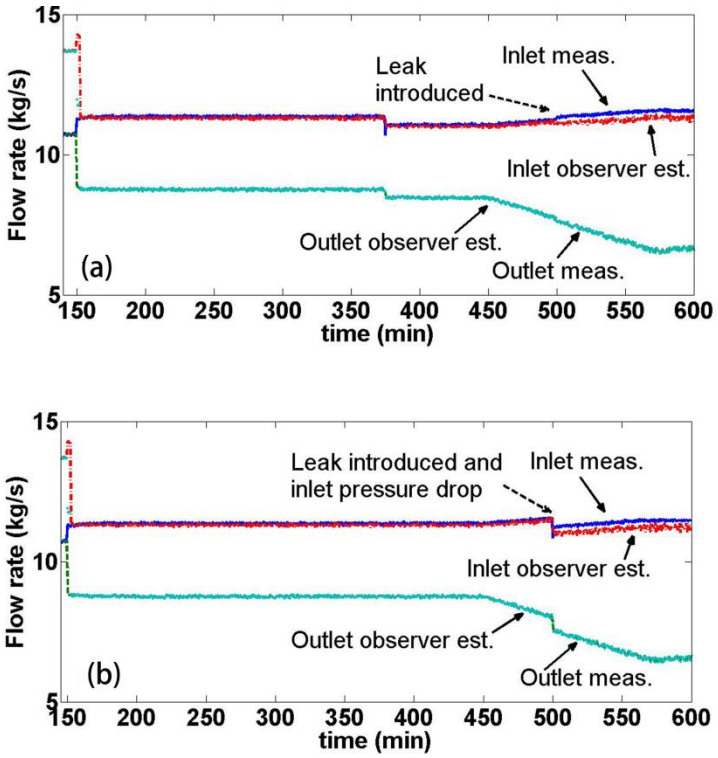

Figure III.9. Comparison of boundary flow rate between observer estimation and 'measurement' data from non-isothermal model

Estimation of leak location

A new leak location estimation algorithm is proposed to include the process disturbances of pressure drop and temperature change. The first step is to identify a leak from a process disturbance based on the pattern of the residual signal. If a disturbance is identified, indicated by a temporary drop of the residual signal, the reduced linear model in Equation (3.7) and Equation (3.8) are updated by recalculating $q_{st.}$, adding the disturbance information into the model. If a leak is identified, indicated by a constant increase of the residual signal, the leak location is estimated using the linear model estimation in Equation (3.7) and Equation (3.8) and the measurement of boundary flow rate.

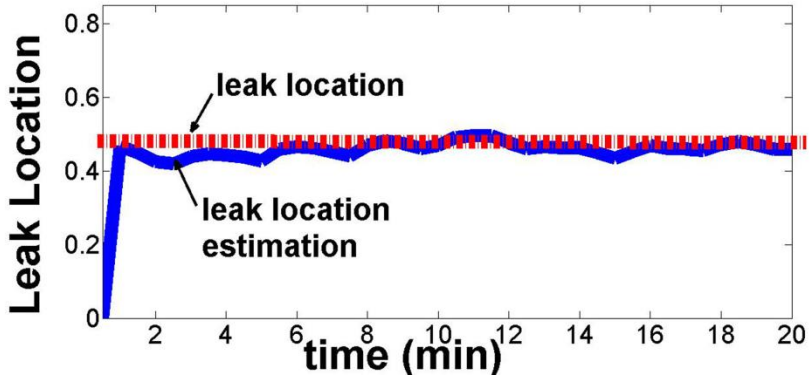

Figure III.10. Estimation of leak location

The leak location is estimated using the following equation, which is a simplified form of Equation (3.5d):

$$X_L = \frac{L}{\left(1 - \frac{E(q_{in} - q_{est.in})}{E(q_{out} - q_{est.out})}\right)}$$

where the variables $q_{est.in}$ and $q_{est.out}$ represent the estimated inlet and outlet flow rate from the linear model in Equation (3.7) and Equation (3.8) and the variables q_{in} and q_{out} represent the measured inlet and outlet flow rate from a pipeline. X_L is the estimated leak location and L is the length of the pipeline. E is the aveage of the previous ten measurements. The results of our methodology are demonstrated in Figure III.10. As shown, the location estimation from the observer can quickly converge to the accurate leak location within several minutes.

Summary of the chapter

One of the biggest safety concerns in the chemical manufacturing industry is the leakage of pipelines during chemical transportation. Software-based analysis is one of the main methods for detecting and locating a leak from pipelines without the need for extensive instrumentation. However, software-based methods are generally very sensitive to process disturbances, which cause the method to fail. In order to deal with these disturbances without increasing the number of measurements, a software-based observer is designed for leak detection in transportation pipelines using a natural gas as a case study. The proposed design implements a linear unknown input observer with time-delays that considers changes of temperature and pressure as unknown inputs and includes measurement noise in the process. The unknown input observer is modified from an existing observer for application of leak detection and the necessary and sufficient condition is provided. Non-isothermal modeling and simulation of a natural

gas pipeline with time-variant consumer usage is performed to test the proposed method. Effects of pressure drop and temperature change on observer estimation are simulated and compared to a simulated leak event. Finally, an algorithm is proposed to incorporate the disturbance information for estimating the location of a leak.

CHAPTER IV

OBSERVER AND PARTIAL DEIFFERENTIAL EQUATION-CONSTRAINED OPTIMIZATION FOR DETECTION OF MULTIPLE LEAKS

Introduction

Algorithms for estimation of a single leak have been studied extensively and reviewed in Chapter II and Chapter III, basing on both isothermal and non-isothermal modeling of liquid/gas transportation in a pipeline.

Detection of subsequent multiple leaks from a natural gas pipeline have not been studied. Multiple leaks from a pipeline can be categorized into subsequent multiple leaks and simultaneous multiple leaks. Detection of subsequent two leaks from a water pipeline has been demonstrated by using multiple observers by Verde et al.[123] A major difference between a liquid and a gas pipeline is the change of gas phase along with temperature change. Hydraulic models for isothermal (liquid) and non-isothermal transportation have different structures due to the presence of thermal-related parameters. We showed the effect of temperature change on the flow of natural gas in pipeline in Chapter II. In this chapter, we extended the content of Chapter III to a case for detection of multiple subsequent leaks.

The above-mentioned or other methods for detection of a single leak cannot be applied directly to detect simultaneous leaks because they use steady-state value of the boundary flow rate. For a pipeline with simultaneous multiple leaks, multiple leaks can be mistakenly interpreted as a single leak at a different location when the steady-state

value of boundary flow rate was used. Thus, it is necessary to investigate the dynamic response of the flow rate to locate simultaneous multiple leaks. Detection of simultaneous multiple leaks from a water pipeline has been showed by Verde et al. [124,125] However, this method cannot be applied directly to a non-isothermal natural gas pipeline due to the high complexity of the non-isothermal natural gas flow model. As we have examined, the isothermal model cannot reproduce the non-isothermal dynamic response of the flow rate, which is due to the effect of thermal properties, so the detection of multiple simultaneous leaks from a natural gas pipeline requires non-isothermal model.

Detection of simultaneous multiple leaks from a natural gas pipeline can be solved as a partial differential equation-constrained global optimization problem with both continuous and integer variables. The objective function of the global optimization is to minimize the error between measurement and estimation of the boundary flow rate. The existence of the integer variable, which is the leak location, hinders the application of gradient-based algorithm for optimization. Partial differential equation -constrained optimization has been studied by many researchers.[126–129] However, due to the specificity of the optimization problem for simultaneous multiple leaks, the current optimization algorithm cannot be directly applied to solve the problem. Current derivative-free global optimization algorithms such as genetic algorithm[129], Monte Carlo simulation[130,131], or particle swarm[132] need extensive computation cycles and time. However, estimating leak locations is an urgent task which aims at reducing financial lost and potential explosion risk.

To solve this optimization problem in a time-efficient manner, a new global optimization algorithm is proposed. The algorithm first discretizes the pipeline with large mesh size (the integer variable) and the Newton's method is applied to find the first approximate locations. Then further discretization is performed around the approximate location and the Newton's method is repeated. After repeated further discretization, a more and more accurate location approximation can be achieved. Due to the sensitivity of the environment temperature on the flow rate of the natural gas in the pipeline, a prior knowledge of temperature, either from measurement or estimation was needed for the optimization algorithm to detect multiple simultaneous leaks. In the study of detecting simultaneous multiple leaks, no process disturbance was considered.

Methodology for detecting multiple leaks

Detection of subsequent multiple leaks: observer design

Based on the non-isothermal models and isothermal model introduced in Chapter II and Chapter III, the same procedure can be applied for designing an observer as explained in Chapter III.

The following summarize the steps for designing such observer for a pipeline system.

First step is to reduce the isothermal flow model into a discrete-time linear model. For a pipeline with consumer usage at known location, a reduced linear model is given as followed.

$$q_{in}(t)=q_{in.st.}+\sum_{i=0}^{n} a_i\, q_{usage}(t-i)$$

$$q_{out}(t)=q_{out.\,st.}+\sum_{i=0}^{n} b_i q_{usage}(t-i)$$

q_{usage} represents the consumer usage in the pipeline, in a case of straight pipeline without any consumer usage, the parameter associated with the consumer usage becomes zero. $q_{in}(t)$ and $q_{out}(t)$are the time-variant inlet and outlet flow rate due to the existence of consumer usage. $q_{in.st.}$ and $q_{out.st.}$ are the inlet and outlet flow rate at steady state. The detailed model reduction can be found from Chapter III.

The second step is to design an unknown input observer and solve the parameters of the unknown input observer through a linear matrix inequality method. An unknown input observer is a state estimation method for a system with certain unexpected process disturbance. The detailed development of the unknown input observer and model reduction are explained in Chapter III.

$$x(t)=\sum_{i=0}^{n} A_i x\left(t-\tau_i\right)+\sum_{i=0}^{n} B_i u\left(t-\tau_i\right)+Ww(t)$$

$$y(t)=Cx(t)+Md(t)$$

In which, $x(t)$ is the state, $y(t)$ is the measurement, $u\left(t-\tau_i\right)$ is the input (consumer usage), $d(t)$ is measurement noise which is assumed white noise, and $w(t)$ is the unknown input. W is the parameter matrix for the unknown input, which was determined by the simulation study on effect of the unknown inputs to the system. An unknown input observer can be designed as shown below.

$$z(t)=\sum_{i=0}^{n} F_i z\left(t-\tau_i\right)+\sum_{i=0}^{n} TB_i u\left(t-\tau_i\right)+\sum_{i=0}^{n} G_i y\left(t-\tau_i\right)$$

$$\hat{x}(t)=z(t)+Ny(t)$$

in which, *F*, *T*, *B*, and *G* are process parameters for the unknown input observer that need to be determined. $\hat{x}(t)$ is the estimation of the state and $y(t)$ is the measurement

from the system. Method to solve the parameters of the observer was given in Chapter III, which is not shown here. Process disturbances such as temperature change and pressure oscillation at pump station were treated as unknown inputs. The effects of process disturbance were studied in our previous study and applied for constructing the observer.

Third step is to apply unknown input observer to estimate the flow rate of the natural gas, and compare the estimation value of flow rate with flow rate measurement. Detection of leaks from a pipeline is based on the analysis of a residual value. A residual value is defined as the difference between measurement and estimation from the observer of flow rate. Our previous study shows that the designed unknown input observer can distinguish the process disturbance such as pressure and temperature change from a leak event basing on the residual value as shown in Chapter III. Multiple leaks can be detected subsequently according to the residual value which will be shown in the results section.

The fourth step involves identifying the leak from the residual signal and locating the leak in a pipeline. Equation (2.29) is applied to calculate the leak location.[12]

$$X_L = L/\left(1 - \frac{E(q_{in} - q_{in.est.})}{E(q_{out} - q_{out.est.})}\right)$$

X_L is the estimated leak location and L is the total length of the pipe. $q_{in.}$ and q_{out} are the measured inlet and outlet flow rate. $q_{in.est.}$ and $q_{out.est.}$ are inlet and outlet flow rate estimated from the reduced model.

When a leak was identified basing on the residual value, the steady state values $q_{in.st.}$ and $q_{out.\ st.}$ are updated to so $q_{in}(t)$ and $q_{out}(t)$ will match the flow rate measurement at steady state. The updated reduced linear model can also account for any temperature change and pressure change. The updated equations are used for detecting possible more leaks and estimating the leak location.

Detection of simultaneous multiple leaks: development of an optimization algorithm

A new global optimization algorithm is proposed to locate multiple leaks in a natural gas pipeline. The objective function of the optimization is to minimize the error of the dynamic response of boundary flow rate between measurement and model estimation. The optimization problem assumes a prior knowledge of temperature and does not consider oscillation of pump pressure. There are both integer variables (leak location) and continuous variables (leak size) in the optimization problem. The optimization problem is formatted as the following.

$$\min_{u\,(q_L)} \sum_{i=0}^{N} (\hat{y}_i-\bar{y}_i)^T Q\ (\hat{y}_i-\bar{y}_i)$$

$$\text{s.t.} \qquad \frac{\partial P}{\partial t}_{x=0}=0,\ \frac{\partial P}{\partial t}_{x=L}=0;\ q_{L1x}, q_{L2x} \in \Theta; \qquad q_{L1s} \in \Gamma$$

$$y_i=\begin{bmatrix} q_l \\ q_0 \end{bmatrix};\ u=\begin{bmatrix} q_{L1x} & q_{L2x} & q_{L1s} \end{bmatrix}$$

$$\frac{\partial P}{\partial t}=\frac{-\frac{1}{A}\frac{\partial q}{\partial x}-\frac{1}{A\Delta x}q_L+\left(\frac{1}{ZC_P}\frac{\partial Z}{\partial T}+\frac{1}{TC_P}\right)\left(\frac{fq^3z^2R^2T^2}{2DA^3P^2}-\frac{4U(T-T_g)}{D}-\frac{q}{A}C_P\frac{dT}{dx}+\left(\frac{T}{Z}\frac{\partial Z}{\partial T}+1\right)\frac{q}{AP}ZRT\frac{dP}{dx}\right)}{\left(\frac{1}{ZRT}-\frac{P}{Z^2RT}\frac{\partial Z}{\partial P}-\left(\frac{\partial Z}{\partial T}\right)^2\frac{T}{Z^2C_P}-\frac{2}{ZC_P}\frac{\partial Z}{\partial T}-\frac{1}{TC_P}\right)}$$

$$\frac{\partial q}{\partial t}=-A\frac{\partial P}{\partial x}-\frac{AP}{ZRT}g\sin\theta-\frac{fq^2}{2DAP}ZRT-\frac{1}{A}\frac{q_L}{\Delta x}\left(\frac{q}{P}\right)ZRT$$

$$\frac{\partial T}{\partial t}=\frac{\left(\frac{1}{ZRT}-\frac{P}{Z^2RT}\frac{\partial Z}{\partial P}\right)\frac{\partial P}{\partial t}}{\left(\frac{P}{Z^2RT}\frac{\partial Z}{\partial T}+\frac{P}{ZRT^2}\right)}+\frac{\frac{1}{A}\frac{\partial q}{\partial x}}{\left(\frac{P}{Z^2RT}\frac{\partial Z}{\partial T}+\frac{P}{ZRT^2}\right)}+\frac{q_L}{A\Delta x}\frac{1}{\left(\frac{P}{Z^2RT}\frac{\partial Z}{\partial T}+\frac{P}{ZRT^2}\right)} \quad (4.1)$$

$\hat{y}_i$ is the measured boundary flow rate at time step i, and $\bar{y}_i$ is the estimated boundary flow rate at time step i. *N* refers to the total time of dynamic response. Boundary conditions (fixed boundary pressure) are applied to the optimization problem and assumed validated during the dynamic response. q_{L1x} and q_{L2x} refer to the leak location, which are constrained variable. q_{L1s} represents the first leak size. The other leak size can be calculated by subtracting q_{L1s} from total leak (considering a two-leak case). To avoid massive computational time and improve the calculation efficiency, a new adaptive discretization method was developed and applied in our solution. The optimization problem was solved using the Hessian-based Newton's method. The goal of the optimization problem is to locate multiple leaks and their corresponding leak sizes. The accuracy of location estimation depends on the mesh size of the discretization.

The adaptive discretization method is illustrated in Figure IV.1. q_{L1x} and q_{L2x} are integer variables (leak location) that need to be searched as accurate as possible.

As shown in Figure IV.1, a middle point was first calculated to locate two leaks in two sections along the pipe, in which $q_{in.st.}$ and $q_{out.st.}$ are inlet and outlet flow rate before leak occurrence at steady state.

The second step is to discretize the pipeline into several large sections, and perform a global search of leak locations from each possible combination of discretized sections as shown in Figure IV.1. In the second step, because the leak locations (the

integer variables) are fixed by each possible combination of discretized sections, the Newton's method is only used to search for a possible leak size (continuous variable) to minimize the objective function. Two possible sections from both ends (divided by the middle point) were chosen as the first approximate locations basing on the numerical value of the objective function. Two pairs of possible locations with smallest objective function values were selected after screening all the possible combination of the discretized pipe sections (leak location).

The third step is to further discretize the chosen two pair of approximate locations in the step two and repeat step two to calculate the second approximate locations. The third step is repeated until satisfied estimation accuracy of leak locations were achieved basing on the discretization size.

We demonstrated two examples on the detection of simultaneous multiple leaks with different leak locations and leak sizes. The two leaks have close leak sizes in the first case and big difference in the second case. Both leaks are smaller than 5%. Newton's method was applied to find the minimal objective function in all these combinations of possible leak locations. The Hessian matrix was calculated numerically in Newton's method.

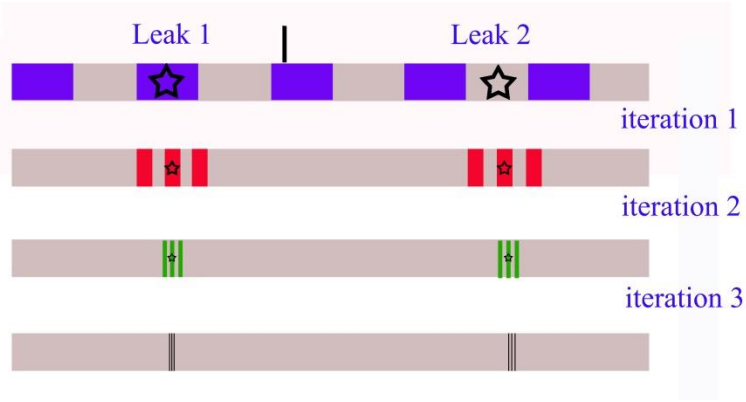

Figure IV.1. Illustration of the optimization algorithm

Results and discussion

Detection of subsequent multiple leaks

Several research papers have proposed methods to detect subsequent leaks from a water pipeline including multiple observers. Due to the complicity of the natural gas flow model, the method proposed for water pipeline cannot been applied for detecting a natural gas pipeline when considering process noise in terms of temperature change or pressure drop. Furthermore, our observer method can be directly applied to three or more subsequent leaks without modifying the algorithm. Simulation results of detecting subsequent leaks are shown in Figure IV.2.

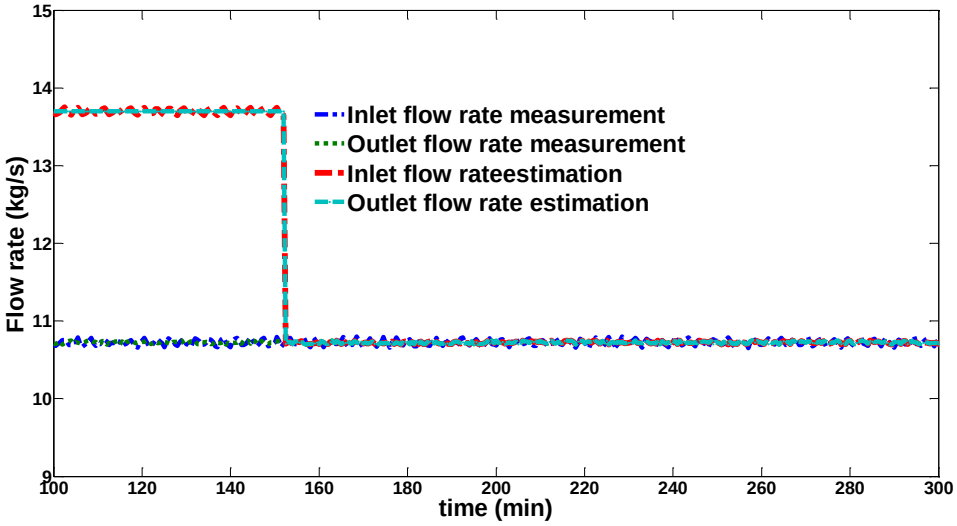

Figure IV.2. Comparison of boundary flow rate between measurement and observer estimation

Figure IV.2 shows the comparison of the flow rate estimation from the observer and flow rate measurement from the simulation when the consumer usage is zero. The observer estimation starts from 150 min. As can be seen in the figure, the estimation from the unknown input observer overlaps with the measurement which indicates a good estimation of the boundary flow rate.

Current available method to deal with the process disturbance is to perform the real-time modeling/simulation when the pressure and temperature information is available. However, our observer method provides easier way to study the effect of pressure and temperature drop without the measurements of pressure and temperature, which reduce the requirement of extra instrumentation.

The residual value of two leaks is shown in Figure IV.3, which shows the detection of subsequent second leak. As can be seen in the figure, a subsequent two

increase of residual value indicated two leaks at different time. Without changing any structure and parameter of the observer, the observer is able to identify more leaks basing on the residual value. To estimate the location of the second leak, $q_{in.st.}$ and $q_{out.st.}$ are updated so that $q_{in}(t)$ and $q_{out}(t)$ equal to the measured inlet and outlet flow rate. The estimation of leak location for the first two leaks is showed in Figure IV.4. As shown in the figure, the estimation of leak location can converge within 20 minutes. The oscillation of the location estimation is due to the process measurement noise.

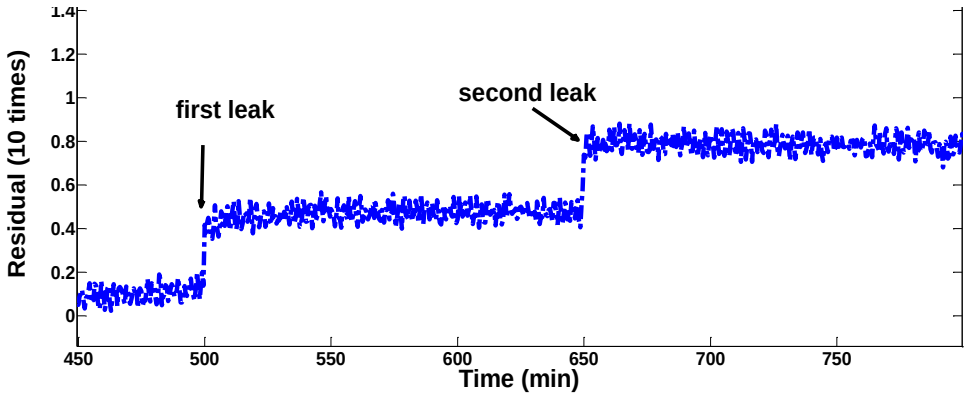

Figure IV.3. Residual value of the observer in the presence of two leaks

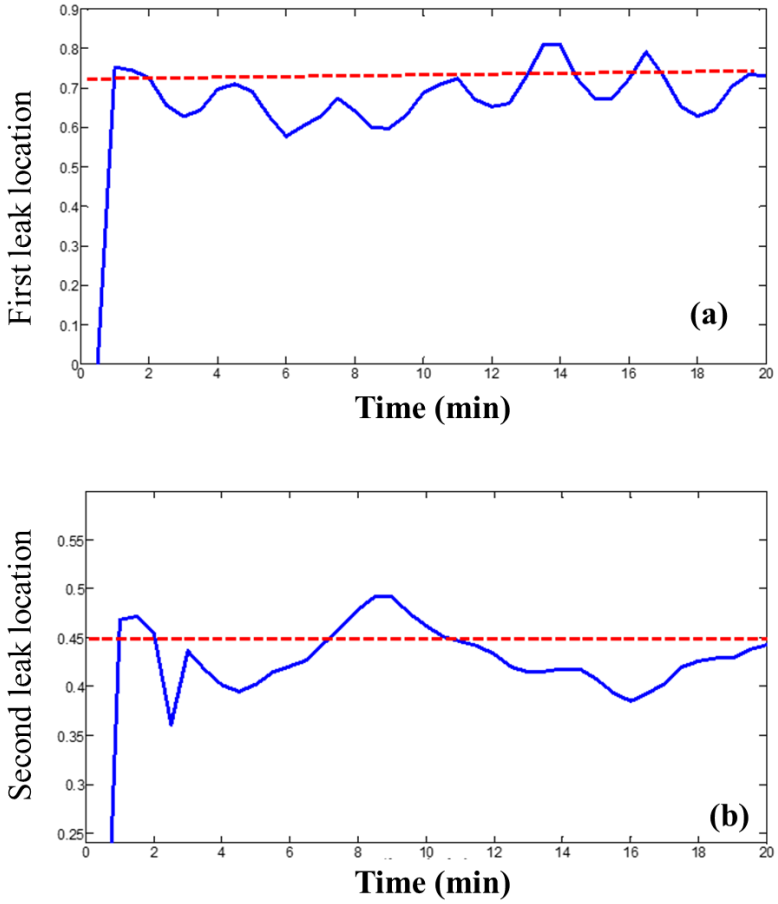

Figure IV.4. Leak location estimation for the first and second leak

Further examples of more leaks are not demonstrated here, which can be applied the same principle demonstrated in the second leak.

Detection of simultaneous multiple leaks

Table IV.1. Case study of two simultaneous leaks

	Leak I location (% of Length)	Leak I size	Leak II location (% of Length)	Leak II size
Case I	0.736	4.0%	0.277	1.6%
Case II	0.418	3.6%	0.797	1.2%

Table IV.1 shows the information of two-case study for detection of simultaneous two leaks. Two leaks with both less than 5% were introduced into a straight pipeline at different locations. For both cases, the pipeline is discretized into 8, 16, 32, and 64 sections in each step. Numerical values of each optimization circle are demonstrated.

The optimization problem contains an integer variable, which is a location-related variable. Calculating the gradient of the integer variable is not possible for this problem. It is required to have a faster way to search for the integer variable in a time-efficient way rather than the global derivative-free optimization. Following the procedure introduced in the previous section, a middle point is calculated based on the steady state flow rate with leaks. For the first circle in case I, the pipeline is discretized into 8 sections, and 20 optimizations are performed. The first optimization involve optimizing the discretized section-pairs of (1,4), (1,5), (1,6), (1,7), and (1,8). Same principles are applied to section-pairs starting with section 2, 3, and 4. Each optimization uses the Newton's method. To shorten the calculation time, the initial guess of the continuous variable (one of the leak size) is set as the half of the total leak size. And

eight Newton's steps are performed. As shown in Table IV.2, section-pairs of (3, 6), (3, 7), (4, 6), and (4, 7) were selected which has the minimal objective function value. For the second optimization circle, the pipeline is further divided into 16 sections, and 16 optimizations were performed by further dividing the selected sections in circle I. In circle III and circle IV, the pipeline is discretized into 32 and 64 sections, and 16 optimizations were performed for each circle. In our study, we perform 4 optimization circles, and further optimization circle with more discretization can be continued. Table III shows the optimization result for leak detection of case II, which followed the exact same procedure.

For each circle of iteration, after the integer variable is fixed, Newton's method is applied to calculate the corresponding leak size. It is worth noticing that the PDE constraint in Equation (4.12) is not a second-order differentiable, because the higher order term of the compressibility factor is not available. Both first order derivative and second-order derivative are both calculated numerically. The numerical error of calculating first and second order derivative will bring in optimization error. To account for these possible numerical errors, for each circle of iteration, the lowest four pairs of possible of leak location were further discretized instead of one possible pair of leak location. This operation will require more calculating circles, however, it will deliver more accurate results.

Table IV.2. Optimization results of leak detection for simultaneous leaks case I

Circle/ Discretization number	Number of optimizations	Pipeline discretization section number and Value of objective function in Equation(4.1)		
I/8	20	Section number	6	7
		3	1.6519	0.6916
		4	1.9201	0.9056
II/16	16	Section number	12	13
		5	0.3156	0.6648
		6	0.3415	0.4841
III/32	16	Section number	23	24
		8	0.1806	0.1171
		9	0.1481	0.0974
IV/64	16	Section number	48	
		17	0.0763	
		18	0.0766	

Table IV.3. Optimization results of leak detection for simultaneous leaks case II

Circle/ Discretization number	Number of optimizations	Pipeline discretization section number s and Value of objective function in Equation(4.1)		
I/8	20	Section number	6	7
		3	0.6543	0.6953
		4	1.1743	1.0227
II/16	16	Section number	13	14
		7	0.2207	0.1579
		8	0.1289	0.2193

Table IV.3. Continued

Circle/ Discretization number	Number of optimizations	Pipeline discretization section number s and Value of objective function in Equation(4.1)		
III/32	16	Section number	25	26
		13	0.1010	0.1099
		14	0.0782	0.1006
IV/64	16	Section number	52	
		27	0.0600	
		28	0.0564	

Table IV.4 summarizes the comparison between real leak location and location estimation from optimization. As can been seen in the table, after 4 circles of optimization, the estimated leak location is very close to the real location. With the assumption of a pipeline between two stations is 10 km, the average estimation error is 100 m.

Table IV.4. Comparison of real leak and optimization result

	Leak 1: real leak / optimization result	Leak 2: real leak / optimization result
Case 1	0.736 / 0.75	0.277 / 0.273
Case 2	0.797/0.8125	0.418/0.429

Summary of the chapter

Software-based methods are easy-to-implant approaches for detecting faults in chemical process. In this paper, new software-based methodologies were developed for detecting multiple leaks in a natural gas pipeline. Two different types of multiple leaks, subsequent and simultaneous multiple leaks, were studied and two different methods were proposed, separately. For both subsequent and simultaneous leaks, case studies with two-leak occurrence were performed using MATLAB® and simulation results were demonstrated.

For detecting subsequent multiple leaks in a natural gas pipeline, an unknown input observer was designed. Process disturbances from pump station and temperature change were addressed in the design of the observer. In the simulation study, disturbances from pump station and temperature change were introduced separately and the performance of the observer was tested. Simulation results showed that the observer was able to identify and locate subsequent multiple leaks in the presence of process disturbances.

New optimization method for detection of simultaneous multiple leaks from a natural gas pipeline was demonstrated. Leak locations were estimated by solving a global optimization problem. The global optimization problem contains constraints of linear and partial differential equations, integer variable, and continuous variable. An adaptive discretization approach combined with Newton's method was designed to search the leak locations.

CHAPTER V

A METHODOLOGY FOR ESTIMATION OF UNMEASURED STATE IN A BIOREACTOR UNDER DISTURBANCE

Introduction

Process states are key information to evaluate a chemical process for process safety and process improvement such as process monitoring, real-time optimization, and advanced process control.[133,134] In certain chemical processes where some process state information cannot be measured in real-time, process state estimation techniques have been developed to predict the state information simultaneously.

Model-based state estimation is a widely applied and powerful approach to obtain state information. The model-based method requires a high-fidelity model which can describe the chemical process precisely. However, for some complex process such as a bioprocessing, extensive knowledge and effort is required to build a reliable model to describe the whole system. For the scenarios disturbance or unknown input information is not captured by the models, significant model-plant mismatch will occur. In the case of bioprocessing, several situations can generate model-plant mismatch which can be treated as unknown input or disturbance, such as the effect of nutrient limitation, oxygen delivery at high cell density, and carbon dioxide stripping.[135–137]

There are several different attempts to address the model-plant mismatch. One of the solutions is to apply parameter estimation for each run of the experiments.[138,139] However, adaptive parameter estimation requires extensive measurements of states and

cannot be used for state estimation for a new experiment until a new set of parameters is determined. Filters and observers are mathematical methods which offer an alternative method for state estimation in the presence of model-plant mismatch to extract state information from corrupted measurements.[140–142] Filtering and observer based state estimation have been extensively studied for process optimization and advanced process control.[133,143] Kalman filter and extended Kalman filter are the most widely used filtering methods to estimate the state from a noisy measurement.[144] Lee et al. proposed using an extended Kalman filter based nonlinear model predictive control (MPC) method for nonlinear systems.[145] Senthil et al. proposed nonlinear observer based model predictive control using a fuzzy Kalman filter and an augmented state Kalman filter, and a simulation study using a CSTR was provided.[146] Qin et al. integrated white noise disturbance models with model predictive control for disturbances or model-plant mismatch. The author also applied a data-based auto-covariance technique to estimate the appropriate covariance and the filter gain for a Kalman filter.[147] Rohani et al. applied extended Kalman filter for state estimation in nonlinear model predictive control, and a case study of crystallizer was provided.[148] Other nonlinear Kalman filter based filters, such as unscented Kalman filters that do not require the calculation of a Jacobian matrix, are suitable for nonlinear systems with high nonlinearity that makes the calculation of the Jacobian matrix difficult. Shah et al. applied an ensemble Kalman filter and an unscented Kalman filter for state estimation of an autonomous hybrid system.[149]

Design and application of different observers have been demonstrated by researchers.[150–152] Certain types of observers, such as high gain observer and moving horizon observers, are proposed for advanced control.[153] Christofides et al. used a high gain observer to estimate the nonlinear state information and a Lyapunov-based approach to design an economic MPC system.[134] Chehimi et al. developed an unknown input observer based output feedback predictive controller for induction motors. The design of the unknown input observer and its assumptions are discussed.[154] Yan et al. incorporated state estimation into model predictive control by applying probabilistic constraints.[155] Patwardhan et al. developed generalized likelihood ratio− based fault diagnosis and identification scheme to correct the state estimation for MPC.[156]

An unknown input observer was developed to estimate the state when the process is operating with certain types of faults and disturbance.[50] Compared to other observers, unknown input observer can eliminate the effect of certain disturbances or faults despite their size. The design of a linear unknown input observer with both full and reduced order has been provided, and the sufficient and necessary conditions for such an observer have also been discussed.[50,150,152,157,158] However, for most chemical processes, the inherent nonlinearity hinders the application of such linear observers. Some attempts have been made to design a nonlinear observer in a more general format.[49,159] The drawbacks of such operation, including the bilinear work and other research efforts such as the state transformation to change the original nonlinear systems into canonical forms, has been discussed in literature.[160–162] To the best of our knowledge, there is not yet a systematic way to design a nonlinear unknown input observer for any nonlinear system.

The design of a class of unknown input observers for a Lipschitz system has been demonstrated by Chen and Saif through a linear matrix inequality method.[159] However, the nonlinear system proposed in this work is not developed for a general form of a nonlinear system, which limits its applications to certain specific systems.

In this paper, we developed a new design for a nonlinear unknown input observer using a more general nonlinear format, which opens the opportunities for more possible applications. The sufficient and necessary conditions for such observer are discussed. Experimental validation of the design and application of the new unknown input observer is demonstrated using a bioreactor case study.

Design of a nonlinear unknown input observer

An unknown input observer is designed for general nonlinear systems without the restriction of linear state and linear input terms as in Saif's work.[159] To design a nonlinear unknown input observer with linear unknown inputs, a nonlinear system with unknown inputs is written in the following format, in which, $x \in R^n$, $y \in R^k$, and $u \in R^p$ are the state vector, the output vector, and known input vector, $d \in R^d$ is the unknown input in the system, and E is assumed of full rank.

$$\dot{x}=f(x,u)+Ed \tag{5.1}$$

$$y=Cx$$

Remark: In Equation (5.1), the nonlinear system is coupled with a linear disturbance Ed where E is a constant parameter matrix.

An unknown input observer is designed in the following form:

$$\dot{z}=(I-HC)f(z+Hy,u)-K(y-\hat{y}) \tag{5.2}$$

$\hat{x}$=z+Hy

H and K are the parameters for the observer which need to be calculated. $\hat{x}$ is the estimation of the state x. To design the unknown input observer, existence conditions are listed below.

Existence condition: the existence of an unknown input observer needs to satisfy the following conditions:

1. E=HCE (5.3.1)
2. rank (CE)=rank (E) (5.3.2)
3. Local Lipschitz condition:

   $\left|f(x,u)-f(\hat{x},u)\right|\leq\gamma\left|x-\hat{x}\right|$, γ is a positive constant number (5.3.3)
4. K satisfies **Theorem 5.1**

The existence of an observer is needed to verify that the estimation error is asymptotically stable. The Existence conditions (3.1)−(3.3) and Theorem 1 are provided to guarantee asymptotically stable estimation error.

Theorem 5.1: If there exist a symmetric matrix P>0 satisfying the following matrix inequality, then the observer is asymptotically stable

$$(KC)^{T}P+PKC+\gamma P\left(I-HC\right)\left(I-HC\right)^{T}P+\gamma I<0 \quad (5.4)$$

To explain the Existence conditions (3.1)−(3.3) and Theorem 1, the estimation error of the observer is introduced by writing $e=x-\hat{x}$. The estimation error can be derived as shown in Equation (5.5), using Equation (5.1) and Equation (5.2).

$$\dot{e}=\dot{x}-\dot{\hat{x}}=\left(I-HC\right)\left(f(x,u)-f(\hat{x},u)\right)-\left(I-HC\right)Ed+KCe \quad (5.5)$$

The Existence condition is used to simplify the dynamics of the estimation error. By applying Equation (5.3.1), the estimation error in Equation (5.5) can be reduced to Equation (5.6).

$$\dot{e}=\left(I-HC\right)\left(f(x,u)-f(\hat{x},u)\right)+KCe \tag{5.6}$$

The asymptotically stable estimation error is proved using a Lyapunov function. **Theorem 5.1** is provided to guarantee the existence of such a Lyapunov function. The proof of such the Lyapunov function is given in the following.

A Lyapunov function is chosen as $V=e^{T}Pe$, and the derivative of the Lyapunov function can be written the the following form, which is modified from Saif's paper[159] :

$$\dot{V}=\dot{e^{T}}Pe+e^{T}P\dot{e}$$

$$= \left(KCe+(I-HC)\left(f(x,u)-f(\hat{x},u)\right)\right)^{T}Pe+e^{T}P\left(KCe+(I-HC)\left(f(x,u)-f(\hat{x},u)\right)\right)$$

$$=e^{T}((KC)^{T}P+PKC)e+\left(f(x,u)-f(\hat{x},u)\right)^{T}\left(I-HC\right)^{T}Pe+e^{T}P\left(I-HC\right)\left(f(x,u)-f(\hat{x},u)\right)$$

(6a)

By applying Existence condition (3.3) in Equation (5.6a), the following inequality can be obtained.

$$\leq e^{T}((KC)^{T}P+PKC)e+2\|e^{T}(I-HC)P\|\gamma\|e\|$$

$$\leq e^{T}((KC)^{T}P+PKC)e+\gamma(\|e^{T}(I-HC)P\|^{2}+\|e\|^{2})$$

$$=e^{T}((KC)^{T}P+PKC+\gamma P\left(I-HC\right)\left(I-HC\right)^{T}P+\gamma I)e \tag{5.7}$$

By applying Shur complement method [122], Equation (5.4) in Theorem 1 can be rewritten as a linear matrix inequality in the form of Equation (5.8)

$$\begin{bmatrix} -I & \sqrt{r}P \\ (I-HC)^T\sqrt{r}P & PKC+C^TK^TP+\gamma I \end{bmatrix}<0 \tag{5.8}$$

To solve this nonlinear matrix problem, we introduce a new variable as $Y=PKC$ and $W=PH$, so the previous nonlinear matrix inequality can be transformed into Equation (5.9).

$$\begin{bmatrix} -I & \sqrt{r}P-\sqrt{r}WC) \\ \sqrt{r}P-\sqrt{r}C^TW^T & Y+Y^T+\gamma I \end{bmatrix}<0 \tag{5.9}$$

To solve this linear matrix inequality equation, parameter matrix H from Equation (5.3.1) is solved first and then applied to $W=PH$ in Equation (5.9). Equation (5.9) can be then solved using linear matrix inequality toolbox in MATLAB.

Parameter matrix H is solved similarly to the previous publication. [47] To solve parameter matrix H, define the following matrix equation in Equation (5.10) using condition Equation (5.3.1).

$$\begin{bmatrix} I-HC & H \end{bmatrix}\begin{bmatrix} I & E \\ C & 0 \end{bmatrix}=[I \quad 0] \tag{5.10}$$

H can be solved as shown in Equation (11).

$$H=[I \quad 0]\begin{bmatrix} I & E \\ C & 0 \end{bmatrix}^+[0 \quad I]+\theta(I-\begin{bmatrix} I & E \\ C & 0 \end{bmatrix}\begin{bmatrix} I & E \\ C & 0 \end{bmatrix}^+)[0 \quad I] \tag{5.11}$$

In which, $\begin{bmatrix} I & E \\ C & 0 \end{bmatrix}^+$ is a generalized inverse of $\begin{bmatrix} I & E \\ C & 0 \end{bmatrix}$, and θ is a parameter matrix with appropriate dimension which needs to be determined when solving the Equation (5.9).

The matrix inequality can be readily solved using the linear matrix inequality toolbox in MATLAB.

Experimental section

A bioreactor example is shown to demonstrate the application the more general nonlinear unknown input observer. Briefly, the cultivation of *Saccharomyces cerevisiae* strain mutant SM14 was performed in both a batch and a fed-batch scheme to produce β-carotene. The details of the bioprocessing system are described in our previous study.[163,164]

Operation and modeling of a bioreactor

A *S. cerevisiae* strain mutant SM14 engineered to produced β-carotene was used in this study. The yeast strain was stored in frozen vials at -80℃ and in plates at 4℃ which were sub-cultured every three weeks for maintenance. The cells were grown in fresh Yeast Nitrogen Base (YNB) media in all the experiments with supplemented D-glucose.

The inoculum for the bioreactor and shake-flask cultures in the following experiments were prepared from single colonies to inoculate 50 ml of YNB media (20 g/L glucose) and incubated at 30℃ for 72h with constant agitation at 200 rpm. The bioreactor studies were carried out in a 7 L, glass, autoclavable bioreactor (Applikon®, Foster City, CA). The bioreactor was inoculated with the entire seed culture. The temperature, pH, agitation speed, and airflow were set at 30℃, 4, 800 rpm, and 6 L/min. The experiments are performed using both batch and fed-batch modes.

Kinetic modeling and parameter estimation studies were performed in our previous work.[163,164] The kinetic model involves the cell growth, glucose consumption, ethanol production and consumption, acetic acid production and consumption, and β-carotene production, which is shown in Equation (5.12) − (5.17).

$$\frac{dX}{dt} = (\mu_G + \mu_E + \mu_A)\, X \tag{5.12}$$

where X is the biomass concentration and μ_G, μ_E and μ_A represents the specific growth rate on glucose, ethanol and acetic acid, respectively, which are defined in Equations (5.13a), (5.13b) and (5.13c).

$$\mu = \mu_G + \mu_E + \mu_A$$

$$\mu_G = \left(\frac{\mu_{max,G} \cdot \chi_E \cdot \chi_A \cdot G}{K_{SG} + G + a_{ge} E + a_{ga} A} \right) \tag{5.13a}$$

$$\mu_E = \left(\frac{\mu_{max,E}\, E}{K_{SE} + E + a_{eg} G + a_{ea} A} \right) \tag{5.13b}$$

$$\mu_A = \left(\frac{\mu_{max,A}\, A}{K_{SA} + A + a_{ag} G + a_{ae} E} \right) \tag{5.13c}$$

where a_{ij} represents the inhibition effect of the jth substrate on the utilization of the ith substrate by the organism. The glucose, ethanol and acetic acid concentrations are given by G, E and A. The parameters $\mu_{max,G}$, $\mu_{max,E}$, and $\mu_{max,A}$ are the maximum specific growth rates on glucose, ethanol and acetic acid, respectively. The variables χ_E and χ_A are polynomial functions fit to experimental data to account for ethanol and acetic acid inhibition on the glucose growth rate.

$$\frac{dG}{dt} = -\frac{\mu_G X}{Y_{X/G}} \tag{5.14}$$

$$\frac{dE}{dt} = k_1\ \mu_G X - \frac{\mu_E X}{Y_{X/E}} \tag{5.15}$$

$$\frac{dA}{dt} = \left(k_2\mu_G + k_3\mu_E\right)X - \frac{\mu_A X}{Y_{X/A}} \tag{5.16}$$

$$\frac{dP}{dt} = (\alpha_1\mu_G + \alpha_2\mu_E + \alpha_3\mu_A)X + \beta X \tag{5.17}$$

where $Y_{X/G}$ is the biomass yield coefficient on glucose. $Y_{X/E}$ is the biomass yield coefficient on ethanol. $Y_{X/A}$ is the biomass yield coefficient on acetic acid, where α_i represents the coefficients for growth-associated product formation related to the yeast growth on each substrate, and β is the coefficient for non-growth-associated carotenoid production. Estimation of process parameter is demonstrated in our previous work. The parameters are the same as our previous paper.[163,164] The variable *P* is used to denote the concentration of the product, β-carotene. The parameters for the model (5.12)-(5.17) given in our pervious paper.[163]

Validation experiments

Two batch and two fed-batch experiments were performed to demonstrate the application of the unknown input observer. The batch experiments start with different inoculum size, each with a slightly different level of initial glucose, ethanol, β-carotene, biomass, and acetic acid. Fed batch experiments were performed by feeding glucose with set bulk concentrations, 200 g/L or 20 g/L of glucose in YNB medium, for a defined time period. The fed-batch model was derived from the batch model with the same model parameters. Details of the validation experiment are listed in the Table V.1.

The fed batch model is developed from the batch model as shown in the following equation:

$$\frac{dX}{dt} = (\mu_G+\mu_E+\mu_A)\, X - X\cdot\frac{F_g}{V} \tag{5.18}$$

$$\frac{dG}{dt} = -\frac{\mu_G X}{Y_{X/G}} - G\cdot\frac{F_g}{V} + G_{in}\cdot\frac{F_g}{V}$$

$$\frac{dE}{dt} = k_1\,\mu_G X - \frac{\mu_E X}{Y_{X/E}} - E\cdot\frac{F_g}{V}$$

$$\frac{dA}{dt} = \left(k_2\mu_G+k_3\mu_E\right)X - \frac{\mu_A X}{Y_{X/A}} - A\cdot\frac{F_g}{V}$$

$$\frac{dP}{dt} = \left(\alpha_1\mu_G+\alpha_2\mu_E+\alpha_3\mu_A\right)X + \beta X - P\cdot\frac{F_g}{V}$$

$$\frac{dV}{dt} = F_g$$

where F_g represents the feeding flow rate of glucose. G_{in} is concentrations of glucose in the feeding stock solution, which is 200 g/L. The fed batch 2 was fed with 20 g/L of glucose stock. *V* is the volume (L).

Table V.1. Details of validation experiments

Batch number	Initial conditions (g/L) [glucose, biomass, product, ethanol, acetic acid, volume (L)]	Feeding
Batch 1	[19.00; 0.20; 0.0058; 0.030; 0.024; 3.0]	None
Batch 2	[17.79; 0.084; 0.0058; 0; 0.083; 3.0]	None
Fed-batch 1	[19.57; 0.12; 0.0060; 0; 0; 3.0]	0.0213 L/h of glucose (200 g/L) for 46 h

Table V.1. Continued

Batch number	Initial conditions (g/L) [glucose, biomass, product, ethanol, acetic acid, volume (L)]	Feeding
Fed-batch 2	[19.47; 0.17; 0.0060; 0.57; 0; 2.0]	0.1574 L/h of glucose (20 g/L) for 6 h

Application of unknown input observer

Validation of Existence condition and estimation of the unknown input matrix

The Existence condition for the observer in Equation (5.3.3) limits the application of the unknown input observer for nonlinear systems. It is necessary to check if Equation (5.3.3) is satisfied. It is the local Lipschitz condition of the kinetic model of the bioreactor. From the fed-batch model in Equation (5.18), the following equation can be derived.

$$f(x,u)-f(\hat{x},u)=\begin{bmatrix} ((\mu_G+\mu_E+\mu_A)-\frac{F_g}{V})(X-\hat{X}) \\ -\frac{\mu_G(X-\hat{X})}{Y_{X/G}}-(G-\hat{G})*\frac{F_g}{V} \\ \left(k_1\,\mu_G-\frac{\mu_E}{Y_{X/E}}\right)(X-\hat{X})-(E-\hat{E})\frac{F_g}{V} \\ \left((k_2\mu_G+k_3\mu_E)-\frac{\mu_A}{Y_{X/A}}\right)(X-\hat{X})-(A-\hat{A})*\frac{F_g}{V} \\ \left((\alpha_1\mu_G+\alpha_2\mu_E+\alpha_3\mu_A)+\beta\right)(X-\hat{X})-(P-\hat{P})*\frac{F_g}{V} \\ 0 \end{bmatrix} \quad (5.18b)$$

In which, $\hat{X}$, $\hat{G}$, $\hat{E}$,$\hat{A}$, and $\hat{P}$ are the estimated states of biomass, glucose, ethanol, acetic acid, and product. Equation (5.18b) contains only linear term of the state. Using the

definition of Euclidean norm, it is easy to verify that Equation (5.3.3) can be satisfied from Equation (5.18b) when the feeding flow rate of glucose (F_g) are limited in a range.

In the design of unknown input observer in Equation (5.2), the unknown input matrix E is assumed constant. The estimation of matrix E is based on fitting the observer estimation to an experiment measurement data of Batch 1 by adjusting the parameter matrix E. Three unknown inputs were considered in the states of biomass, product, and ethanol in matrix E. The parameters in matrix E are obtained through a similar curve fitting process described by our previous paper.[163,164]

Implementation of unknown input observer for a bioreactor

In the validation experiments, Batch 2, Fed-batch 1, and Fed-batch 2 were performed to apply the unknown input observer to estimate the process states. The unknown input matrix E was kept the same for all the batches as obtained. The only on-line measurement for the observer is biomass, which can be done using either hardware or software measurement.[165] Different initial conditions were used in the invalidation experiments and are listed in Table V.1. To compare the difference between the original kinetic model prediction and the observer estimation, the normalized root mean square (RMS) error is calculated using the following equation.

$$\text{RMS error}=\sqrt{\sum_1^n \frac{(X_{est.}-X_{mea.})^2}{n}}/X_{max} \tag{5.19}$$

In which, $X_{mea.}$ is the value of states from measurement. $X_{est.}$ is the estimated value of states from either original kinetic model prediction or estimation from unknown

input observer. *n* is the measurement points and X_{max} is the biggest measurement value of the state recorded in each experiment.

Comparison between parameter estimation with unknown input observer

A new set of parameters was estimated using the data from Batch 1. The new estimated parameters were applied to estimate Batch 2, Fed-batch 1, and Fed-batch 2, and results are compared to the state estimation from unknown input observer.

Results and discussion

Comparison between original kinetic model and validation experiments

The parameters for the kinetic model were obtained from two batch experimental runs as demonstrated in our previous paper.[163,164] Bioprocess is a more complex system than other chemical processes due to many unknowns in the microbial systems. For the kinetic modeling point of view, for example in our system, six states are considered including glucose, ethanol, product, acetic acid, biomass, and bioreactor volume. The growth and inhibition rates of the ethanol are considered in the model. However, there are many factors, which have not been considered in the model, e.g. for a bioreactor with high cell density, unmodeled uncertainty may involve nutrient limitation, oxygen insufficiency, and carbon dioxide accumulation, and inhibition of chemicals. To fully understand and model these effects, extensive scale-down experiments are required to perform studies on individual effects. Due to certain unexpected inputs or unmodeled effects of the biosystem, the model-plant mismatch is observed when applying our original kinetic model to the validation experiments. The unexpected inputs of the bioprocess are not fully understood. New experiments have different inoculum sizes and

different feeding strategies. The mismatch between the kinetic model and plant will affect the state estimation for process optimization and control. Figure V.1 and Figure V.2 show the model-plant mismatch for different validation experiments listed in Table V.1.

Figure V.1 shows the mismatch between original kinetic model and measurements from batch experiments. The parameters in the original process model was obtained from two batch experiments, so the model-plant mismatch in other batch experiment is expected to be small. From Figure V.1, it is worth noticing that the original kinetic model estimated less biomass and ethanol but more product. Model predicts faster ethanol and glucose consumption rate, which eventually turns the substrate (glucose and ethanol) into product. For our bioprocess system, the ultimate goal is to enhance the production of β-carotene through optimization or model-based control, so more attention will be given to the product (a state) for the rest of the paper. The figure also shows that for the first 10 h of the experiments in Figure 1a and first 30 h in Figure 1b, the original model can predict the behavior of the experiments. However, the predicted behavior the bioreactor differs from the experiment data after the initial stage. Glucose, ethanol, and acetic acid are considered as carbon source for the bioprocess, which are plotted using a same scale.

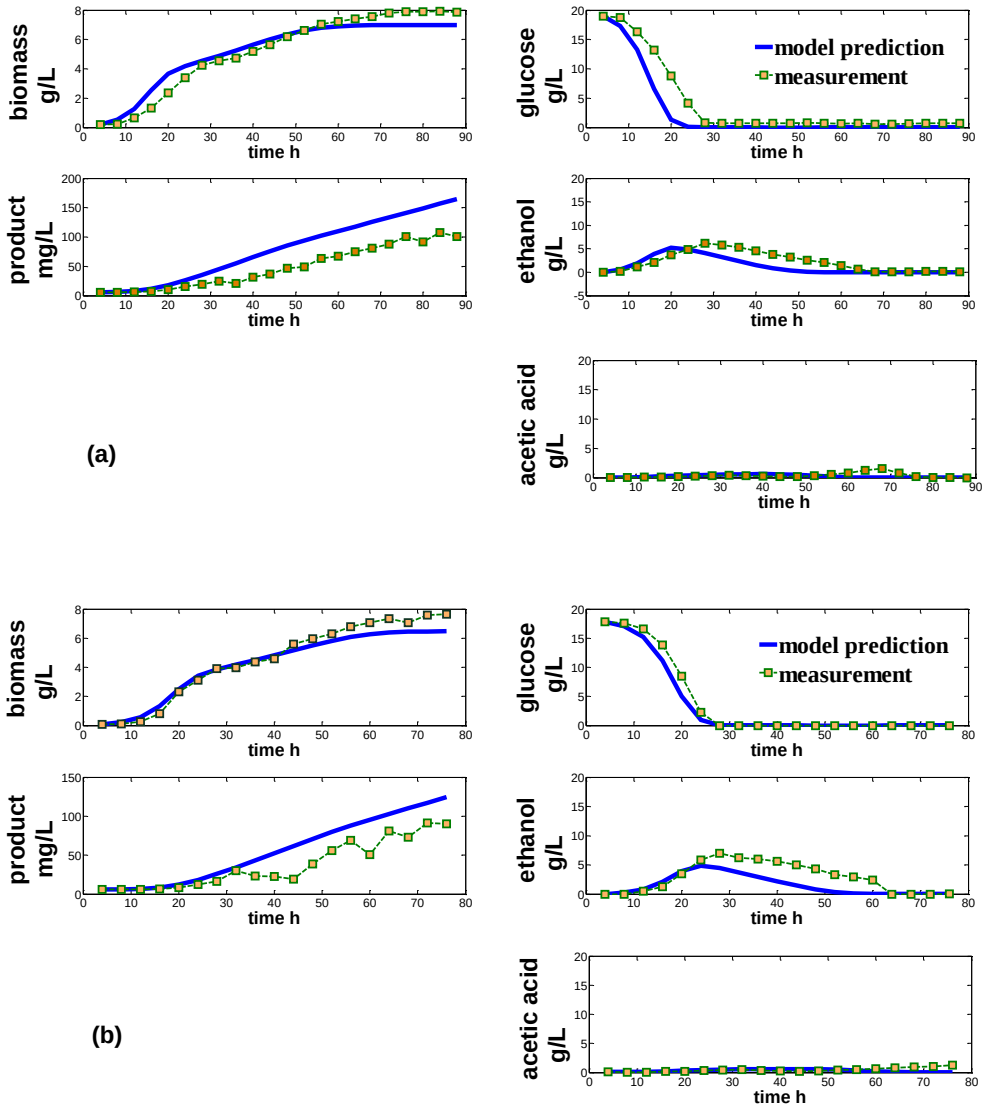

Figure V.1. Comparison between prediction from original kinetic model and measurement for experiment Batch 1(a) and Batch 2 (b)

Figure V.2 demonstrates the model-plant mismatch between prediction from original kinetic model and fed-batch experiments. As listed in Table V.1, Fed-batch 1 and Fed-batch 2 both feed glucose into the bioreactor. The major difference between Fed-batch 1 and Fed-batch 2 is the amount and time span of the feeding of glucose. Fed-

batch 1 fed glucose at a high concentration for a prolonged period of time. As can be seen in Figure V.2a, the measurement of glucose concentration in Fed-batch 1 indicates the high level of glucose in the bioreactor. Fed-batch 2 fed a small amount of glucose into the bioreactor for a short time as shown in Figure V.2b.

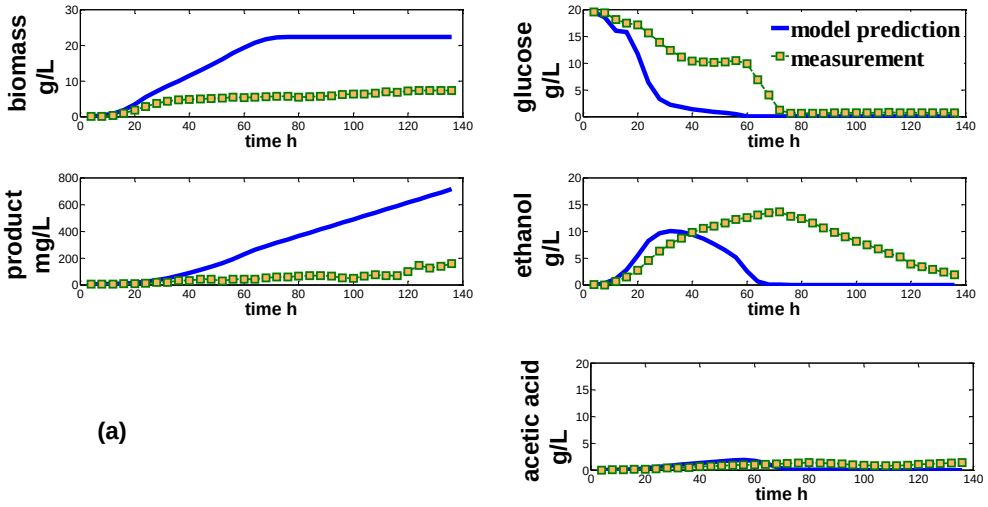

Figure V.2. Comparison between prediction from original kinetic model and measurement for experiment Fed-batch 1 (a) and Fed-batch 2 (b)

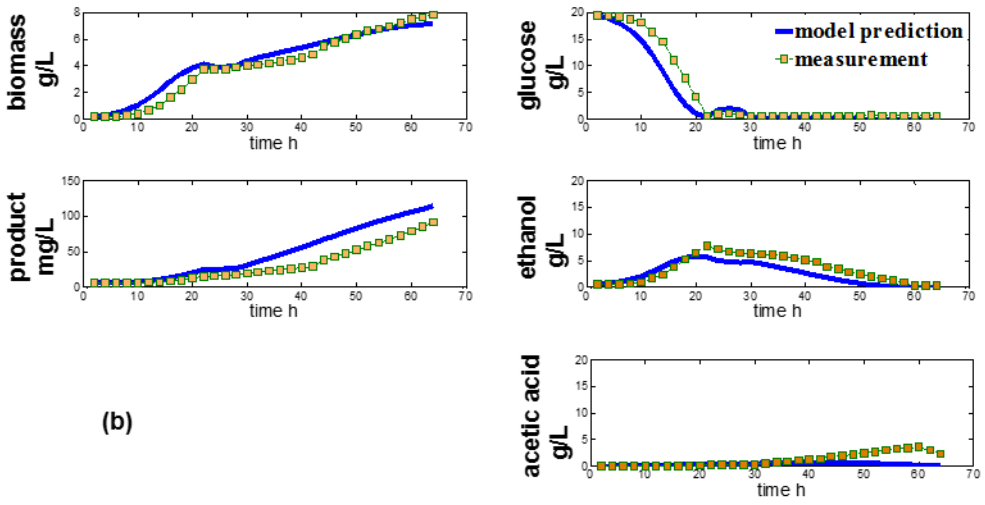

Figure V.2. Continued.

As can be seen in Figure V.2a, significant differences between the prediction from original kinetic model and the measurements were observed for biomass, glucose, and product. According to our batch model, cells grow basing on the food source of glucose, ethanol, and acetic acid. After constant feeding of glucose for a prolonged period of time, the biomass is predicted by the model to increase to a very high level as shown in Figure V.2a. The low level of measured biomass may be due to the nutrient limitation. The large amount of biomass quickly consumes the glucose, as shown by the low level of glucose predicted by the model, as seen in Figure V.2a. The model predicted a higher increase of product compared to the measured data due to the higher predicted biomass. Figure V.2b shows smaller model-plant mismatch than Figure V.2a, which can be attributed to the lower amount of glucose fed to the process in a shorter amount of time. The difference between the model prediction and the actual

measurements in Fed-batch 2 is similar to the batch experiment as shown in Figure V.1. This fact provides the possibility of an extension of the batch process to a fed-batch process using our previous process model.

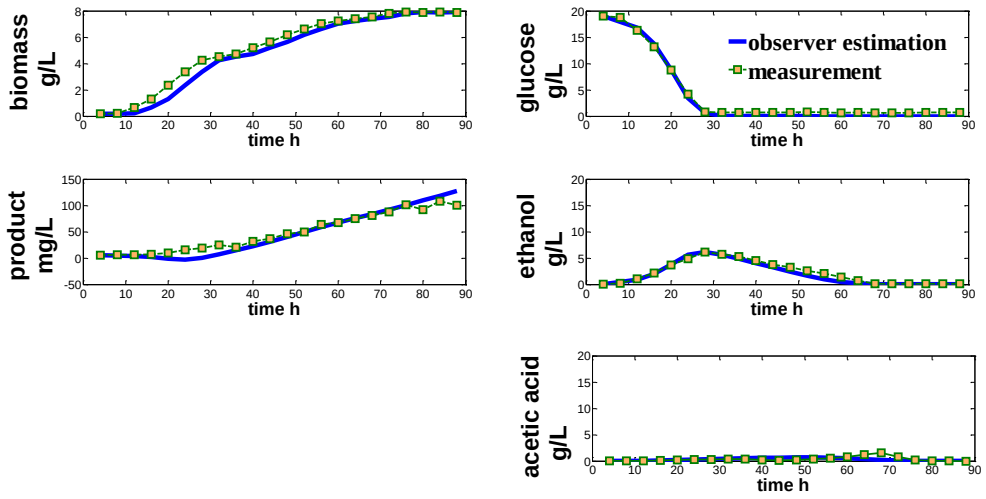

Figure V.3. Comparison of observer estimation and measurement of Batch 1 for estimating unknown input matrix

Estimation of unknown input matrix

To design the unknown input observer and solve the parameters for the observer, the first step is to obtain the unknown input matrix, which is matrix *E* in Equation (5.1). Equation (5.1) is a mathematical description of a nonlinear system, which is a combination of a known nonlinear model and linear unknown inputs. It is still an open question whether any nonlinear system can be described as such combination especially for the linear unknown inputs. Some unknown inputs can be reasonably assumed to be nonlinear. However, it is difficult to configure the exact effect of the unknown inputs due to the possible combination of many different inputs. In this paper, we assume the

overall effect of unknown inputs is linear. To estimate the parameter matrix of the unknown inputs, we apply the same parameter estimation as described in our previous paper. A line fitting is used to estimate parameter for the unknown input matrix. Figure V.3 shows the fitting of the observer estimation and measurements. Experimental data from Batch 1 is used for estimating the unknown input matrix and the results for the comparison between experimental data and the observer with estimated parameters are shown in Figure V.3. As can be seen in Figure V.4, after the estimation of the unknown input matrix parameter, the state estimation from the observer can predict the measurements in all the states except the small error in acetic acid. The production and utilization of acetic acid by the organism is still not fully understood. Due to the relatively low amount of acetic acid in the bioreactor, the estimation from the observer is acceptable. The unknown input matrix E is obtained and is depicted as follows: [0; -1/1000; -6.6/1000; 0.35/1000; 0]. The other parameters for the observer in Equation (5.2) are shown below.

$$C=\begin{bmatrix} 0 & 0 & 0 & 0 & 0 & 0 \\ 0 & 1 & 0 & 0 & 0 & 0 \\ 0 & 0 & 0 & 0 & 0 & 0 \\ 0 & 0 & 0 & 0 & 0 & 0 \\ 0 & 0 & 0 & 0 & 0 & 0 \end{bmatrix};\ H=\begin{bmatrix} 0 & 0 & 0 & 0 & 0 & 0 \\ 0 & 1 & 0 & 0 & 0 & 0 \\ 0 & 6.6 & 0 & 0 & 0 & 0 \\ 0 & -0.35 & 0 & 0 & 0 & 0 \\ 0 & 0 & 0 & 0 & 0 & 0 \end{bmatrix};\ K=\begin{bmatrix} 0 & 0 & 0 & 0 & 0 & 0 \\ 0 & -23.4953 & 0 & 0 & 0 & 0 \\ 0 & -23.7426 & 0 & 0 & 0 & 0 \\ 0 & 1.4994 & 0 & 0 & 0 & 0 \\ 0 & 0 & 0 & 0 & 0 & 0 \end{bmatrix}$$

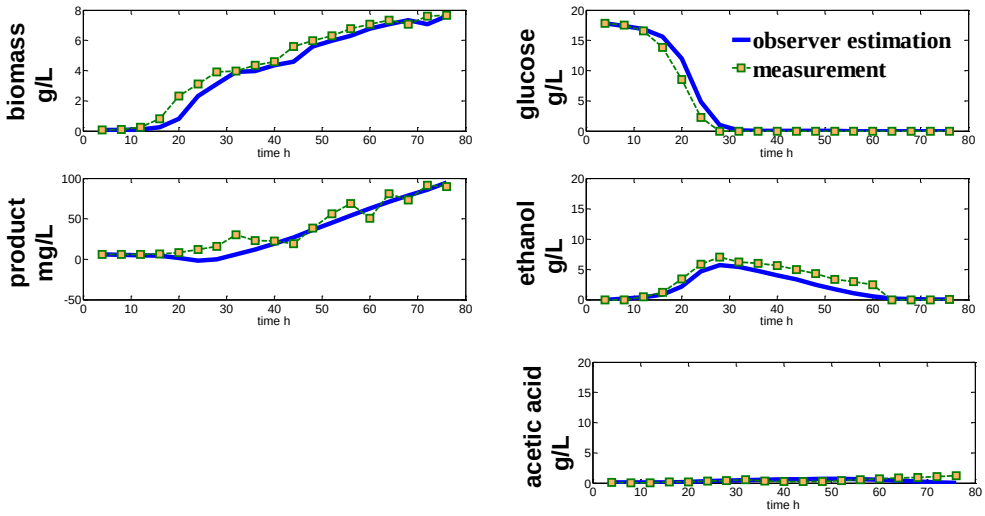

Figure V.4. Comparison of states between estimation from unknown input observer and measurement for experiment Batch 2

Comparison between observer estimation and experiments

After the estimation of the unknown input matrix *E*, the unknown input observer can be applied to other validation experiments such as Batch 2, Fed-batch 1, and Fed-batch 2 to test its ability for state estimation. Figure IV shows the state estimation results from the unknown input observer and its comparison to the off-line measurements. In the application of the unknown input observer, the biomass on-line measurements are available. In the figure, the biomass state is estimated from the unknown input observer rather than the measurement, which explains the difference between the unknown input observer and actual measurements in biomass. Ethanol and product are the two states that show improved estimation compared to the estimation shown in Figure V.1b. The batch experiment is the most studied and understood operation mode. Estimation of original model parameters and the unknown input parameter matrix are both performed

in the batch mode, so the good performance of the unknown input observer in batch mode can be expected. Although some estimation error can be observed in the glucose and ethanol prediction, the estimation of product has a better fit of the measurement which is the main focus of the state estimation. Table V.2 provides the calculated RMS error for Batch 1 and Batch 2 from both the original model and the unknown input observer. Batch 1 is used to estimate the unknown input matrix. The results in Batch 2 indicate the estimation error of ethanol and product is reduced.

Table V.2. RMS error from original model and observer for batch experiment

	Batch 1		Batch 2	
	Original kinetic model	Observer	Original kinetic model	Observer
Biomass	0.0850	0.0594	0.0759	0.0741
Glucose	0.1301	0.0336	0.0616	0.0621
Ethanol	0.2793	0.0811	0.2985	0.1653
Product	0.3354	0.0992	0.2624	0.1114
Acetic acid	0.3294	0.2725	0.4030	0.3542

Batch and fed-batch are the two main operation modes in pharmaceutical industry. The original kinetic model is based on the batch operation. In this paper, we have tested the application of our unknown input observer to the fed-batch operation. In an ideal case of process modeling, the batch model can be directly modified into a fed-batch model. However, due to some unmodeled processes or certain disturbances, significant model-plant mismatch can exist, as shown in Figure V.2a. The significant model-plant mismatch will limit the application of the modeling of fed-batch or

continuous operation. In our results obtained by applying an unknown input observer to a fed-batch system, estimation from an unknown input observer can significantly reduce the model-plant mismatch. The difference in the results shown in Figure V.5a and Figure V.5b is due to the feeding strategy of glucose. As shown in Table V.1, the experiment whose results are shown in Figure V.5a involved feeding a large amount of glucose over 46 hours.

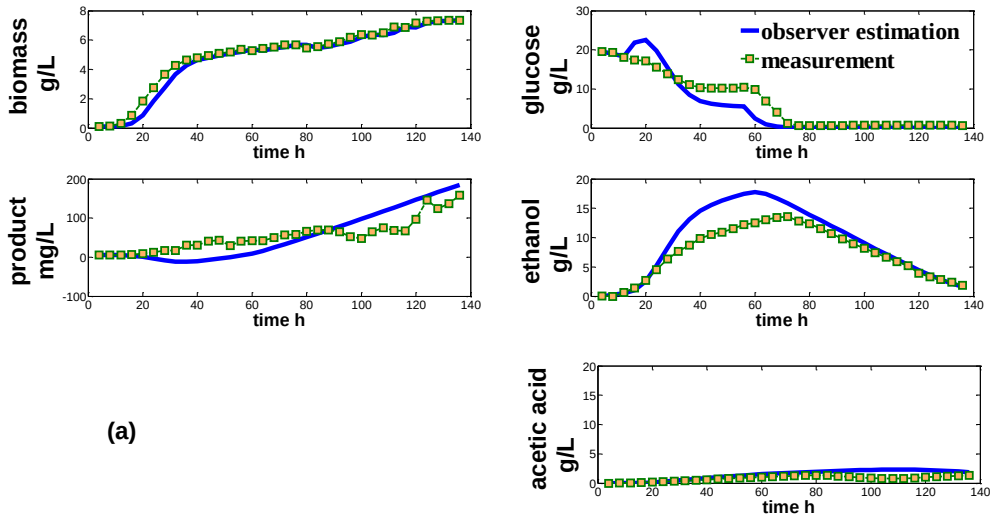

Figure V.5. Comparison of states between estimation from unknown input observer and measurement for experiment Fed-batch 1(a) and Fed-batch 2 (b)

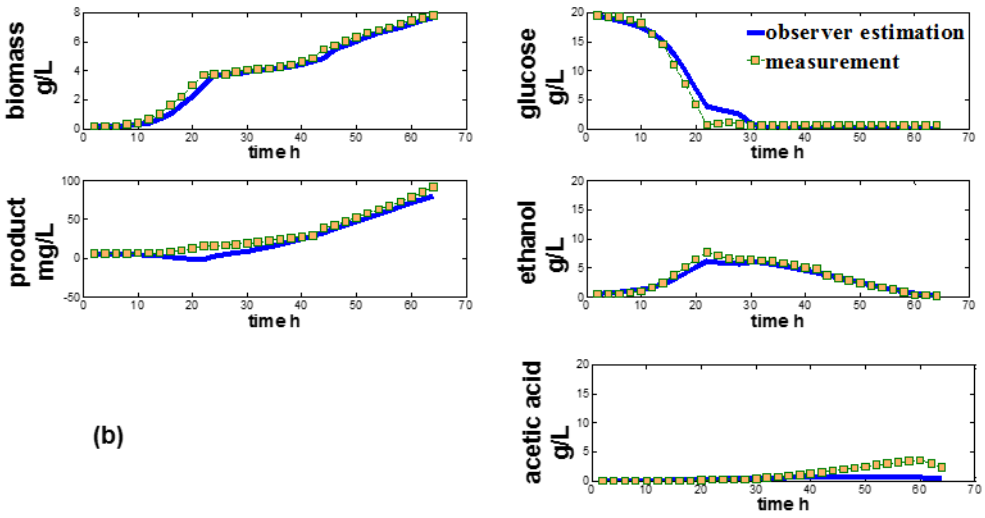

Figure V.5. Continued.

In the experiment whose results are shown in Figure V.5b, a small amount of glucose is fed into the bioreactor for a short amount of time. The glucose measurement data in Figure V.5a confirms the addition of large amount of glucose. In Figure V.5a, state estimations of glucose, ethanol, and product have been greatly improved compared to the original model prediction shown in Figure V.2a. Although there is certain error in the estimation of the state of final product, the observer can predict the overall trend of the product. The error in model-plant mismatch is not currently well-understood. As we discussed in the previous section, we use a process model in Equation (5.1) to represent the whole system, which considers a linear disturbance. Although some disturbance or uncertainty certainly have a nonlinear effect, due to the lack of information of the disturbance, it is not possible to determine the exact nonlinear effect of each disturbance. Additionally, the error in the model-plant mismatch is the combination of all the possible

disturbances, which further complicates the problem. The results in Figure V.5a show the disturbance caused by a large amount of glucose feed is a nonlinear effect. However, the linear disturbance is the only possible method in the design of the observer for tackling such a problem. Figure V.5b shows a relatively small error in all the state estimations from the unknown input observer. The small error is due to the small amount of glucose fed into the bioreactor, which makes the process close to a batch process. Table V.3 summarizes the calculated RMS error for Fed-batch 1 and Fed-batch 2 experiments. As indicated in the table, all the state estimations from the unknown input observer have reduced error when compared to the original kinetic model, especially for the prediction of the product state.

Table V.3. RMS error from original model and observer for the fed-batch experiment

	Fed-batch 1		Fed-batch 2	
	Original kinetic model	Observer	Original kinetic model	Observer
Biomass	1.7291	0.0476	0.0740	0.0403
Glucose	0.2819	0.1467	0.1082	0.0622
Ethanol	0.5294	0.1977	0.2021	0.0760
Product	2.0213	0.2099	0.2212	0.0857
Acetic acid	0.6569	0.5970	0.3963	0.3505

Comparison between model with updated parameters and unknown input observer

An ideal process model will have a fixed set of parameters for different operations. However, the biological experiments demonstrate that the existence of such a process model is almost impossible. One of the methods is to update the parameters for

each experiment run. However, the parameter estimation requires the measurements of as many states as possible, which contradicts the intent of process modeling. In our study, a comparison between the parameter update and unknown input observer is shown in Figure V.6, although the parameter update is based on the measurements of all the states and unknown input observer is based on the measurement of biomass only. In the comparison, we re-estimate the parameters for Batch 1 using the same method we used in our previous study, and we apply the re-estimated parameters for the Batch 2, Fed-batch 1, and Fed-batch 2 experiments.[163,164] The results are shown in Figure V.6. Batch 1 is used to update the parameters (shown in Figure V.6a). Figure V.6b applies the same updated parameters for experiment Batch 2. Figure V.6c and Figure V.6d shows the results for fed-batch experiments. As can be seen in the figure, the updated model can predict the batch experiment, but all not the fed-batch experiment, which indicates that there are key unmodeled disturbances.

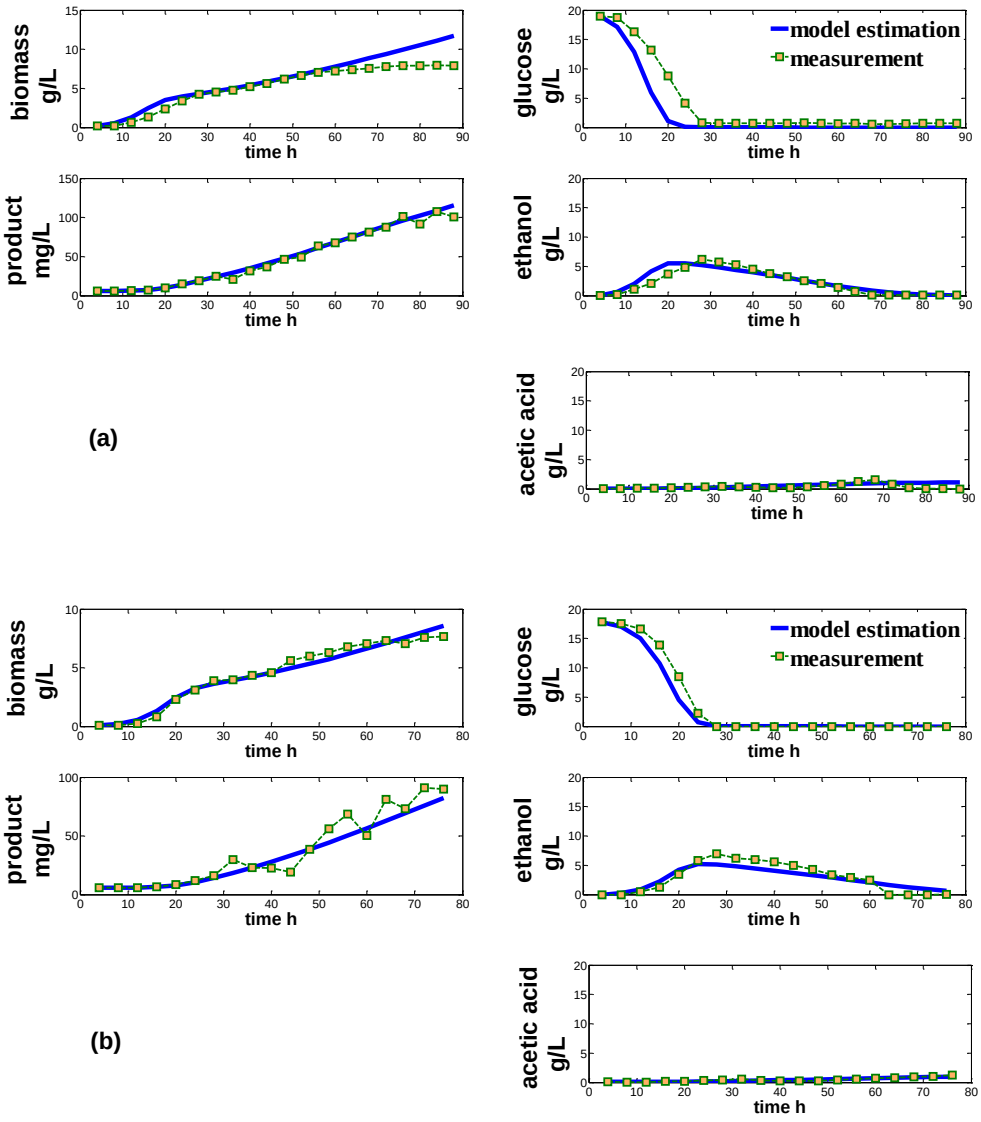

Figure V.6. Prediction of the states from model with updated parameter for Batch 1 (a), Batch 2 (b), Feb-batch 1 (c), and Fed-batch 2(d)

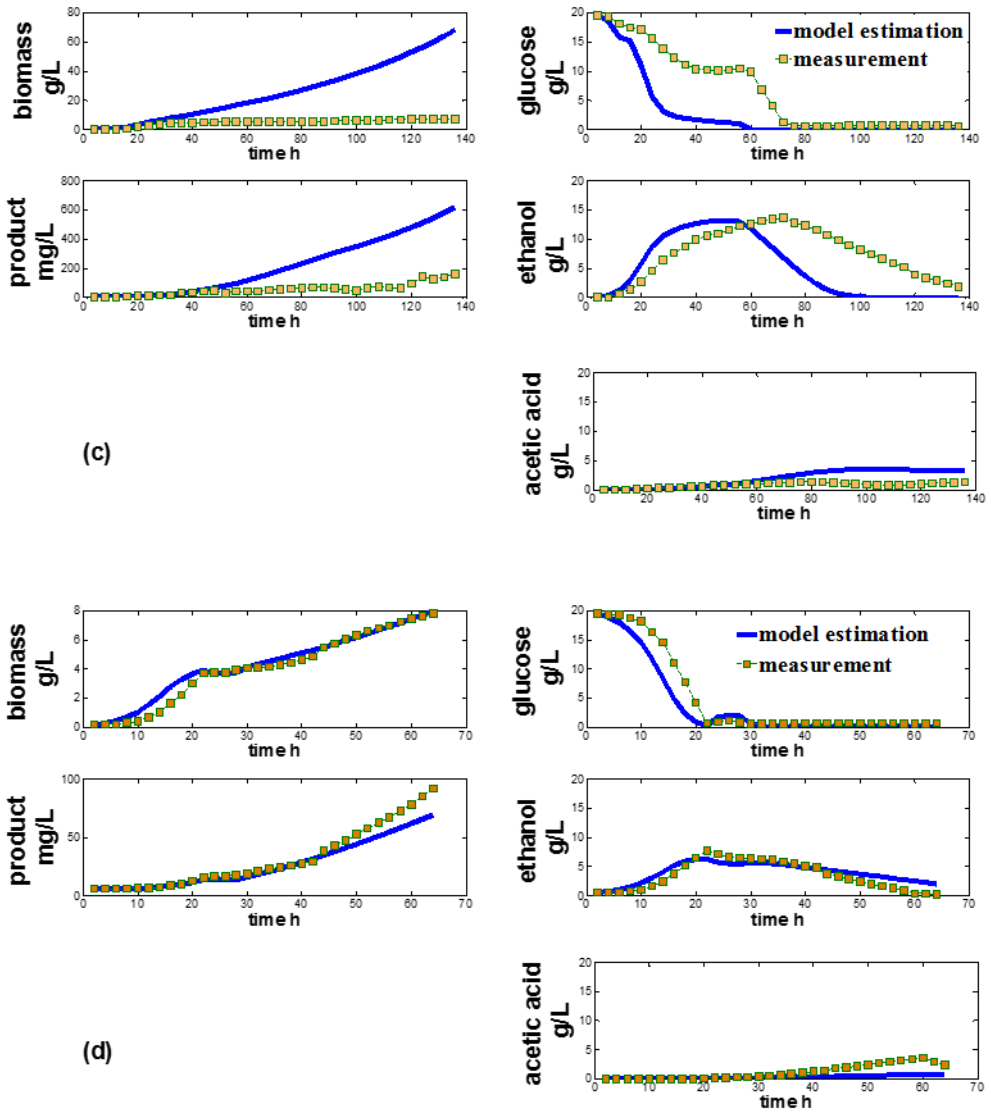

Figure V.6. Continued.

RMS error from the kinetic model prediction with updated parameters and the unknown input observer is shown in Table V.4 and Table V.5. The 'updated model' in the table indicates the model with re-estimated parameters. Since Batch 1 is the batch used for both parameter re-estimation and estimation of unknown input matrix, it is not

used for comparison purpose. As indicated in the table, Batch 2 has comparable estimation error when comparing the model with the parameter update and the unknown input observer. As shown in Table V.3 and Table V.5, kinetic models with updated parameters can reduce the estimation error for Fed-batch 2. However, the Fed-batch 1 results indicate that the parameter re-estimation using a batch experiment still can't estimate the fed-batch experiment efficiently. The result indicated that for a fed-batch experiment with large amount of glucose feeding, an adaptive update of parameter is preferred for the parameter estimation method. However, the adaptive parameter estimation requires off-line measurements of many state values, while the application of observer only requires online biomass measurement.

Table V.4. RMS error from kinetic model with updated parameters and observer for batch experiment

	Batch 1		Batch 2	
	Updated kinetic model	Observer	Updated kinetic model	Observer
Biomass	0.1804	0.0594	0.0573	0.0741
Glucose	0.1374	0.0336	0.0713	0.0621
Ethanol	0.1265	0.0811	0.1496	0.1653
Product	0.0438	0.0992	0.0976	0.1114
Acetic acid	0.3085	0.2725	0.1273	0.3542

Table V.5. RMS error from kinetic model with updated parameters and observer for fed-batch experiment

	Fed-Batch 1		Fed-Batch 2	
	Updated kinetic model	Observer	Updated kinetic model	Observer
Biomass	3.7944	0.0476	0.0584	0.0403
Glucose	0.2799	0.1467	0.1183	0.0622
Ethanol	0.3807	0.1977	0.1522	0.0760
Product	1.4221	0.2099	0.0858	0.0857
Acetic acid	1.1547	0.5970	0.3557	0.3505

Comparison of three carbon sources

As can be seen in Table V.2 to Table V.5, state estimation for acetic acid in both original model and observer has larger normalized RMS error than the other states. In this bioprocess, acetic acid is considered as a third carbon source for β-carotene production after glucose and ethanol. To compare contributions of the three carbon source, carbon molecules (mole) from each carbon source are calculated. Quantity of glucose is calculated by its initial concentration. Quantities of ethanol and acetic acid are calculated by their maximal concentration, which occurs at the end of their production phase. It is assumed that ethanol starts acting as a carbon source after glucose is all consumed. And acetic acid acts as a carbon source after ethanol is all consumed. It also can be seen in the figures, such as in Figure 1a, ethanol reaches its maxima at 28 h, when glucose is all consumed. Acetic acid reaches its maximal concentration at 68 h when ethanol is all consumed. The inhibitory effort of ethanol on cell growth and toxic effect of acetic acid may lead to the priority sequence of the carbon source.[166–168] For the fed-batch experiments, the addition of substrate is also calculated.

The comparison results are shown in Figure V.7. As can be seen in the figure, acetic acid contributes less than 6% of the carbon source except Fed-batch 2. This is significantly less compared to glucose and ethanol. Due to the low impact of acetic acid, the relatively large estimation error for acetic acid is accepted.

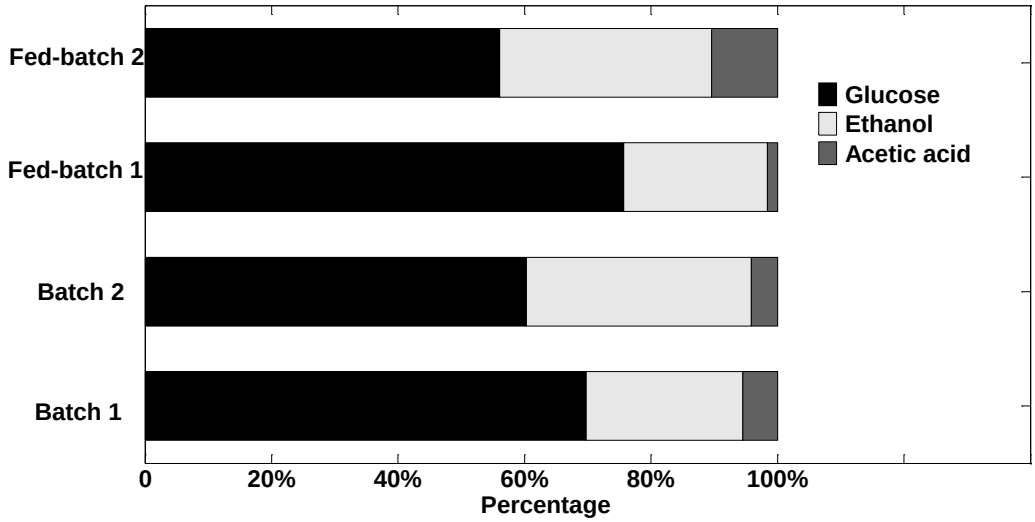

Figure V.7. Contribution of carbon from three carbon source (carbon mole quantity)

Summary of the chapter

The measurement or estimation of process states is critical for process monitoring, advanced process control, and process optimization. For chemical processes where state information cannot be measured directly, techniques such as state estimation need to be developed. Model-based state estimation is one of the most widely applied methods for estimation of unmeasured states basing on a high-fidelity process model. However, certain disturbances or unknown inputs not considered by process models will

generate model-plant mismatch, and in some cases the mismatch is significant. To estimate the process state in the presence of process disturbances or unknown inputs, a new design of a nonlinear unknown input observer is proposed and applied to the estimation of states in a bioreactor. The design of such an observer is provided and sufficient and necessary conditions of the observer are discussed.

Experimental studies of batch and fed-batch operation of a bioreactor are performed using *Saccharomyces cerevisiae* strain mutant SM14 to produce β-carotene. Based on the mathematical modeling of the process which is demonstrated in our previous study, an unknown input observer for the bioreactor is developed. Model-plant mismatch is observed when changes are made to the initial conditions or operating mode of the reactor. The state estimation of the process from the designed observer is demonstrated to alleviate the model-plant mismatch and is compared to the experimental measurements.

CHAPTER VI

CONCLUSIONS AND FUTURE WORK

Conclusions

In this dissertation, different model-based state estimation techniques were proposed and applied to chemical processes.

In Chapter II, non-isothermal natural gas flow equations in pipeline were developed to study the effect of inlet temperature, ground temperature, and heat transfer coefficient on the flow phenomena. The results showed that all the above-mentioned thermal properties have an observable impact on the flow rate and a relatively smaller impact on the pressure profile. The natural gas leak from the pipeline will change the flow rate, pressure, and temperature profile across the length of the pipeline depending on the size and location of the leak. The non-isothermal model can be conditionally reduced to an isothermal model when only considering the flow rate along the pipeline. The constant parameter '*c'* in the isothermal model was estimated for different thermal conditions and leak occurrences. Unscented Kalman filter provides better flow rate estimation than extended Kalman filter. In the dual unscented Kalman filter with parameter update, the isothermal model can be used as an observer to estimate the gas flow rate under non-isothermal situations at steady state. With the non-isothermal model generating the data in place of real pipeline data, the proposed dual unscented Kalman filter can detect the leak location efficiently.

In Chapter III, a methodology for constructing a linear unknown input observer for a natural gas flow process was developed. Existence, stability, and robustness analysis of the observer was also provided. The method was illustrated by first approximating the nonlinear isothermal model with a linear model. A linear unknown input observer is proposed and solved through a linear matrix inequality method. It was shown that the observer is able to identify the effects of pressure oscillation and temperature changes without requiring the thermal measurement and real-time modeling. An adaptive linear model was also proposed for leak location estimation while considering the effects of changes in temperature and boundary pressure.

Chapter IV chapter developed two different approaches to detect subsequent and simultaneous leaks from a natural gas pipeline. An unknown input observer-based estimation method was adapted to detect the subsequent multiple leaks with the ability to deal with process noise such as temperature and pressure change. An adaptive discretization global optimization algorithm method was proposed to locate the multiple leaks. The new optimization algorithm will significantly reduce the computation circles and can efficiently estimate the multiple leak locations.

In Chapter V, A new design of a nonlinear unknown input observer was proposed and implemented using a bioreactor case study. The existence and stability of the observer was provided. The unknown input matrix was determined by one batch experiment and applied to other batch and fed-batch validation examples. The unknown input observer used the biomass measurement as a feedback to estimate the other states. Results indicated the unknown input observer can improve the prediction of the states in

both batch and fed-batch experiments. The assumption of a linear disturbance in the design of unknown input observer can be validated for certain batch and fed-batch experiments.

Future work

Development of hybrid fault detection observers

New observer for fault detection and isolation is needed for complex system. Among the observers applied in the chemical system, process fault or unknown inputs are estimated from the first principle concept or experimental setting. However, for a complex system that process fault or disturbance cannot be measured directly, new observer technique needs to be developed. Hybrid observers integrate various observer developing techniques, which can be a candidate for state estimation for complex systems.

Currently, most of the observer designs are based on the first principle modeling of a process. For certain systems, first principle modeling is hard to obtain. The observer design based on the incomplete knowledge of process modeling is still under development.

Process monitoring of virus production and separation

In our previous study, a novel strategy is proposed for preparing cellulose fiber monolith by partially dissolving and reshaping Lyocell cellulose fiber into monolith shape, which enhances the mechanical property of the monolith. Process modeling and simulation is primarily studied. However, due to the numerous proteins participating in the separation process, process simulation of separating virus from cell proteins and

DNA remain a challenge. Process modeling and monitoring technique need to be developed for a complicated process with little knowledge of process variables. Limited sensor numbers could also be a bottleneck to overcome.

REFERENCES

(1) Bachinger, T.; Haugen, J.-E. Process Monitoring. In *Handbook of Machine Olfaction: Electronic Nose Technology*; Wiley-VCH: German, 2004; pp 481–503.

(2) Chiang, L. H.; Russell, E.; Braatz, R. D. *Fault Detection and Diagnosis in Industrial Systems*; Springer: London, 2001.

(3) Isermann, R. Supervision, Fault-Detection and Fault-Diagnosis Methods - An Introduction. *Control Eng. Pract.* **1997**, *5* (5), 639.

(4) Venkatasubramanian, V.; Rengaswamy, R.; Kavuri, S. N.; Yin, K. A Review of Process Fault Detection and Diagnosis Part III: Process History Based Methods. *Comput. Chem. Eng.* **2003**, *27* (3), 327.

(5) Venkatasubramanian, V.; Rengaswamy, R.; Kavuri, S. N. A Review of Process Fault Detection and Diagnosis Part II: Qualitative Models and Search Strategies. *Comput. Chem. Eng.* **2003**, *27* (3), 313.

(6) Gertler, J. *Fault Detection and Diagnosis in Engineering Systems*; CRC Press: New York, 1998.

(7) Venkatasubramanian, V.; Rengaswamy, R.; Yin, K.; Kavuri, S. N. A Review of Process Fault Detection and Diagnosis Part I: Quantitative Model-Based Methods. *Comput. Chem. Eng.* **2003**, *27* (3), 293.

(8) MacGregor, J. F.; Kourti, T. Statistical Process Control of Multivariate Processes. *Control Eng. Pract.* **1995**, *3* (3), 403.

(9) Montgomery, D. *Introduction to Statistical Quality Control*; John Wiley & Sons Inc.: Singapore, 2009.

(10) Martin, E. B.; Morris, A. J.; Zhang, J. Process Performance Monitoring Using Multivariate Statistical Process Control. *IEE Proc. - Control Theory Appl.* **1996**, *143* (2), 132.

(11) Bakshi, B. R. Multiscale PCA with Application to Multivariate Statistical Process Monitoring. *AIChE J.* **1998**, *44* (7), 1596.

(12) Kourti, T.; MacGregor, J. F. J. F. Process Analysis, Monitoring and Diagnosis, Using Multivariate Projection Methods. *Chemom. Intell. Lab. Syst.* **1995**, *28*, 3.

(13) Höskuldsson, a; Hoskuldsson, A. PLS Regression Methods. *J. Chemom.* **1988**, *2* (July), 211.

(14) Ge, Z.; Song, Z.; Gao, F. Review of Recent Research on Data-Based Process Monitoring. *Ind. Eng. Chem. Res.* **2013**, *52*, 3543.

(15) MacGregor, J.; Cinar, A. Monitoring, Fault Diagnosis, Fault-Tolerant Control and Optimization: Data Driven Methods. *Comput. Chem. Eng.* **2012**, *47*, 111.

(16) Ding, S. X. Data-Driven Design of Monitoring and Diagnosis Systems for Dynamic Processes: A Review of Subspace Technique Based Schemes and Some Recent Results. *J. Process Control* **2014**, *24* (2), 431.

(17) Yin, S.; Ding, S. X.; Haghani, A.; Hao, H.; Zhang, P. A Comparison Study of Basic Data-Driven Fault Diagnosis and Process Monitoring Methods on the Benchmark Tennessee Eastman Process. *J. Process Control* **2012**, *22* (9), 1567.

(18) Qin, S. J. Survey on Data-Driven Industrial Process Monitoring and Diagnosis. *Annu. Rev. Control* **2012**, *36* (2), 220.

(19) Phanomchoeng, G.; Rajamani, R. Observer Design for Lipschitz Nonlinear

Systems Using Riccati Equations. *Proc. Am. Control Conf.* **2010**, 6060.

(20) Rawlings, J. B.; Ji, L. Optimization-Based State Estimation: Current Status and Some New Results. *J. Process Control* **2012**, *22* (8), 1439.

(21) Simon, D. Kalman Filtering with State Constraints: A Survey of Linear and Nonlinear Algorithms. *IET Control Theory Appl.* **2010**, *4* (8), 1303.

(22) Kravaris, C.; Sotiropoulos, V.; Georgiou, C.; Kazantzis, N.; Xiao, M.; Krener, A. J. Nonlinear Observer Design for State and Disturbance Estimation. *Syst. Control Lett.* **2007**, *56* (11–12), 730.

(23) Saif, M. Sliding Mode Observer for Nonlinear Uncertain Systems. *IEEE Trans. Automat. Contr.* **2001**, *46* (12), 2012.

(24) Chen, W.-H. Disturbance Observer Based Control for Nonlinear Systems. *IEEE/ASME Trans. Mechatronics* **2004**, *9* (4), 706.

(25) Zeitz, M. The Extended Luenberger Observer for Nonlinear Systems. *Syst. Control Lett.* **1987**, *9* (2), 149.

(26) Kruger, U.; Xie, L. *Statistical Monitoring of Complex Multivariate Processes: With Applications in Industrial Process Control*; Wiley-VCH: Chichester, 2012.

(27) Sheriff, M. Z.; Harrou, F.; Nounou, M. Univariate Process Monitoring Using Multiscale Shewhart Charts. In *Proceedings - 2014 International Conference on Control, Decision and Information Technologies, CoDIT 2014*; 2014; pp 435–440.

(28) Arunasakthi, K.; KamatchiPriya, L. A Review on Linear and Non-Linear Dimensionality Reduction. *Mach. Learn. Appl.* **2014**, *1* (1), 65.

(29) Van Der Maaten, L. J. P.; Postma, E. O.; Van Den Herik, H. J. Dimensionality Reduction: A Comparative Review. *J. Mach. Learn. Res.* **2009**, *10*, 1.

(30) Fodor, I. K. A Survey of Dimension Reduction Techniques. *Cent. Appl. Sci. Comput. Lawrence Livermore Natl. Lab.* **2002**, *9*, 1.

(31) Villalba, S. D.; Cunningham, P. An Evaluation of Dimension Reduction Techniques for One-Class Classification. *Artif. Intell. Rev.* **2007**, *27* (4 SPEC. ISS.), 273.

(32) Abdi, H. Partial Least Squares Regression and Projection on Latent Structure Regression (PLS Regression). *Wiley Interdiscip. Rev. Comput. Stat.* **2010**, *2* (1), 97.

(33) Mohd Ali, J.; Ha Hoang, N.; Hussain, M. A.; Dochain, D. Review and Classification of Recent Observers Applied in Chemical Process Systems. *Comput. Chem. Eng.* **2015**, *76*, 27.

(34) De Santis, E.; Di Benedetto, M. D.; Pola, G. Observability and Detectability of Linear Switching Systems: A Structural Approach. *Math.DS* **2008**, *1*, 1.

(35) Li, Z. Y.; Wang, Y.; Zhou, B.; Duan, G. R. Detectability and Observability of Discrete-Time Stochastic Systems and Their Applications. *Automatica* **2009**, *45* (5), 1340.

(36) Moreno, J. A.; Dochain, D. Global Observability and Detectability Analysis of Uncertain Reaction Systems. In *IFAC Proceedings Volumes (IFAC-PapersOnline)*; 2005; Vol. 16, pp 37–42.

(37) Wei, X. J.; Wu, Z. J.; Karimi, H. R. Disturbance Observer-Based Disturbance

Attenuation Control for a Class of Stochastic Systems. *Automatica* **2016**, *63*, 21.

(38) Chen, X. S.; Yang, J.; Li, S. H.; Li, Q. Disturbance Observer Based Multi-Variable Control of Ball Mill Grinding Circuits. *J. Process Control* **2009**, *19* (7), 1205.

(39) Stobart, R. K.; Kuperman, A.; Zhong, Q. C. Uncertainty and Disturbance Estimator–Based Control for Uncertain LTI-SISO Systems With State Delays. *J. Dyn. Syst. Meas. Control* **2011**, *133*, 245021.

(40) Zhong, Q. C.; Rees, D. Control of Uncertain LTI Systems Based on an Uncertainty and Disturbance Estimator. *J. Dyn. Syst. Meas. Control* **2004**, *126* (4), 905.

(41) Li, S.; Yang, J.; Chen, W. H.; Chen, X. Generalized Extended State Observer Based Control for Systems with Mismatched Uncertainties. *IEEE Trans. Ind. Electron.* **2012**, *59* (12), 4792.

(42) Chen, W.-H.; Yang, J.; Guo, L.; Li, S. Disturbance Observer-Based Control and Related Methods: An Overview. *IEEE Trans. Ind. Electron.* **2015**, *46* (c), 1.

(43) Guo, B. Z.; Zhao, Z. L. On the Convergence of an Extended State Observer for Nonlinear Systems with Uncertainty. *Syst. Control Lett.* **2011**, *60* (6), 420.

(44) Zhao, Z. L.; Guo, B. Z. Extended State Observer for Uncertain Lower Triangular Nonlinear Systems. *Syst. Control Lett.* **2015**, *85*, 100.

(45) Xiong, S.; Wang, W.; Liu, X.; Chen, Z.; Wang, S. A Novel Extended State Observer. *ISA Trans.* **2015**, *58*, 309.

(46) Yoo, D.; Yau, S. S. T.; Gao, Z. On Convergence of the Linear Extended State

Observer. In *IEEE International Symposium on Intelligent Control - Proceedings*; 2006; pp 1645–1650.

(47) Koenig, D.; Bedjaoui, N.; Litrico, X. Unknown Input Observers Design for Time-Delay Systems Application to an Open-Channel. In *Proceedings of the 44th IEEE Conference on Decision and Control, and the European Control Conference*; Seville, Spain, 2005; pp 5794–5799.

(48) Kudva, P.; Viswanadham, N.; Ramakrishna, A. Observers for Linear Systems with Unknown Inputs. *IEEE Trans. Automat. Contr.* **1980**, *25* (1), 113.

(49) Pertew, A. M.; Marquez, H. J.; Zhao, Q. Design of Unknown Input Observers for Lipschitz Nonlinear Systems. In *Proceedings of the American Control Conference*; 2005; pp 4198–4203.

(50) Bhattacharyya, S. Observer Design for Linear Systems with Unknown Inputs. *Autom. Control. IEEE Trans.* **1978**, *23* (3), 483.

(51) Stobart, R. K.; Kuperman, A.; Zhong, Q.-C. Uncertainty and Disturbance Estimator-Based Control for Uncertain LTI-SISO Systems With State Delays. *J. Dyn. Syst. Meas. Control - Trans. ASME 2011* **2011**, *133* (2), 1.

(52) Rocha-Cózatl, E.; Wouwer, A. Vande. State and Input Estimation in Phytoplanktonic Cultures Using Quasi-Unknown Input Observers. *Chem. Eng. J.* **2011**, *175* (1), 39.

(53) Lemesle, V.; Gouze, J. L. Hybrid Bounded Error Observers for Uncertain Bioreactor Models. *Bioprocess Biosyst Eng* **2002**, *27*, 311.

(54) Moisan, M.; Bernard, O.; Gouzé, J. L. Near Optimal Interval Observers Bundle

for Uncertain Bioreactors. *Automatica* **2009**, *45* (1), 291.

(55) Farza, M.; M'Saad, M.; Maatoug, T.; Kamoun, M. Adaptive Observers for Nonlinearly Parameterized Class of Nonlinear Systems. *Automatica* **2009**, *45* (10), 2292.

(56) Ghanmi, A.; Hajji, S.; Kamoun, S. Nonlinear Discrete High-Gain Observer: Application to Bioreactor Model. *Proc. Eng. Technol.* **2016**, 282.

(57) D'Hères, S. M. Nonlinear Observers and Applications. In *Lecture Notes in Control and Information Sciences*; Springer: Berlin, 2007.

(58) Krener, a. J.; Respondek, W. Nonlinear Observers with Linearizable Error Dynamics. *J. Control Optim.* **1985**, *23* (2), 197.

(59) Besançon, G. *Nonlinear Observers and Applications*; Springer-Verlag Berlin Heidelberg: Berlin, 2007.

(60) Besançon, G. Remarks on Nonlinear Adaptive Observer Design. *Syst. Control Lett.* **2000**, *41* (4), 271.

(61) Zhang, Q. Revisiting Different Adaptive Observers through a Unified Formulation. In *Proceedings of the 44th IEEE Conference on Decision and Control, and the European Control Conference, CDC-ECC '05*; 2005; Vol. 2005, pp 3067–3072.

(62) Geiger, I. G. *Principles of Leak Detection*; KROHNE Oil and Gas Brochure: Breda, 2008.

(63) Stouffs, P.; Giot, M. Pipeline Leak Detection Based on Mass Balance: Importance of the Packing Term. *J. Loss Prev. Process Ind.* **1993**, *6* (5), 307.

(64) Wan, J.; Yu, Y.; Wu, Y.; Feng, R.; Yu, N. Hierarchical Leak Detection and Localization Method in Natural Gas Pipeline Monitoring Sensor Networks. *Sensors* **2011**, *12* (1), 189.

(65) Zhang, J. Designing a Cost-Effective and Reliable Pipeline Leak-Detection System. *Pipes Pipelines Int.* **1997**, *42* (1), 20.

(66) Frank, P. M. Analytical and Qualitative Model-Based Fault Diagnosis - A Survey and Some New Results. *European Journal of Control*. 1996, pp 6–28.

(67) Isermann, R. Model-Based Fault-Detection and Diagnosis - Status and Applications. *Annu. Rev. Control* **2005**, *29* (1), 71.

(68) Behbahani-Nejad, M.; Bagheri, a. A MATLAB Simulink Library for Transient Flow Simulation of Gas Networks. *Proc. World Acad. Sci. Eng. Technol.* **2008**, *33* (September), 153.

(69) Behbahani-Nejad, M.; Shekari, Y. The Accuracy and Efficiency of a Reduced-Order Model for Transient Flow Analysis in Gas Pipelines. *J. Pet. Sci. Eng.* **2010**, *73* (1–2), 13.

(70) Ke, S. L.; Ti, H. C. Transient Analysis of Isothermal Gas Flow in Pipeline Network. *Chem. Eng. J.* **2000**, *76* (2), 169.

(71) Kralik, J.; Stiegler, P.; Vostru, Z.; Zavorka, J. Modeling the Dynamics of Flow in Gas Pipelines. *IEEE Trans. Syst. Man. Cybern.* **1984**, *14* (4), 586.

(72) Noorbehesht, N.; Ghaseminejad, P. Numerical Simulation of the Transient Flow in Natural Gas Transmission Lines Using a Computational Fluid Dynamic Method. *Am. J. Appl. Sci.* **2013**, *10* (1), 24.

(73) Reddy, H. P.; Narasimhan, S.; Bhallamudi, S. M. Simulation and State Estimation of Transient Flow in Gas Pipeline Networks Using a Transfer Function Model. *Ind. Eng. Chem. Res.* **2006**, *45* (11), 3853.

(74) Brouwer, J.; Gasser, I.; Herty, M. Gas Pipeline Models Revisited: Model Hierarchies, Nonisothermal Models, and Simulations of Networks. *Multiscale Model. Simul.* **2011**, *9* (2), 601.

(75) Herrangonzalez, A.; Delacruz, J.; Deandrestoro, B.; Riscomartin, J. Modeling and Simulation of a Gas Distribution Pipeline Network. *Appl. Math. Model.* **2009**, *33* (3), 1584.

(76) Reddy, H. P.; Narasimhan, S.; Bhallamudi, S. M.; Bairagi, S. Leak Detection in Gas Pipeline Networks Using an Efficient State Estimator. Part-I: Theory and Simulations. *Comput. Chem. Eng.* **2011**, *35* (4), 651.

(77) Wan, E. a; Van Der Merwe, R. The Unscented Kalman Filter for Nonlinear Estimation. In *Adaptive Systems for Signal Processing, Communications, and Control Symposium 2000. AS-SPCC. The IEEE 2000*; 2002; pp 153–158.

(78) Wan, E. A.; Merwe, R. van der. *The Unscented Kalman Filter, in Kalman Filtering and Neural Networks*; John Wiley & Sons, Inc.: New York, 2001.

(79) Wan, E. a.; van der Merwe, R. The Unscented Kalman Filter. In *Kalman Filtering and Neural Networks*; Wiley-VCH: New York, 2002; pp 1–49.

(80) Benkherouf, A.; Allidina, A. Y. Leak Detection and Location in Gas Pipelines. *IEE Proc. D Control Theory Appl.* **1988**, *135* (2), 142.

(81) Liu, M.; Zang, S.; Zhou, D. Fast Leak Detection and Location of Gas Pipelines

Based on an Adaptive Particle Filter. *Int. J. Appl. Math. Comput. Sci.* **2005**, *15* (4), 541.

(82) Emara-Shabaik, H. E.; Khulief, Y. A.; Hussaini, I. A Non-Linear Multiple-Model State Estimation Scheme for Pipeline Leak Detection and Isolation. *Proc. Inst. Mech. Eng. Part I J. Syst. Control Eng.* **2002**, *216* (6), 497.

(83) Hauge, E.; Aamo, O.; Godhavn, J.-M. Model-Based Monitoring and Leak Detection in Oil and Gas Pipelines. *SPE Proj. Facil. Constr.* **2009**, *4* (3), 53.

(84) Verde, C. Multi-Leak Detection and Isolation in Fluid Pipelines. *Control Eng. Pract.* **2001**, *9* (6), 673.

(85) Helgaker, J. F.; Oosterkamp, A.; Langelandsvik, L. I.; Ytrehus, T. Validation of 1D Flow Model for High Pressure Offshore Natural Gas Pipelines. *J. Nat. Gas Sci. Eng.* **2014**, *16*, 44.

(86) Dranchuk, P. M.; Abou-Kassem, J. H. Calculation of Z Factors for Natural Gases Using Equations of State. *J. Can. Pet. Technol.* **1975**, *14* (3), 34.

(87) Wan, E. a; van der Merwe, R.; Nelson, A. Dual Estimation and the Unscented Transformation. In *Nips*; 2000; pp 666–672.

(88) Tang, W. Modeling, Estimation, and Control of Nonlinear Time-Variant Complex Processes, Texas Tech University, 2013.

(89) Wang, S.; Carroll, J. Leak Detection for Gas and Liquid Pipelines by Online Modeling. *Energy Process.* **2007**, *39* (4), 21.

(90) Osiadacz, A. J.; Chaczykowski, M. Comparison of Isothermal and Non-Isothermal Pipeline Gas Flow Models. *Chem. Eng. J.* **2001**, *81* (1), 41.

(91) Chaczykowski, M. Transient Flow in Natural Gas Pipeline - The Effect of Pipeline Thermal Model. *Appl. Math. Model.* **2010**, *34* (4), 1051.

(92) Abbaspour, M.; Chapman, K. S. Nonisothermal Transient Flow in Natural Gas Pipeline. *J. Appl. Mech.* **2008**, *75* (3), 31018.

(93) Bai, Y.; Bai, Q. *Subsea Pipelines and Risers*; Elsevier: New York, 2005.

(94) Murvay, P. S.; Silea, I. A Survey on Gas Leak Detection and Localization Techniques. *J. Loss Prev. Process Ind.* **2012**, *25* (6), 966.

(95) Peter Black. A Review of Pipeline Leak Detection Technology. In *Pipeline Systems*; Springer: Dordrecht, 1992; pp 287–298.

(96) Jiang, R.; Jiang, Y. Leak Detection and Localization of Gas Pipeline Network Based on a Steady State Model. In *2014 Seventh International Symposium on Computational Intelligence and Design*; Hangzhou, China, 2014; pp 10–13.

(97) Chatzigeorgiou, D.; Youcef-Toumi, K.; Ben-Mansour, R. Detection & Estimation Algorithms for in-Pipe Leak Detection. In *2014 American Control Conference*; Portland, USA, 2014; pp 5508–5514.

(98) Scott, Stuart, L.; Barrufet, Maria, A. *Worldwide Assessment of Industry Leak Detection Capabilities for Single & Multiphase Pipelines*; College Station, 2003.

(99) Abbaspour, M.; Chapman, K. S. Nonisothermal Transient Flow in Natural Gas Pipeline. *J. Appl. Mech.* **2008**, *75* (3), 31018.

(100) Reddy, H. P.; Narasimhan, S.; Bhallamudi, S. M. Simulation and State Estimation of Transient Flow in Gas Pipeline Networks Using a Transfer Function Model. *Ind. Eng. Chem. Res.* **2006**, *45* (11), 3853.

(101) Osiadacz, A. J.; Maciej, C. Verification of Transient Gas Flow Simulation Model. In *PSIG Annual Meeting*; Bonita Springs, Florida, 2010.

(102) Herty, M.; Mohring, J.; Sachers, V. A New Model for Gas Flow in Pipe Networks. *Math. Methods Appl. Sci.* **2010**, *33* (7), 845.

(103) Bagajewicz, M.; Valtinson, G. Leak Detection in Gas Pipelines Using Accurate Hydraulic Models. *Ind. Eng. Chem. Res.* **2014**, *53* (44), 16964.

(104) Emara-Shabaik, H. E.; Khulief, Y. a.; Hussaini, I. A Non-Linear Multiple-Model State Estimation Scheme for Pipeline Leak Detection and Isolation. *Proc. Inst. Mech. Eng. Part I J. Syst. Control Eng.* **2002**, *216* (6), 497.

(105) Reddy, H. P.; Narasimhan, S.; Bhallamudi, S. M.; Bairagi, S. Leak Detection in Gas Pipeline Networks Using an Efficient State Estimator. Part-I: Theory and Simulations. *Comput. Chem. Eng.* **2011**, *35* (4), 651.

(106) Wu, B.; Ding, Z. Pipeline Leak Location Using Optimization Method. In *PSIG Annual Meeting*; New Orleans, Louisiana, 2015.

(107) Abdulla, M. B.; Herzallah, R. Probabilistic Multiple Model Neural Network Based Leak Detection System: Experimental Study. *J. Loss Prev. Process Ind.* **2015**, *36*, 30.

(108) Geiger, G.; Werner, T.; Matko, D. Leak Detection and Locating - A Survey. In *PSIG Annual Meeting*; Bern, Switzerland, 2003.

(109) Fu, Y.; Duan, G.; Song, S. Design of Unknown Input Observer for Linear Time-Delay Systems. *Int. J. Control* **2004**, *2* (4), 530.

(110) Zhang, X.; Polycarpou, M. M.; Parisini, T. Fault Diagnosis of a Class of

Nonlinear Uncertain Systems with Lipschitz Nonlinearities Using Adaptive Estimation. *Automatica* **2010**, *46* (2), 290.

(111) Edwards, C.; Spurgeon, S. K.; Patton, R. J. Sliding Mode Observers for Fault Detection and Isolation. *Automatica* **2000**, *36* (4), 541.

(112) Torres, L.; Verde, C.; Besancon, G.; Gonzalez, O. High-Gain Observers for Leak Location in Subterranean Pipelines of Liquefied Petroleum Gas. *Int. J. Robust Nonlinear Control* **2014**, *24* (6), 1127.

(113) Rahiman, W.; Bo, L.; Buzhou, W.; Zhengtao, D. Circle Criterion Based Nonlinear Observer Design for Leak Detection in Pipelines. In *2007 IEEE International Conference on Control and Automation, ICCA*; Hangzhou, China, 2008; pp 2993–2998.

(114) Guillén, M.; Dulhoste, J. F.; Besançon, G.; S, I. R.; Santos, R.; Georges, D. Leak Detection and Location Based on Improved Pipe Model and Nonlinear Observer. In *2014 European Control Conference*; Strasbourg, France, 2014; pp 958–963.

(115) Espinoza-Moreno, G.; Begovich, O.; Sanchez-Torres, J. Real Time Leak Detection and Isolation in Pipelines: A Comparison between Sliding Mode Observer and Algebraic Steady State Method. *World Autom. Congr. Proc.* **2014**, 748.

(116) Dulhoste, J. F.; Besancon, G.; Torres, L.; Begovich, O.; Navarro, A. About Friction Modeling for Observer-Based Leak Estimation in Pipelines. In *Proceedings of the IEEE Conference on Decision and Control*; Orlando, USA, 2011; pp 4413–4418.

(117) Sename, O. Unknown Input Robust Observers for Time-Delay Systems. In *36th IEEE Conference on Decision and Control*; San Diego, USA, 1997; pp 1629–1630.

(118) Miller, R. J.; Mukundan, R. On Designing Reduced-Order Observers for Linear Time-Invariant Systems Subject to Unknown Inputs. *Int. J. Control* **1982**, *35* (1), 183.

(119) Hui, S.; Żak, S. Observer Design for Systems with Unknown Inputs. *Int. J. Appl. Math. Comput. Sci.* **2005**, *15* (4), 431.

(120) Szoplik, J. The Gastransportation in a Pipeline Network. In *Advances in Natural Gas Technology*; Hamid, A.-M., Ed.; InTech Europe: Rijeka, 2001; pp 339–357.

(121) Weitian, C.; Saif, M. Fault Detection and Isolation Based on Novel Unknown Input Observer Design. In *2006 American Control Conference*; Minneapolis, USA, 2006.

(122) Mahmoud, M. S. *Robust Control and Filtering for Time-Delay Systems*; CRC Press: New York, 2000.

(123) Verde, C.; Visairo, N. Bank of Nonlinear Observers for the Detection of Multiple Leaks in a Pipeline. In *Proceedings of the 2001 IEEE International Conference on Control Applications*; 2001; pp 714–719.

(124) Verde, C.; Visairo, N.; Gentil, S. Two Leaks Isolation in a Pipeline by Transient Response. *Adv. Water Resour.* **2007**, *30* (8), 1711.

(125) Verde, C.; Molina, L.; Torres, L. Parameterized Transient Model of a Pipeline for Multiple Leaks Location. *J. Loss Prev. Process Ind.* **2014**, *29* (1), 177.

(126) Biegler, L.; Ghattas, O. *Large Scale PDE Constrained Optimization: An Introduction*; Springer-Verlag Berlin Heidelberg: Berlin, 2003.

(127) Protas, B. Adjoint-Based Optimization of PDE Systems with Alternative Gradients. *J. Comput. Phys.* **2008**, *227* (13), 6490.

(128) Cioaca, A.; Alexe, M.; Sandu, A. Second-Order Adjoints for Solving PDE-Constrained Optimization Problems. *Optim. Methods Softw.* **2012**, *27* (4/5), 625.

(129) Storn, R.; Price, K. Differential Evolution -- A Simple and Efficient Heuristic for Global Optimization over Continuous Spaces. *J. Glob. Optim.* **1997**, *11* (4), 341.

(130) Hesselbo, B.; Stinchcombe, R. B. Monte Carlo Simulation and Global Optimization without Parameters. *Phys. Rev. Lett.* **1995**, *74* (12), 2151.

(131) Vanderbilt, D.; Louie, S. G. A Monte Carlo Simulated Annealing Approach to Optimization over Continuous Variables. *J. Comput. Phys.* **1984**, *56* (2), 259.

(132) Rios, L. M.; Sahinidis, N. V. Derivative-Free Optimization: A Review of Algorithms and Comparison of Software Implementations. *J. Glob. Optim.* **2013**, *56* (3), 1247.

(133) Ricker, N. L. Model Predictive Control with State Estimation. *Ind. Eng. Chem. Res.* **1990**, *29* (3), 374.

(134) Heidarinejad, M.; Liu, J.; Christofides, P. D. State-Estimation-Based Economic Model Predictive Control of Nonlinear Systems. *Syst. Control Lett.* **2012**, *61* (9), 926.

(135) Ozturk, S. S.; Hu, W. *Cell Culture Technology for Pharmaceutical and Cell-Based Therapies*; CRC Press: New York, 2005.

(136) Meilhoc, E.; Wittrup, K. D.; Bailey, J. E. Influence of Dissolved Oxygen Concentration on Growth, Mitochondrial Function and Antibody Production of Hybridoma Cells in Batch Culture. *Bioprocess Eng.* **1990**, *5* (6), 263.

(137) Gray, D. R.; Chen, S.; Howarth, W.; Inlow, D.; Maiorella, B. L. CO2 in Large-Scale and High-Density CHO Cell Perfusion Culture. *Cytotechnology* **1996**, *22* (1–3), 65.

(138) Kreisselmeier, G.; Anderson, B. D. O. Robust Model Reference Adaptive Control. *Autom. Control. IEEE Trans.* **1986**, *31* (2), 127.

(139) Eaton, J. W.; Rawlings, J. B. Feedback Control of Chemical Processes Using on-Line Optimization Techniques. *Comput. Chem. Eng.* **1990**, *14* (4), 469.

(140) Seliger, R.; Frank, P. M. Fault-Diagnosis by Disturbance Decoupled Nonlinear Observers. In *Proceedings of the 30th IEEE Conference on Decision and Control*; 1991; pp 277–282.

(141) Zhang, R.; Gao, F. State Space Model Predictive Control Using Partial Decoupling and Output Weighting for Improved Model/plant Mismatch Performance. *Ind. Eng. Chem. Res.* **2013**, *52* (2), 817.

(142) Wang, D.; Lum, K. Y. Adaptive Unknown Input Observer Approach for Aircraft Actuator Fault Detection and Isolation. *Int. J. Adapt. Control Signal Process.* **2007**, *21* (1), 31.

(143) Roset, B.; Nijmeijer, H. Observer-Based Model Predictive Control. *Int. J. Control* **2004**, *77* (17), 1452.

(144) Ali, E.; Zafiriou, E. Optimization-Based Tuning of Nonlinear Model Predictive

Control with State Estimation. *J. Process Control* **1993**, *3* (2), 97.

(145) Lee, J. H.; Ricker, N. L. Extended Kalman Filter Based Nonlinear Model Predictive Control. *Ind. Eng. Chem. Res.* **1994**, *33*, 1530.

(146) Prakash, J.; Senthil, R. Design of Observer Based Nonlinear Model Predictive Controller for a Continuous Stirred Tank Reactor. *J. Process Control* **2008**, *18* (5), 504.

(147) Rajamani, M.; Rawlings, J.; Qin, S. Achieving State Estimation Equivalence for Misassigned Disturbances in Offset Free Model Predictive Control. *AIChE J.* **2009**, *55* (2), 396.

(148) Tadayyon, A. Extended Kalrnan Filter-Based Nonlinear Model Predictive Control of KCl-NaCl Crystallizer. *Can. J. Chem. Eng.* **2001**, *79* (4), 255.

(149) Prakash, J.; Patwardhan, S. C.; Shah, S. L. State Estimation and Nonlinear Predictive Control of Autonomous Hybrid System Using Derivative Free State Estimators. *J. Process Control* **2010**, *20* (7), 787.

(150) Boutayeb, M. Observers Design for Linear Time-Delay Systems. *Syst. Control Lett.* **2001**, *44* (2), 103.

(151) Wang, Z.; Huang, B.; Unbehauen, H. Robust H∞ Observer Design of Linear State Delayed Systems with Parametric Uncertainty: The Discrete-Time Case. *Automatica* **1999**, *35* (6), 1161.

(152) Yang, F.; Wilde, R. W. Observers for Linear Systems with Unknown Inputs. *IEEE Trans. Automat. Contr.* **1988**, *33* (7), 677.

(153) Findeisen, R.; Imsland, L. S.; Allgöwer, F. State and Output Feedback Nonlinear

Model Predictive Control: An Overview. *Eur. J. Control* **2003**, *9* (2–3), 190.

(154) Chehimi, H.; Sa, S. H. Unknown Inputs Observer Based Output Feedback Controller for Rotor Resistance Estimation in IMs. *Int. J. Sci. Tech. Autom. Cotrol Comput. Eng.* **2011**, *5* (6), 1532.

(155) Yan, J.; Bitmead, R. R. Incorporating State Estimation into Model Predictive Control and Its Application to Network Traffic Control. *Automatica* **2005**, *41* (4), 595.

(156) Deshpande, A. P.; Patwardhan, S. C.; Narasimhan, S. S. Intelligent State Estimation for Fault Tolerant Nonlinear Predictive Control. *J. Process Control* **2009**, *19* (2), 187.

(157) Park, T. G.; Kim, D. Design of Unknown Input Observers for Linear Systems with Unmatched Unknown Inputs. *Trans. Inst. Meas. Control* **2014**, *36* (3), 399.

(158) Hou, M.; Muller, P. C. Design of Observers for Linear Systems with Unknown Inputs. *Autom. Control. IEEE Trans.* **1992**, *37* (6), 871.

(159) Chen, W. C. W.; Saif, M. Unknown Input Observer Design for a Class of Nonlinear Systems: An LMI Approach. In *2006 American Control Conference*; 2006; pp 834–838.

(160) Ding, X.; Frank, P. M.; Guo, L. Nonlinear Observer Design via an Extended Observer Canonical Form. *Syst. Control Lett.* **1990**, *15* (4), 313.

(161) Seliger, R.; Frank, P. M. Robust Component Fault Detection and Isolation in Nonlinear Dynamic Systems Using Nonlinear Unknown Input Observers. In *Proceedings of the IFAC/IMACS Symposium SAFE PROCESS*; Baden-Baden,

Germany, 1991; pp 277–282.

(162) Yang, H.; Saif, M. Monitoring and Diagnostics of a Class of Nonlinear Systems Using a Nonlinear Unknown Input Observer. In *Proceeding of the 1996 IEEE International Conference on Control Applications*; 1996; pp 1006–1011.

(163) Ordoñez, M.; Raftery, J.; Jaladi, T.; Chen, X.; Kao, K.; Karim, M. Modelling of Batch Kinetics of Aerobic Carotenoid Production Using Saccharomyces Cerevisiae. *Biochem. Eng. J.* **2016**, *144*, 226.

(164) Karim, M. N.; Raftery, J. P.; Pan, X. Optimal Control of a Continuous Bioreactor for Maximized Betacarotene Production. In *Integrated Continuous Biomanufacturing II*; ECI Symposium Series: Berkeley, USA, 2015.

(165) Wechselberger, P.; Sagmeister, P.; Herwig, C. Real-Time Estimation of Biomass and Specific Growth Rate in Physiologically Variable Recombinant Fed-Batch Processes. *Bioprocess Biosyst. Eng.* **2013**, *36* (9), 1205.

(166) Ludovico, P.; Sousa, M. J.; Silva, M. T.; Leão, C.; Côrte-Real, M. Saccharomyces Cerevisiae Commits to a Programmed Cell Death Process in Response to Acetic Acid. *Microbiology* **2001**, *147* (9), 2409.

(167) Zhang, Q.; Wu, D.; Lin, Y.; Wang, X.; Kong, H.; Tanaka, S. Substrate and Product Inhibition on Yeast Performance in Ethanol Fermentation. *Energy and Fuels* **2015**, *29* (2), 1019.

(168) Narendranath, N. V; Thomas, K. C.; Ingledew, W. M. Effects of Acetic Acid and Lactic Acid on the Growth of Saccharomyces Cerevisiae in a Minimal Medium. *J. Ind. Microbiol. Biotechnol.* **2001**, *26* (3), 171.

APPENDIX

Development of non-isothermal natural gas flow models

Nomenclature

A	Area of cross section
D	Inner diameter of pipeline
F	Friction force
G	Gravity force
H	Enthalpy
p	Pressure
Pr	Force due to pressure drop
q	Mass flow rate
q_L	Mass flow rate of leak
Q	Heat transfer rate
U	Heat transfer coefficient
ρ	Gas density

The mass, momentum, and energy balance of the gas flow in a pipeline is shown below.

Mass balance

$\dot{q}_{in}-\dot{q}_{out}=\dot{q}_{accu}$

$\dot{q}_{in}=\rho Av; \quad \dot{q}_{out}=\rho Av+\frac{\partial \rho Av}{\partial x}\Delta x+q_L; \qquad \dot{q}_{acc}=\frac{\partial \rho A\Delta x}{\partial t}$

Momentum balance

$\dot{M}_{element}=\dot{M}_{in}-\dot{M}_{out}+G+Pr+F$

$\dot{M}_{in}=\rho Av\cdot v;\quad \dot{M}_{out}=\rho Av\cdot v+\frac{\partial \rho Av\cdot v}{\partial x}\Delta x+q_L\cdot v;\quad \dot{M}_{element}=\frac{\partial(\rho A\Delta xv)}{\partial t}$

$G=-\rho A\Delta x g sin\theta$

$Pr=PA-\left(P+\frac{\partial P}{\partial x}\Delta x\right)A=-\frac{\partial P}{\partial x}A\Delta x$

$F=\frac{-\rho f v^2}{2D}A\Delta x$

Simplify the equation to the following:

$$\frac{\partial(\rho v)}{\partial t}+\frac{\partial \rho v\cdot v}{\partial x}+\frac{\partial P}{\partial x}+\frac{q_L.v}{A\Delta x}=-\rho g sin\theta-\frac{\rho f v^2}{2D}$$

For the non-isothermal model, the equation can be written as:

$$\frac{1}{A}\frac{\partial q}{\partial t}+\frac{\partial \rho v\cdot v}{\partial x}+\frac{\partial P}{\partial x}+\frac{q_L.v}{A\Delta x}=-\rho g sin\theta-\frac{fq^2}{2DA^2P}ZRT$$

Energy balance

$\dot{E}_{element}=\dot{E}_{in}-\dot{E}_{out}+\dot{W}+\dot{Q}$

$\dot{E}_{in}=(H+\frac{1}{2}v^2)\rho Av$

$\dot{E}_{out}=\left(H+\frac{1}{2}v^2\right)\rho Av+\frac{\partial\left(H+\frac{1}{2}v^2\right)\rho Av}{\partial x}\Delta x+\left(H+\frac{1}{2}v^2\right)q_L$

$\dot{E}_{element}=\frac{\partial\left(U_T+\frac{1}{2}w^2\right)\rho A\Delta x}{\partial t}$

$\dot{W}=-\rho gAv sin\theta\Delta x$

$\dot{Q}=-\frac{4UA(T-T_G)}{D}\Delta x$

So the energy balance equation can be written as:

$$\frac{\partial\left(U_T+\frac{1}{2}v^2\right)\rho}{\partial t}+\frac{\partial\left(H+\frac{1}{2}v^2\right)\rho v}{\partial x}+\frac{\left(H+\frac{1}{2}v^2\right)q_L}{A\Delta x}=-\rho g v\sin\theta-\frac{4U(T-T_G)}{D}$$

Having the following process variables:

$$U_T=H-PV$$

$$dH=C_P dT+\left\{\frac{T}{\rho}\left(\frac{\partial\rho}{\partial T}\right)_P+1\right\}\frac{dP}{\rho}$$

$$\left(\frac{\partial\rho}{\partial T}\right)_P=-\frac{\rho}{T}\left(1+\frac{T}{Z}\frac{\partial Z}{\partial T}\right)$$

The energy balance equation becomes:

$$\rho\frac{\partial H}{\partial t}+\rho v\frac{\partial H}{\partial x}-v\frac{\partial P}{\partial x}-\frac{\partial P}{\partial t}=\frac{\rho f v^3}{2D}-\frac{4U(T-T_G)}{D}$$

So the final non-isothermal process model is:

$$\frac{\partial P}{\partial t}=\frac{-\frac{1}{A}\frac{\partial q}{\partial x}-\frac{1}{A\Delta x}q_L+\left(\frac{1}{ZC_P}\frac{\partial Z}{\partial T}+\frac{1}{TC_P}\right)\left(\frac{fq^3z^2R^2T^2}{2DA^3P^2}-\frac{4U(T-T_g)}{D}-\frac{q}{A}C_P\frac{dT}{dx}+\left(\frac{T}{Z}\frac{\partial Z}{\partial T}+1\right)\frac{q}{AP}ZRT\frac{dP}{dx}\right)}{\left(\frac{1}{ZRT}-\frac{P}{Z^2RT}\frac{\partial Z}{\partial P}-\left(\frac{\partial Z}{\partial T}\right)^2\frac{T}{Z^2C_P}-\frac{2}{ZC_P}\frac{\partial Z}{\partial T}-\frac{1}{TC_P}\right)}$$

$$\frac{\partial q}{\partial t}=-A\frac{\partial P}{\partial x}-\frac{AP}{ZRT}g\sin\theta-\frac{fq^2}{2DAP}ZRT-\frac{1}{A}\frac{q_L}{\Delta x}\left(\frac{q}{P}\right)ZRT$$

$$\frac{\partial T}{\partial t}=\frac{\left(\frac{1}{ZRT}-\frac{P}{Z^2RT}\frac{\partial Z}{\partial P}\right)\frac{\partial P}{\partial t}}{\left(\frac{P}{Z^2RT}\frac{\partial Z}{\partial T}+\frac{P}{ZRT^2}\right)}+\frac{\frac{1}{A}\frac{\partial q}{\partial x}}{\left(\frac{P}{Z^2RT}\frac{\partial Z}{\partial T}+\frac{P}{ZRT^2}\right)}+\frac{q_L}{A\Delta x}\frac{1}{\left(\frac{P}{Z^2RT}\frac{\partial Z}{\partial T}+\frac{P}{ZRT^2}\right)}$$

Proof of Lemma 3.1

The proof of Lemma 1 is similar to the reference.[47]

$$[T\quad N\quad F_0\quad \bar{G}_0\quad F_1\quad \bar{G}_1\quad F_2\quad \bar{G}_2\quad F_3\quad \bar{G}_3\quad F_4\quad \bar{G}_4]\cdot\phi_1=\Psi_1$$

The solution for Equation (13c) exists if and only if

$$\text{rank}\begin{bmatrix}\phi_1\\ \Psi_1\end{bmatrix}=\text{rank}\phi_1$$

By applying the definition of ϕ_1, Ψ_1, and the above equation (AB1), the following equation can be obtained. W is assumed not an identity matrix.

$$\text{rank}\begin{bmatrix}I_n & W\\ C & 0\end{bmatrix}=n+\text{rank } W$$

By multiplying a nonsingular matrix $\begin{bmatrix}I_n & 0\\ C & -I_p\end{bmatrix}$ at the left hand side of the above equation, we have the following equation.

$$\text{rank}\begin{bmatrix}I_n & W\\ 0 & CW\end{bmatrix}=n+\text{rank}W$$

so rank(*CW*) = rank (*W*)

Proof of Theorem 3.2

Theorem 3.2: The observer estimation error will be asymptotically stable if and only if the following conditions hold: there exist matrices $P=P^T>0$ and $Q_i>0$ satisfying the following linear matrix inequality:

$$\Xi=\begin{bmatrix}-P+\sum_{i=1}^{4}Q_i & 0 & 0 & 0 & 0 & F_0^tP\\ * & -Q_1 & 0 & 0 & 0 & F_1^tP\\ * & * & -Q_2 & 0 & 0 & F_2^tP\\ * & * & * & -Q_3 & 0 & F_3^tP\\ * & * & * & * & -Q_4 & F_4^tP\\ * & * & * & * & * & -P\end{bmatrix}<0$$

Briefly, the proof of **Theorem 3.2** begins with the introduction of a discrete type Lyapunov-Karsovskii function, which is given by:

$$V(e_k)=e^t(k)Pe(k)+\sum_{i=1}^{4}\sum_{\theta_i=k-\tau_i}^{k-1}e^t(\theta_i)Q_ie(\theta_i)$$

$$V(e_{k+1})=e^t(k+1)Pe(k+1)+\sum_{i=1}^{4}\sum_{\theta_i=k+1-\tau_i}^{k} e^t(\theta_i)Q_i e(\theta_i)$$

$$\Delta V(e_k)=V(e_{k+1})-V(e_k)=\begin{bmatrix} e(k-\tau_1)\\ e(k-\tau_2)\\ e(k-\tau_3)\\ e(k-\tau_4)\end{bmatrix}^t \Xi \begin{bmatrix} e(k-\tau_1)\\ e(k-\tau_2)\\ e(k-\tau_3)\\ e(k-\tau_4)\end{bmatrix} < 0, \text{ so } \Xi < 0$$

By applying the Schur complement method and some additional mathematical manipulations, the matrix Ξ can be transformed. More details on the application of Lyapunov-Karsovskii function and Schur complement method can be found at the reference.[122]

Proof of Theorem 3.3

Theorem 3.3: The norm of transfer function of T_{en} will be smaller than γ if there exists matrices, and $P = P^T > 0$; $Q_i>0$, which satisfy the following linear matrix inequality. D equals to $(NM+ \sum G_iM)$.

$$\Omega=\begin{bmatrix} -P+\sum_{i=1}^{4}Q_i & 0 & 0 & 0 & 0 & 0 & F_0^tP & F_0^tP & 0\\ * & -Q_1 & 0 & 0 & 0 & 0 & F_1^tP & F_1^tP & 0\\ * & * & -Q_2 & 0 & 0 & 0 & F_2^tP & F_2^tP & 0\\ * & * & * & -Q_3 & 0 & 0 & F_3^tP & F_3^tP & 0\\ * & * & * & * & -Q_4 & 0 & F_4^tP & F_4^tP & 0\\ * & * & * & * & * & -\gamma^2 & D^tP & D^tP & 0\\ * & * & * & * & * & * & -P & 0 & 0\\ * & * & * & * & * & * & * & 0 & P\\ * & * & * & * & * & * & * & * & -I \end{bmatrix} < 0$$

Proof of the above theorem is to introduce a variable: $J_{ed} = \sum (e^T(k)e(k) - \gamma^2 n^T(k)n(k)) < 0$, which is equal to the transfer function $\|T_{en}\| < \gamma$. Then $J_{ed} = \sum (e^T(k)e(k) - \gamma^2 n^T(k)n(k) + \Delta V) + V(0) - V(\infty)$, in which V() is the Lyapunov-Karsovskii function applied in the proof of **Theorem** 2. With $V(\infty) \geq 0$ and assumption of $V(0) = 0$, the proof requires to find matrix parameters so that $e^T(k)e(k) - \gamma^2 n^T(k)n(k) + \Delta V < 0$. Then the equation can be rearranged as follows:

$$\begin{bmatrix} e(k-\tau_1) \\ e(k-\tau_2) \\ e(k-\tau_3) \\ e(k-\tau_4) \\ n(k) \end{bmatrix}^t \Omega \begin{bmatrix} e(k-\tau_1) \\ e(k-\tau_2) \\ e(k-\tau_3) \\ e(k-\tau_4) \\ n(k) \end{bmatrix} < 0 \ , \ \Omega < 0$$

By applying Schur complement method and mathematical manipulation, matrix Ω can be transformed in **Theorem** 3.3. **Theorem** 3.3 provides a validation method to examine the robustness of the design parameters.